JÜLICH
FORSCHUNGSZENTRUM

Institut für Kernphysik
COSY

SPIN@COSY: Looking Inside a Spin Resonance

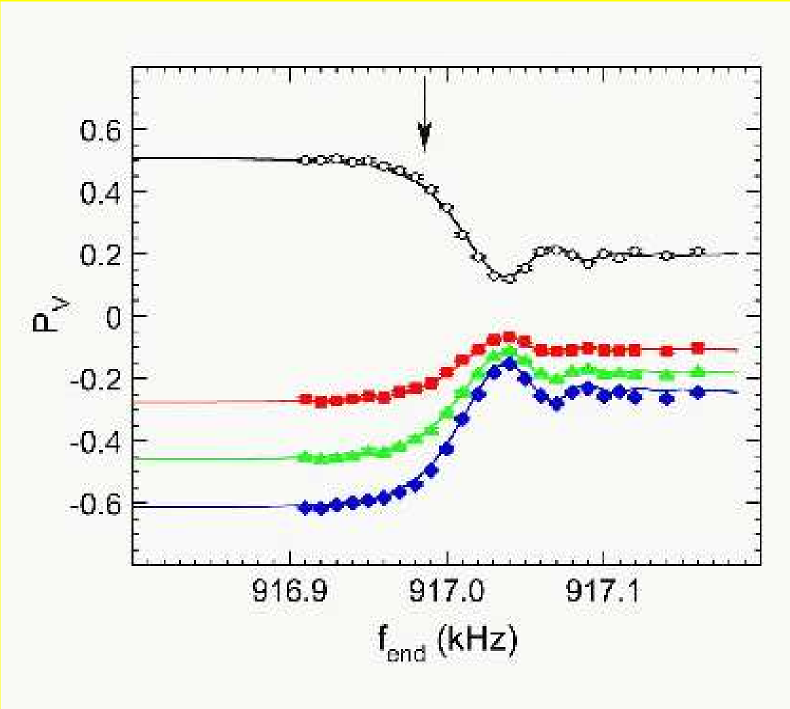

ANNUAL REPORT 2007

Jül-4262

Annual Report 2007

Institut für Kernphysik / COSY

DIRECTORS AT THE IKP:

Experimental Hadron Structure (IKP-1):	**Prof. Dr. James Ritman**
Experimental Hadron Dynamics (IKP-2):	**Prof. Dr. Hans Ströher**
Theoretical Nuclear Physics (IKP-3):	**Prof. Dr. Ulf-G. Meißner**
Large-Scale Nuclear Physics Equipment (IKP-4):	**Prof. Dr. Rudolf Maier (managing director)**

EDITORIAL BOARD:
Priv. Doz. Dr. Markus Büscher
Priv. Doz. Dr. Christoph Hanhart
Prof. Dr. Siegfried Krewald
Prof. Dr. Hartmut Machner
Prof. Dr. Rudolf Maier
Prof. Dr. Ulf-G. Meißner
Prof. Dr. James Ritman
Dr. Hans Stockhorst
Prof. Dr. Hans Ströher

Cover picture:

The SPIN@COSY polarized beam team found striking new results while studying the spin-manipulation of polarized deuterons at COSY. The newly developed Chao formalism (the first generalization of the Froissart-Stora formula) was used to calculate in detail what might happen in a new type of experiment, where a 1 MHz RF-magnet's frequency is swept by a fixed range of 400 Hz, while its end-frequency f_{end} is stepped through many different values near and inside a spin resonance. The calculations predicted that, if the resonance strength of the magnet was not strong enough to fully flip the spin, then there would be large oscillations in the final polarization. The figure shows four measured vertical vector polarization states (P_{V}) (black: $+1$, red: $-1/3$, green: $-2/3$, blue: -1) of 1.85 GeV/c stored deuterons plotted *vs.* the end frequency of the 400 Hz sweep. The calculations (solid lines) predict the oscillations very well, indicating that the experimental results confirm the validity of the Chao formalism. Precise values were obtained for the resonance frequency $f_{\mathrm{R}} = 916985.3 \pm 0.5$ Hz, the frequency spread $\delta p_{\Delta p} = 23 \pm 1$ Hz (FWHM), and the strength $\varepsilon = (1.060 \pm 0.005) \cdot 10^{-5}$. The arrow shows the center of the resonance.

Preface

On November 7/8, 2007 the kick-off event and a symposium on physics at the future FAIR facility took place at GSI-Darmstadt, during which the start of the project was officially announced. This important milestone strongly influences the activities of the IKP. As in previous years, the institute continued its vigorous engagement for the High Energy Storage Ring (HESR) as well as the PANDA and PAX experiments. IKP is in charge of all major HESR components, among them the ion optical design of the ring, the rf systems, the beam-diagnostics and magnets, as well as stochastic cooling. IKP has also taken on central responsibilities for the PANDA central charged particle tracking and vertexing, the PANDA frozen pellet target, as well as establishing a method to achieve a high degree of antiproton polarization for PAX. After the launching of the FAIR project these activities are now continuing to be vigorously pursued.

After the HGF Midterm Review in September, the committee expressed strong support for the theory group and was impressed by the stable operation of COSY and by the developments for the HESR. The ongoing physics program at ANKE was very positively acknowledged as well as progress with WASA, and the new proposal on ”Strangeness Physics at COSY-TOF”.

The inaugural meeting of the Virtual Institute “Spin and strong QCD” (Spokesperson: Ulf-G. Meißner) took place on November 30, 2007 at the IKP. The experimental as well as theoretical research of this Virtual Institute — with participating institutions IKP, GSI, Universities Bern, Bonn, Cracow, Torino, INFN Ferrara — is focused on three of the most important aspects of non-perturbative strong interactions with a direct connection to the hadron physics programs at COSY, PANDA and PAX at FAIR: Hadron spectroscopy, symmetry tests and polarization.

The experimental work at IKP is focused around the COSY accelerator complex:

- The WASA detector at an internal target station of COSY has been completely installed. A first experiment on the $pp \to pp\eta$ reaction has successfully been carried out.
- A first double polarization experiment took place at ANKE (polarized deuteron beam on polarized proton target with a storage cell). The ANKE collaboration also made a first attempt to precisely determine the η-mass by accurately measuring the beam energy of polarized deuterons with a spin-flip technique.
- The Spin@COSY polarized beam team found new striking results while studying the spin manipulation of polarized deuterons (see cover page). A new model, called Chao matrix formalism, that describes the beam polarization behavior inside a spin resonance was verified in detail and effectually applied for the first time at COSY. The result will also help to understand the behavior of polarized beams at other machines and someday also of antiproton beams at FAIR.
- The PAX collaboration has continued its test measurements at COSY to further investigate the possibilities to effectively produce polarized antiprotons for a later upgrade of the HESR.
- The number of COSY users has increased to more than 400. In the coming years new groups will carry out measurements at COSY, *e.g.* the EDM collaboration with preparatory studies aiming at the measurement of the deuteron’s electric dipole moment.

- During the two months summer shut down necessary repairs at cyclotron were accomplished, a barrier bucket cavity and a RF solenoid were installed. The PISA set-up was removed from the ring tunnel and will be send to IMP-Lanzhou, China.

Outstanding results from the theory group are:

- A novel method for the extraction of scattering phases and mixing angles from lattice simulations has been applied to nucleon-nucleon scattering.
- A new Regge model for pion photoproduction at energies above 3 GeV has been developed in order to extract high-lying Baryon resonances.
- It has been demonstrated that the decay properties of the $X(3872) \to \bar{D}D\pi$ and $\to J/\psi\pi\pi$ only allow for an interpretation as a virtual state.
- We have shown that it is possible to extract the neutron-neutron scattering length with an accuracy of $\delta a_{nn} = \pm 0.1$ fm from the differential cross section of the $\gamma d \to \pi^+ nn$ reaction.

Besides the regular physics program at the COSY accelerator, components and prototypes designed and built for HESR are being examined at COSY. New and important steps can be recorded:

- Substantial progress has been made in developing new pickup structures for stochastic cooling at the HESR. With funding of the EU project "DIRAC secondary beams" a prototype tank has been constructed and successfully tested at COSY.
- A prototype barrier bucket cavity came successfully into operation at COSY. This device is foreseen at the HESR to compensate the indispensable strong mean energy loss due to the beam-target interaction.
- The development of a 2 MeV electron cooler for COSY has continued. The new electron cooling system is proposed to further boost the luminosity even with strong heating effects of high-density internal targets. The 2 MeV electron cooler is best qualified to explore new essential features of the high energy electron cooler for the HESR.
- The HESR ring lattice was completely redesigned with normal conducting magnets and stochastic cooling properties were studied in this new lattice version.

We are looking forward to the constitution of the FAIR GmbH and we hope for investment money in order to prepare and build the accelerator HESR and detector components of PANDA and PAX as planned.

Finally we would like to express our sincere gratitude to the colleagues of the infrastructure of the Research Center in particular JSC, ZAT and ZEL. Our special thanks go to the surrounding universities and national research centers and our CANU community. We acknowledge the continuous support by the Helmholtz society, the board of management of the Research Center, by the COSY-FFE program and, in particular, by Dr. Sebastian M. Schmidt who became the new director of the research area "Key technologies and structure of matter" on 1 November 2007.

Jülich, March 2008 Rudolf Maier

Contents

Appendix

1 Physics at COSY

1.1 Overview

From 2007 on **ANKE**, **TOF** and **WASA** are the major experimental facilities at COSY since the remaining other installations — **COSY-11**, **PISA**, **BIG KARL** (with ENSTAR, GEM and HIRES) — have been decommissioned after successfully completing their scientific programs.
The **ANKE** collaboration carried out a first measurement of the charge-exchange deuteron break-up with both polarized beam and target. For such experiments the COSY beam intensity is increased by stacking injection while a storage cell is employed to achieve higher target densities.
WASA started its physics program with a measurement of the $\eta \to 3\pi$ decay, using η-mesons produced in the $pp \to pp\eta$ reaction, and several experiments with a deuterium pellet target.
The **TOF** collaboration has finalized the analysis of a large data sample on the $\vec{p}p \to pK^+\Lambda$ reaction. The spectrometer is now being prepared for an upgrade with a straw-tube tracker which will increase the mass resolution, *e.g.* for associated strangeness production processes. A proposal on their future program "Strangeness Physics at COSY-TOF" was submitted to the COSY Program Advisory Committee that approved the outlined experiments.

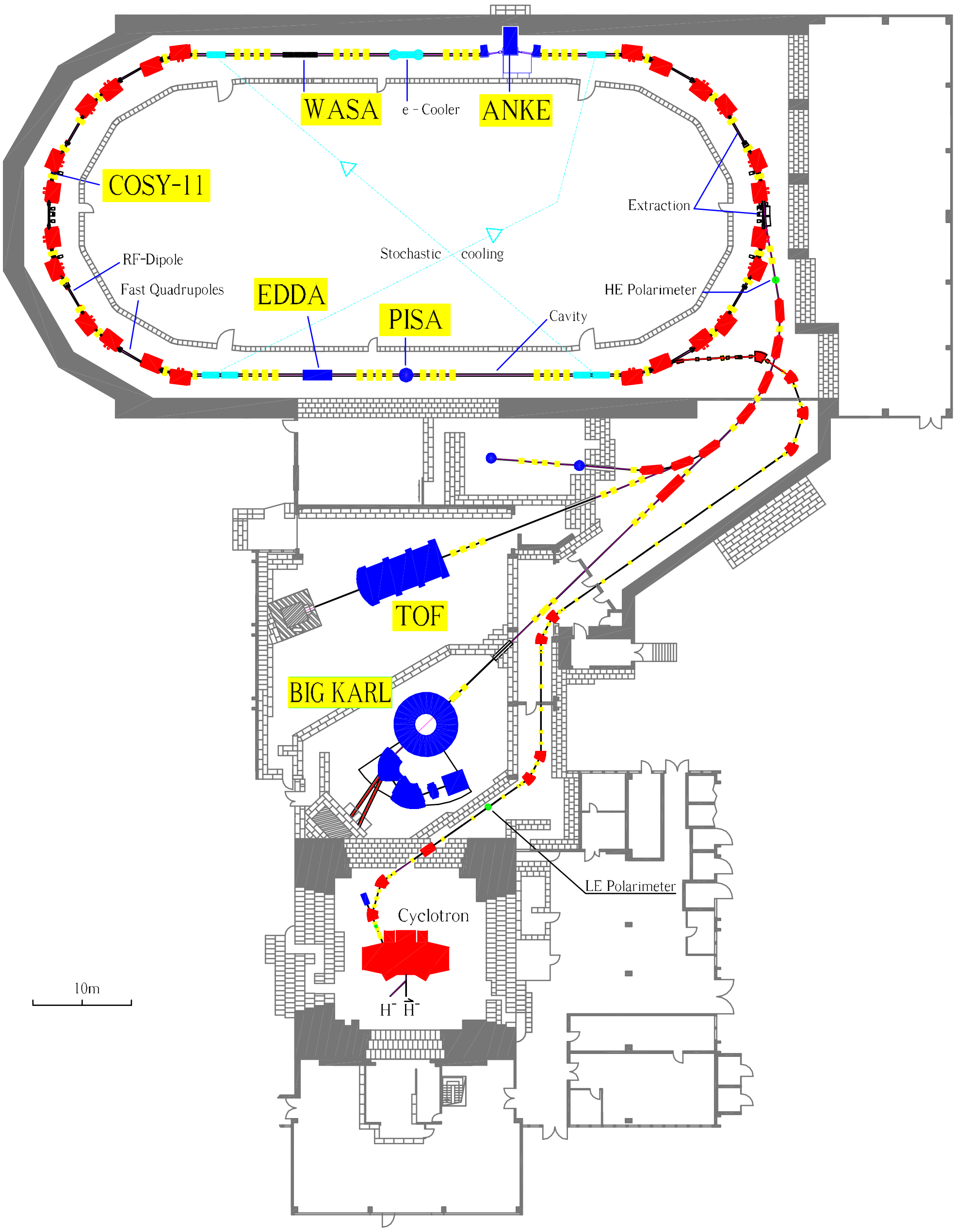

1.2 Major Physics Results at COSY

1.2.1 A possible $\eta\,^3$He quasibound state

The two high precision measurements of the $dp \to {}^3\mathrm{He}\,\eta$ reaction carried out at **ANKE** and **COSY-11** gave consistent results, as illustrated by the total cross section data shown in Fig. 1; the only obvious difference corresponds to a different luminosity estimate. These fascinating results could be achieved by using a slow continuous linear ramp in beam momentum provided by the COSY accelerator (*e.g.* -5 to $+10$ MeV in 300 s for ANKE).

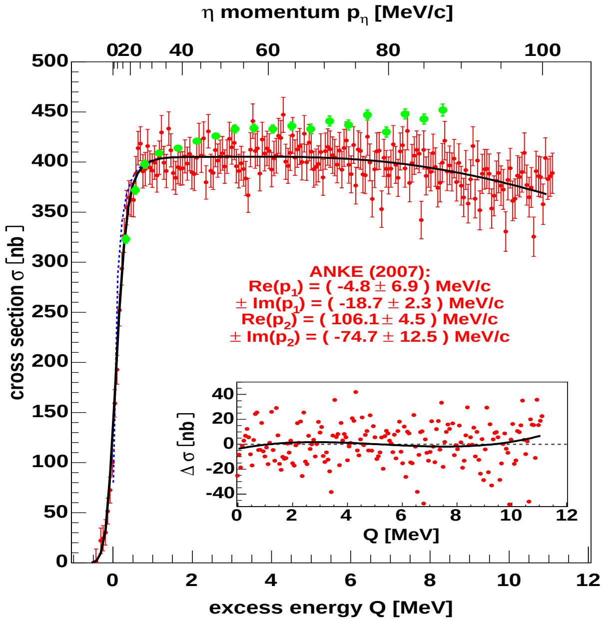

Fig. 1: ANKE (red) and COSY-11 measurements of the $dp \to {}^3\mathrm{He}\,\eta$ total cross section in terms of the excess energy Q and c.m. η momentum p_η. The line corresponds to the two-pole fit of Eq. (1). The inset shows the deviation of the ANKE data from the fitted line.

The precipitous rise in the cross section in terms of the excess energy Q or the η c.m. momentum $p_\eta = \sqrt{2m_{\mathrm{red}}Q}$ suggests a nearby pole in the production amplitude f and to identify its position, both sets of data could be fit with the *ansatz*

$$f_s = \frac{f_B}{(1-p_\eta/p_1)(1-p_\eta/p_2)}\,. \qquad (1)$$

To estimate accurately the parameters it is necessary to take the spread of the COSY beam momentum into account. When this is done, the ANKE data show that there is a pole at $p_1 = [(-5\pm7)\pm i(19\pm2)]$ MeV/c, *i.e.* $Q_0 = [(-0.30\pm0.15)\pm i(0.21\pm0.29)]$ MeV. This pole corresponds to a quasi-bound or virtual state of the $\eta\,^3$He system but, because of the uncertainty regarding the sign of the imaginary part, one cannot tell which. Furthermore, the total cross sections are sensitive mainly to the magnitude of Q_0 rather than its phase. However, important extra information is provided by the angular distributions.

Both COSY experiments show that for all the energies measured the cross section is linear in the ^{3}He c.m. production angle θ and, if the data are fitted in the form $\sigma = \sigma_0(1+\alpha\cos\theta)$, the slope parameter α varies strongly with p_η, as shown in Fig. 2. The shape is also similar to that of previous Saturne measurements, which have far fewer points.

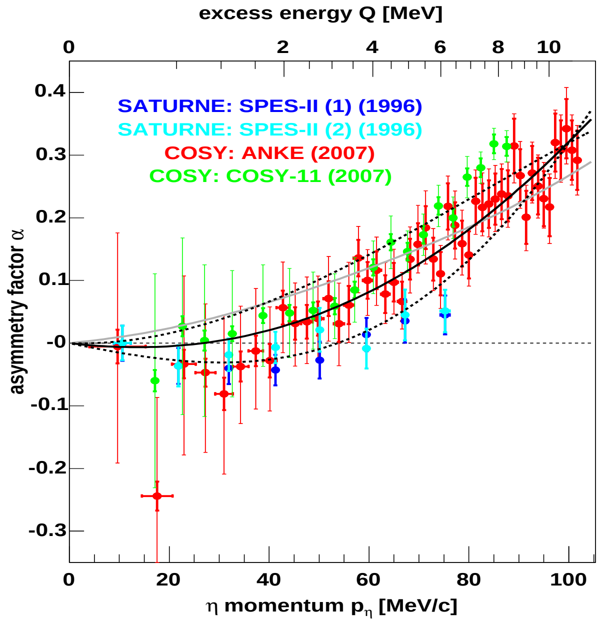

Fig. 2: Momentum dependence of the asymmetry parameter α for the $dp \to {}^3\mathrm{He}\,\eta$ reaction showing data from ANKE (red), COSY-11 (green), and Saturne (blue). The solid line represents a fit with the s-wave amplitude as given by Eq. (1) plus a p-wave with a constant phase. The dashed line neglects the phase variation coming from the pole.

Due to the interference between s- and p-wave production amplitudes, one might expect that α should vary linearly with c.m. momentum. The striking point about Fig. 2 is that this only happens for $p_\eta > 40$ MeV/c. The deviation from linearity due to the rapid decrease in the magnitude of the s-wave amplitude f_s leads to the dashed curve, which clearly does not reproduce the near-threshold data. A much better representation of the ANKE data is achieved when the phase variation of the s-wave amplitude arising from the p_1 pole of Eq. (1) is taken into account. A similar improvement for the COSY-11 data is obtained with slightly different parameters. Thus the angular distributions support the assertion that the anomalous behaviour observed is due to the presence of a nearby quasi-bound or virtual state of $\eta\,^3$He.

The rapid rise of the p waves so close to threshold implies that there should be interesting and informative effects in the angular dependence of $dp \to {}^3\mathrm{He}\,\eta$ polarization observables and a programme to measure these has already started at ANKE.

1.2.2 Observation of a strong K$^-$p final state interaction

Exclusive measurements of the $pp \to ppK^+K^-$ reaction were undertaken at **ANKE** at beam energies 2.65, 2.70, and 2.83 GeV. The prominent ϕ peak in the K^+K^- invariant mass spectrum, illustrated in Fig. 3, led to the determination of the differential and total cross sections for the $pp \to pp\phi$ reaction. In addition, however, Fig. 3 shows a K^+K^- background whose shape approximately resembles phase space.

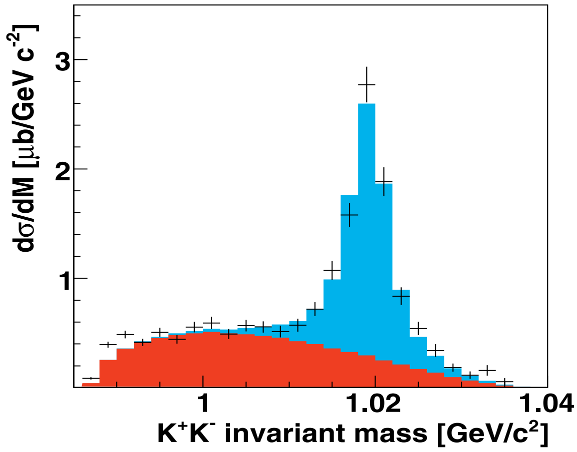

Fig. 3: Differential cross section for the $pp \to ppK^+K-$ reaction at 2.65 GeV as a function of the K^+K^- invariant mass compared to Monte Carlo simulations of ϕ (blue) and non-ϕ (red) contributions.

Similar experiments carried out at **COSY-11** at energies below the ϕ-threshold showed that the distributions of the positive and negative kaons were very different. In particular, low K^-p invariant masses were preferentially populated as compared to those of K^+p. This striking feature is confirmed over wider regions of energy and mass by the new ANKE data.

Figure 4 shows the ratio of the production cross sections for K^-p and K^+p pairs for events outside of the ϕ peak. The ratio changes by an order of magnitude from the lowest to the highest invariant masses. Moreover, the same effect is observed in the ratio of the production cross sections for K^-pp and K^+pp pairs shown in Fig. 5.

In contrast to the relatively weak K^+p force, the K^-p interaction is known to be strong, driven largely by the $\Lambda(1405)$ hyperon. The various non-ϕ distributions measured at ANKE have been modeled assuming that there can be final state interactions simultaneously in pp and both final K^-p systems. This product *ansatz* describes well all the ANKE data at three beam energies if one uses an effective K^-p scattering length of about 1.5 fm. This is illustrated by the simulations of the K^+K^- mass distribution of Fig. 3 and the K^-p/K^+p and K^-pp/K^+pp ratios of Figs. 4 and 5, respectively. The identical *ansatz* also reproduces well the K^-p/K^+p ratios measured at COSY-11.

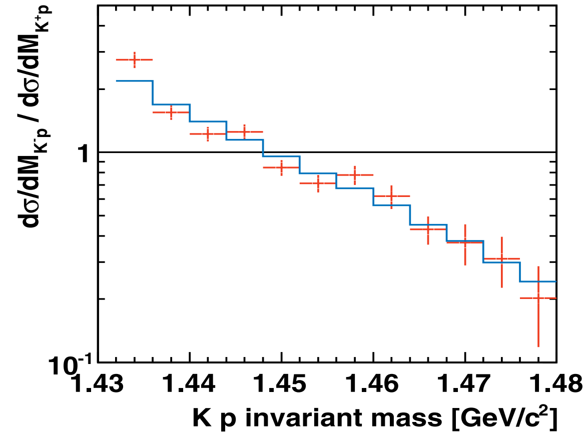

Fig. 4: Ratio of the differential cross sections for the $pp \to ppK^+K^-$ reaction at 2.65 GeV away from the ϕ region as function of the K^-p and K^+p invariant masses. Experimental data (red) are compared to a Monte Carlo simulation (blue).

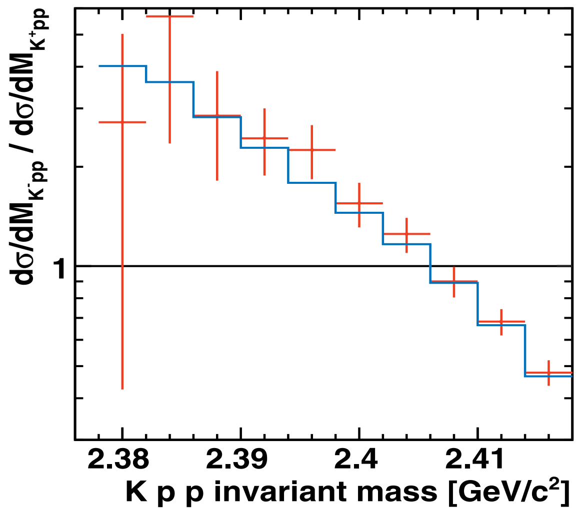

Fig. 5: Ratio of the differential cross sections for the $pp \to ppK^+K^-$ reaction at 2.65 GeV away from the ϕ region as function of the K^-pp and K^+pp invariant masses. Experimental data (red) are compared to a Monte Carlo simulation (blue).

The final state interaction assumptions also lead to a good description of the energy dependence of the non-ϕ contribution to the $pp \to ppK^+K^-$ total cross section. The sole exceptions are the lowest COSY-11 points which are slightly high. The discrepancy here might be connected with the behaviour apparent in Fig. 3, where the lowest mass points are under-predicted. This effect, which is seen at the other two beam energies as well as in the data from the DISTO collaboration, is also present in the ANKE data on $pn \to dK^+K^-$. The most likely explanation is that it is associated with the $K^0\bar{K}^0$ threshold, which is 8 MeV/c^2 above that of K^+K^-. The data may therefore allow one to study the transition $K^0\bar{K}^0 \rightleftharpoons K^+K^-$ at low energy.

1.2.3 Vector meson production

Vector mesons play an important role in meson exchange models of the interaction between nucleons. This is but one aspect that motivates interest in experimental studies of vector meson production of nucleons and light nuclei. Results from COSY currently dominate this field of research while earlier data from the Saturne experiments provided some guidance. Figure 6 shows total cross sections for the isoscalar neutral vector mesons measured in pp interactions. Full coverage of the excitation function for $pp \to pp\omega$ below 300 MeV excitation energy was achieved by COSY experiments which close the gap between excitation energies comparable to the meson widths and several hundred MeV. Only one data point for ϕ production existed prior to the COSY measurements.

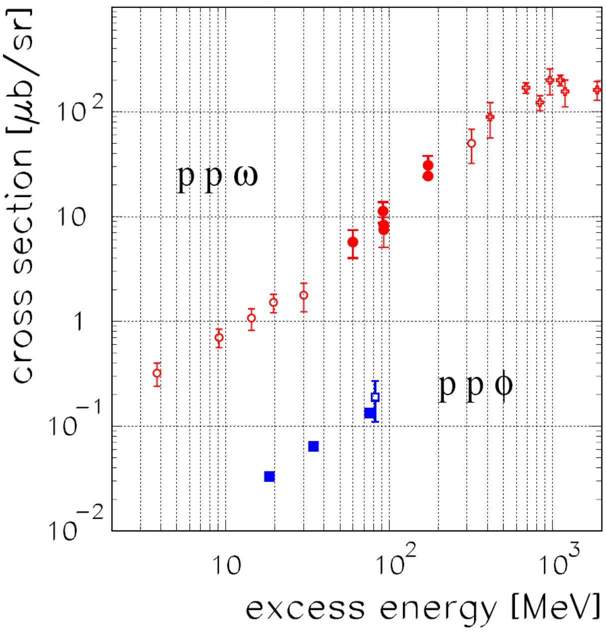

Fig. 6: Excitation functions of vector mesons as measured in pp interactions at COSY (filled symbols, red: $pp \to pp\omega$, blue: $pp \to pp\phi$), data from Saturne experiments (open symbols) and earlier bubble chamber data (crosses).

The apparent change in slope of the $pp \to pp\omega$ cross section at low excess energies of a few tens of MeV is a matter of ongoing debate. It may be a direct consequence of the finite width of the ω meson, but theoretical calculations taking the width into account often fail to reproduce the curvature even though only the smallest possible angular momenta should contribute. This may be a hint at the involvement of resonances in the process. Several candidates for baryon resonances that may couple to $p\omega$ exist, but their decay into this channel is not established. Further measurements, in particular those involving differential observables, can shed light on this question. Such measurements have been and continue to be performed at COSY. While the overall picture is not yet clear, it can be expected that a careful theoretical analysis of the full data set which by now also includes analyzing powers will become feasible in the near future. Theoretical descriptions of the existing data usually give a better description, in particular for the angular distributions, when resonances are included.

Besides the ω production cross sections, a set of measurements on ϕ production is available. In general it was expected that the ϕ production would be strongly suppressed as compared to the ω production because of their quark content. The so-called OZI rule (named after Okubo, Zweig and Iizuka who predicted a strong suppression of newly produced quark flavors in production reactions) suggests that the ϕ contribution in the production should be given by the square of the ϕ/ω mixing ratio of about 4.2 per mille. In this formulation, any deviation from this expectation is viewed as evidence for pre-formed $s\bar{s}$ pairs in the nucleons. Experimentally, the ratio is about one order of magnitude bigger than this naïve expectation. A recent comparison of new differential data for the ω with data for the ϕ finds similar angular distributions in both channels at a given excitation energy, which may point at similar production mechanisms. However, if either channel couples to a resonance close to threshold such a comparison may not yield the simple quark model expectation without any pre-formed strange quark pairs.

Apart from elementary production off the proton, ANKE has measured data on ω production in p-n fusion using deuteron targets. Here, not even the magnitude of the total cross sections has been explained theoretically. Data on the unbound pn final state have not been measured yet. A few measurements in pd fusion, in particular $pd \to {}^3\mathrm{He}\phi$, rather close to threshold were performed in previous years, but a comparison with the ω production is not possible since data are lacking. This channel may be of interest in view of OZI violation, but also since data measured for $pd \to {}^3\mathrm{He}\omega$ at a single spectrometer setting for backward-going mesons indicate a very strong threshold suppression of the cross section.

While theory in vector meson production is lagging behind experiment, the data that have been made available by the COSY experiments, in particular by **ANKE** and **TOF**, have spurred some interest on the side of theory. Understanding elementary neutral vector meson production is an indispensable prerequisite for the interpretation of production data off nuclei, where chiral restoration may manifest itself through changes in the spectral function.

WASA measurements at high energies will provide additional high-statistics measurements of ω production in pp interactions. WASA is particularly suited for the $\omega \to \pi^0\gamma$ decay branch, but also the more abundant $\omega \to \pi^+\pi^-\pi^0$ can be used. This also allows measurements of pd fusion, where comparison of both decay branches will shed light on the origin of the unexplained threshold anomaly.

1.2.4 $^1S_0$ diproton forward production in the $pp \to pp\pi^0$ reaction

Single pion production in nucleon-nucleon collisions, $NN \to NN\pi$, is one of the tools to investigate NN dynamics at intermediate energies. Because of the large momentum transfers involved, even close to threshold, such a meson production process is sensitive to the short-distance part of the NN interaction.

The $pp \to pp\pi^0$ differential cross section has now been measured at **ANKE** for seven proton beam energies T_p between 0.5 and 2.0 GeV at forward angles of the proton pair production $\theta_{pp}^{cm} = 0°–18°$. When proton pairs with excitation energy $E_{pp} < 3$ MeV are selected, these diprotons $\{pp\}_s$ should be in the $^1S_0$ state. This is confirmed in the experiment by the observed E_{pp} spectra and the angular distribution of the protons in the final pp rest frame. Therefore, the reaction $pp \to \{pp\}_s\pi^0$ is the isospin-spin partner of the well known, kinematically analogous process $pp \to d\pi^+$. While the latter has been at the focus of extensive experimental studies for tens of years, for the $pp \to \{pp\}_s\pi^0$ reaction the only published data away from the threshold energy domain were limited to energies $T_p < 0.425$ GeV (CELSIUS).

The ANKE data show a forward dip in the angular distribution of the diprotons for energies $T_p \leq 1.4$ GeV whereas at 2.0 GeV a forward peak is seen. The T_p dependence of the forward cross section reveals a broad peak around 0.6 GeV and a minimum at 1.4 GeV, see Fig. 7. The increase of the cross section at 2.0 GeV together with a drastic change of the angular distribution indicate a transition to a different reaction mechanism at energies where states heavier than the $\Delta(1232)$ are excited.

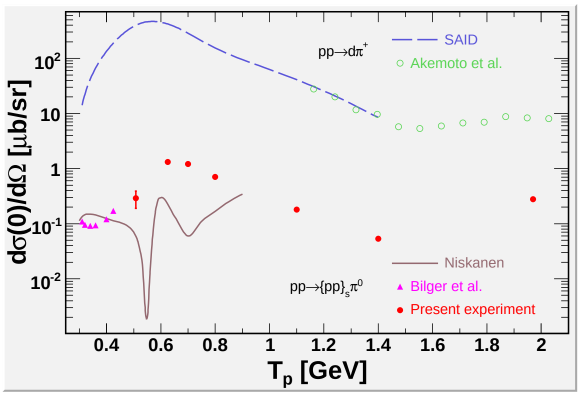

Fig. 7: Energy dependence of the differential cross section for the $pp \to \{pp\}_s\pi^0$ reaction with $E_{pp} < 3$ MeV. The closed circles represent the ANKE results while the triangles show the low energy CELSIUS data. The solid curve corresponds to the prediction from the model of J.A. Niskanen. For comparison the cross section for the $pp \to d\pi^+$ reaction is shown: the dashed curve is the SAID parameterization, the open circles depict the KEK results.

Some of the observed features are similar to those of $pp \to d\pi^+$. However, the ratio of the forward differential cross sections of the two reactions, corrected for different FSI in the relevant nucleon pairs, shows a significant suppression of the single-pion production associated with a spin-singlet final nucleon pair, see Fig. 8. While such a suppression is known and understood in the near-threshold and the $\Delta(1232)$ regions, the observed smallness of the singlet production at higher energies requires further investigations.

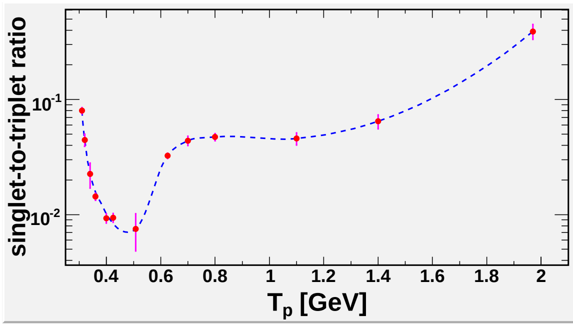

Fig. 8: Ratio of the single-pion production cross sections associated with formation of spin-singlet and spin-triplet nucleon pairs. The curve is to guide the eye.

The obtained data are a part of the ongoing ANKE studies on the $pp \to \{pp\}_s\pi^0$ reaction which includes also measurements of polarization observables. A description of the whole data ensemble will be a significant challenge for theories treating this, one of the simplest, pion-production reaction.

1.2.5 Coalescence and "fireball" processes in non-equilibrium emission of light charged particles from p+Au collisions

A unique data set on the energy and angular dependence of double differential cross sections $d^2\sigma/d\Omega dE$ was measured and recently published by the **PISA** collaboration for $p, d, t, {}^{3,4,6}$He, ^{6,7,8,9}Li, ^{7,9,10}Be, and ^{10,11,12}B produced in collisions of 1.2, 1.9 and 2.5 GeV p+Au target.

The double differential cross sections for light charged particles were analysed in the frame of the microscopic model of intranuclear cascade with coalescence of nucleons (INCL4.3 model) and statistical model (GEM2) for evaporation of particles from excited residual nuclei. It is observed that energy and angular dependencies of data do not agree satisfactorily with either predictions of microscopic intranuclear cascade calculations for protons, or with coalescence calculations for other light charged particles.

The phenomenological inclusion of another reaction mechanism — emission of light charged particles from a "fireball", *i.e.*, fast and hot moving source — combined with the microscopic model calculations of intranuclear cascade, coalescence INCL4.3 and evaporation GEM2 of particles leads to very good description of the data, as is shown for example for deuteron emission in Fig.9.

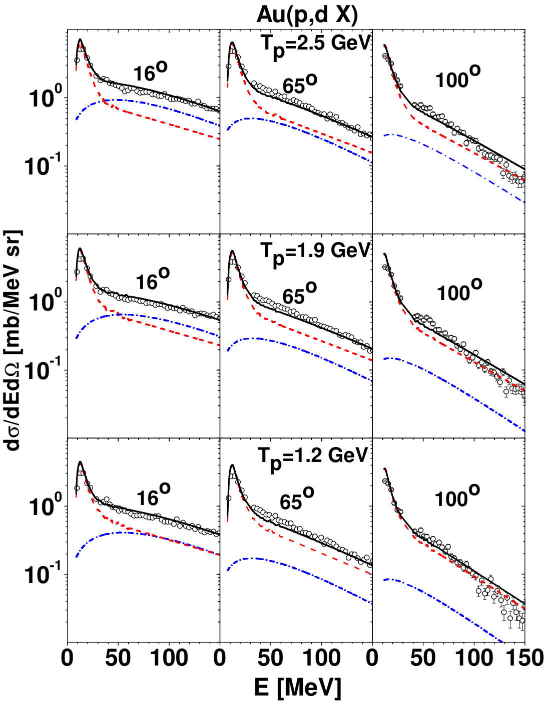

Fig. 9: Open circles represent experimental energy spectra of protons measured at 16°, 65°, and 100° for three proton beam energies. Dot-dashed lines present the contribution of deuteron emission from the "fireball", the dashed lines show INCL4.3+GEM2 calculations. The solid lines show sum of all these contributions.

A new result of the present work is the observation of non-equilibrium emission of LCP's and IMF's mediated by two competing mechanisms: surface coalescence of outgoing nucleons and the contribution from a mechanism similar to a fast break up of the target nucleus leading to three moving sources appearing as result of the break up. The need to introduce the presence of a "fireball" contribution seems to indicate that the lack of correlation between nucleons, which is inherent to intranuclear cascade models, leads to oversimplified microscopic description of the reaction mechanism. A detailed discussion on the "fireballs" characteristics, its velocity, apparent temperature, production cross section and the number of nucleons it is built of has recently been published by the PISA collaboration.

The present investigations allowed to find the beam energy variation of the contribution of non-equilibrium processes to the studied emission of LCP's. It was found that the non-equilibrium processes are very important for production of light charged particles. They exhaust 40 – 80% of the total cross sections — depending on the emitted particles. Coalescence and "fireball" emission give comparable contributions to the cross sections with exception

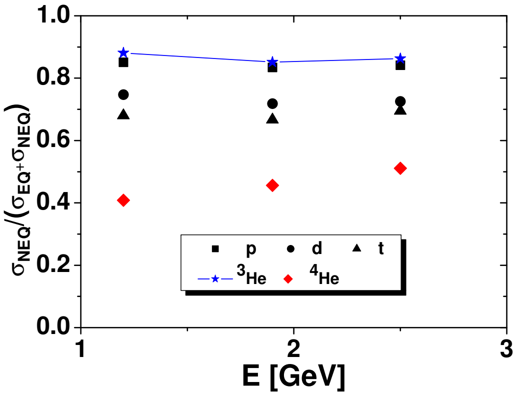

Fig. 10: Ratio of non-equilibrium processes (coalescence&"fireball") to total cross sections (non-equilibrium&evaporation) as function of beam energy.

of ^{3}He data where coalescence dominates. The ratio of sum of all non-equilibrium processes to those proceeding through stage of statistical equilibrium does almost not change in the beam energy range from 1.2 to 2.5 GeV for all light charged particles with the exception of the α-particles, where this relative contribution increases by 20% from lowest to highest beam energy as is shown in Fig.10. Such an almost constant fraction of the contribution of non-equilibrium processes seems to be rather unexpected in view of strong increase of the total production cross sections in the studied broad range of beam energies.

To obtain more insight into the reaction mechanism it is necessary to systematically investigate the energy dependence of the reaction processes for various targets. Energy and angular dependences of double differential cross sections for lighter target systems are currently analysed.

1.3 Status of Experimental Facilities

1.3.1 First double-polarization measurements at ANKE

A key feature of the experiments planned at ANKE is the use of polarized beams and targets which allow one to perform double-polarization measurements. The focus is on the study of three-body final states with the aim of extracting basic spin-dependent two-body scattering information close to threshold. Since summer 2005 ANKE can be equipped with a Polarized Internal Target (PIT) located between the dipole magnets D1 and D2 (see Fig. 11).

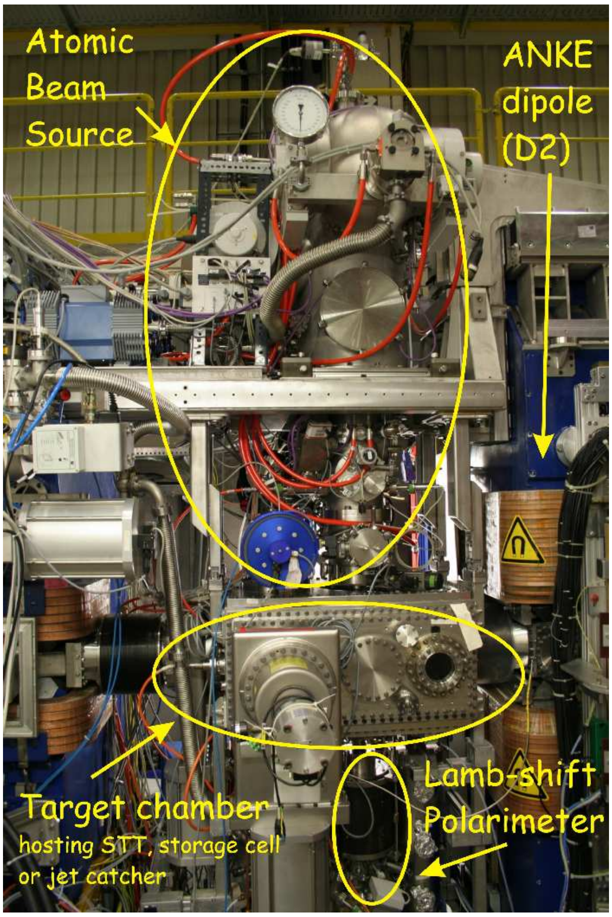

Fig. 11: Photo of ANKE with the Polarized Internal Target (PIT) in front of the spectrometer dipole D2. The main components of the PIT system: Atomic Beam Source (ABS), Lamb-shift Polarimeter (LSP), and the target chamber hosting Storage Cell (SC) together with Silicon Tracking Telescope (STT) system are indicated.

During one week of commissioning experiment in January 2007 allocated to measure the Charge-Exchange break-up of polarized deuterons on a polarized hydrogen target $\vec{d}\vec{p} \to (pp)n$, the following achievements have been made:

- For the first time, studies with the COSY polarized deuteron beam were performed using a storage cell (25 μm aluminum foil, with the inner surface covered by Teflon, of 20×15 mm^2 cross section and 390 mm length). For this purpose the machine group furnished a polarized deuteron beam, electron cooled, stacked at injection and accelerated to T_d=1.2 GeV;

- To improve the COSY beam intensity, a longer stacking injection was implemented. In double-polarized measurements a cycle of 45(50) minutes duration was used: 15(20) minutes for stacking (90(120) stacks separated by 10 s for cooling) and 30 minutes for the flat top. Under these conditions 7×10^9 polarized deuterons were accelerated to the flat-top energy of 1.2 GeV;

- It has been shown that the procedure of scraping the accelerated beam before the data-taking minimized the background events coming from the interactions of the beam halo particles with the cell wall. Even without stochastic cooling (this is not possible at COSY at the beam energy of $T_d = 1.2$ GeV), the achieved beam quality generally allowed the deuterons to pass through the cell without hitting the walls;

- The expected density for the polarized hydrogen ($\vec{\mathrm{H}}$ gas) storage cell target of $d_t = 1.34 \times 10^{13}$ cm^{-2} was achieved. This value, together with the beam intensity of 7×10^9 stored polarized deuterons, led to a luminosity of $L \simeq 1.0 \times 10^{29}$ s^{-1}cm^{-2};

- The clean identification of events for the $\vec{d}\vec{p}$-induced reactions when using a long cell target has been demonstrated. This was done on the basis of experimental information obtained from the $\vec{\mathrm{H}}$ gas target and on the known shape of the background from the cell walls, which is imitated through the use of N_2 gas in the cell. The exact shape of the background under the missing-mass peak from the cell-wall events has been determined in real experimental conditions and was controlled during online measurements;

- Using the missing-mass technique for the measured single- and double-track events in ANKE, it has been shown that very clean identification of the following reactions is possible: $\vec{d}\vec{p} \to dp_{sp}\pi^0$ (both branches of quasi-free $\vec{n}\vec{p} \to d\pi^0$), $\vec{d}\vec{p} \to (pp)n$, $\vec{d}\vec{p} \to {}^3\mathrm{He}\,\pi^0$, and $\vec{d}\vec{p} \to dp$. The last channel was identified unambiguously with very little background (see Fig. 12) by using the silicon detectors, placed close to the storage cell in vacuum target chamber, in coincidence with the forward detector system;

- In parallel to the data taking, the ABS source has been tuned with Lamb-shift Polarimeter (LSP)

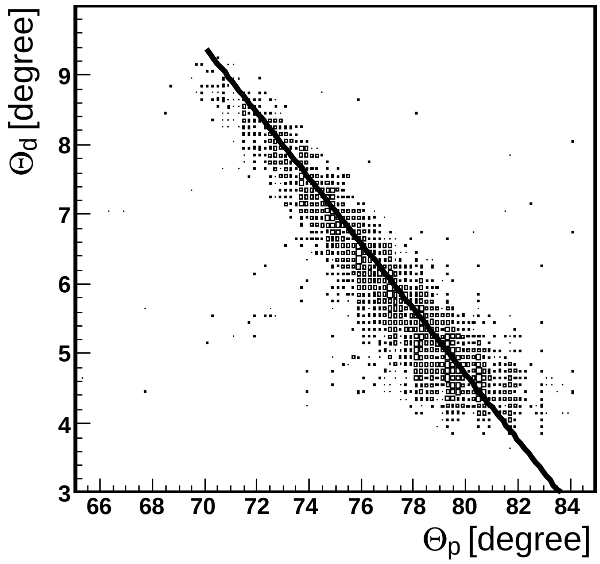

Fig. 12: Angular correlation between the protons and deuterons detected in the STT and forward detector, respectively. The expected kinematical correlation for the dp elastic reaction is shown by the black line.

measurements (see Fig. 13). The goal was to determine the target polarization (Q_y) from the quasi-free $n\vec{p} \to d\pi^0$ reaction (see Fig. 14). The achieved value of average target polarization of $\langle Q_y \rangle = 0.75 \pm 0.06$ is much higher than it was in the first measurements in 2006. Thus, the target polarization has been maximized and the equality of positive and negative polarizations has been verified on the level of a couple of percent by using online measurements from the LSP, repeated every 24 hours;

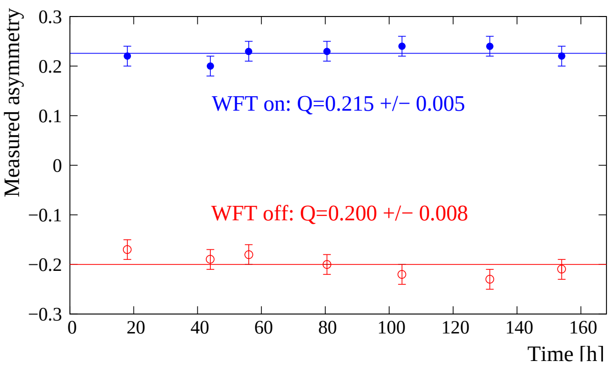

Fig. 13: Online measurements of the Lyman-α peak asymmetry from the LSP when the weak field transition unit (WFT) was switched **on** ('spin-up') and **off** ('spin-down').

- The value of the deuteron beam vector polarization P_z has been extracted from the quasi-free $\vec{n}p \to d\pi^0$ reaction using the angular dependence of the analyzing power of the $\vec{p}p \to d\pi^+$ reaction, which was also used to determine the target polarization. The result, $\langle P_z^{\mathrm{ANKE}} \rangle = 0.60 \pm 0.10$, is compatible with the value of $\langle P_z^{\mathrm{LEP}} \rangle = 0.660 \pm 0.003$, obtained from the Low Energy Polarimetry (LEP) measurements.

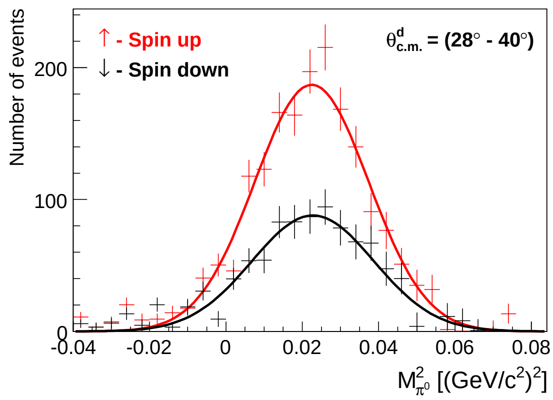

Fig. 14: Angular dependence of the missing-mass squared distribution for the reaction $d\vec{p} \to dp_{sp}X$ measured with the storage cell and 1.2 GeV deuteron beam. Red and black histograms stands, respectively, for data with target polarization 'spin-up' and 'spin-down', after background subtraction using N_2 data.

Given the above successes in the *first* handling of the double-polarized data, it can be concluded that ANKE is ready to embark on the experimental program which includes the double-polarization measurements.

1.3.2 Status of the COSY-TOF Experiment

The analysis of first data on Λ production with polarised protons has been completed, results are obtained for the Λ analysing power and for the spin transfer coefficient at 2.75 and 2.95 GeV/c beam momentum.
A data sample, consisting of more than 320.000 fully reconstructed $pp \to pK^+\Lambda$ events, is now available at a beam momentum of 3.06 GeV/c. The corresponding preliminary Dalitz plot is shown in Fig. 15.
For the first time the analysing power for the two pion production in proton proton interactions was analysed. The evaluation of the analysing power of the reaction $\vec{p}p \to pp\eta$ is in progress, more than 50,000 η events have been analysed.
With installation of a new roots vacuum booster for the COSY-TOF vacuum tank the pumping capacity was increased by a factor of four. Together with the increased vacuum tube cross section this assures a pressure of lower than $3 \cdot 10^{-3}$ mbar, which is needed for the operation of the straw tube tracker inside the tank. More than 3000 signal lines, high-voltage cables, and gas tubes have to be fed into the vacuum for this internal operation. For this

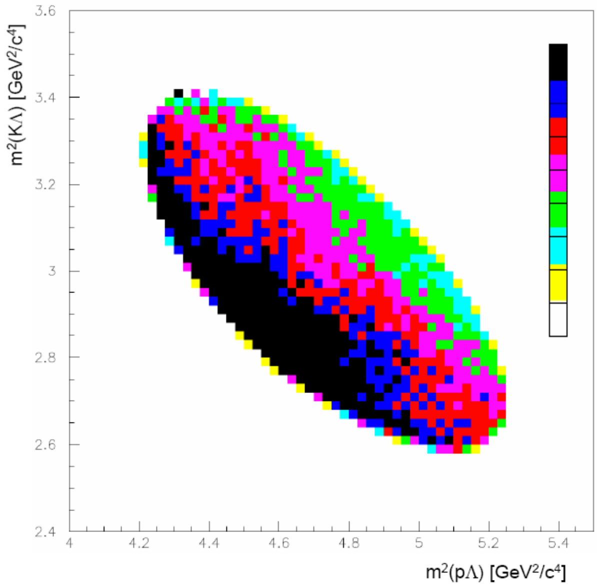

Fig. 15: Preliminary Dalitz plot of the reaction $pp \to pK^+\Lambda$ for a beam momentum of 3.06 GeV/c. The sample contains about 320,000 events covering the full phase space.

task a hexagonal shaped vacuum vessel was constructed, which will be installed between the tank and the tube to connect the tank to the pumping station (see Fig. 16). This vessel was fabricated in the ZAT workshops.

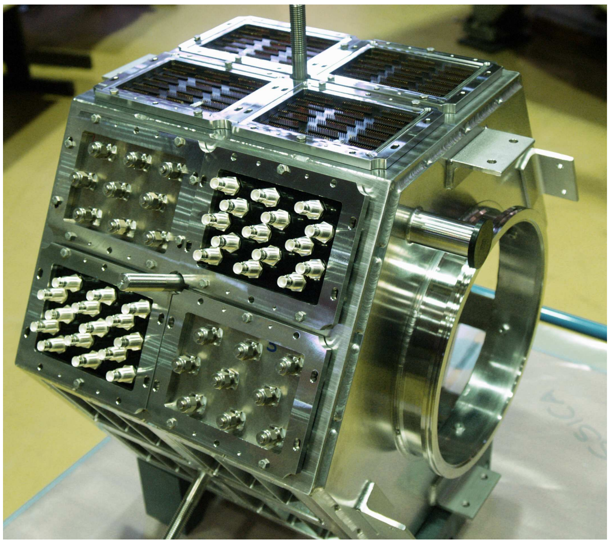

Fig. 16: The hexagonal vacuum vessel, which allows for the lead through of more than 3000 signal lines, high-voltage cables, and gas tubes.

1.3.3 First Experiments with the WASA Detector

The installation of a new Forward Window Counter (FWC) allowing for runs at higher luminosities, the data acquisition system reaching its design goal of $\approx 20\,\mu s$ dead-time per event already during the first production run, the production of extremely stable working nozzles for pellet target operation, and a pellet target uptime for operation with deuterium of more than 84 % mark the technical milestones reached during the past year.

In April and May 2007, WASA-at-COSY has started its physics program with first data on the isospin violating $\eta \to 3\pi^0$ decay and dedicated experiments using deuterium pellets. η mesons have been produced in the reaction $pp \to pp\eta$ at a kinetic energy of $T_p = 1400\,\mathrm{MeV}$ and are tagged via the missing mass with respect to two protons identified in the Forward Detector. The $3\pi^0$ channel is identified from the subsequent $\pi^0 \to \gamma\gamma$ decay, *i.e.* the three π^0 are reconstructed from a 6γ final state. Experimental data are shown in Fig. 17 in a symmetrized Dalitz plot, with a background contribution from non-resonant $3\pi^0$ production estimated to be less than 10 %. Transformation to a one-dimensional distribution in terms of the density of events as a function of the radial distance from the centre of the Dalitz plot allows the extraction of the slope parameter α in the linear parameterization $\left|A(\eta \to 3\pi^0)\right|^2 \approx 1 + 2\alpha z$ of the decay amplitude (Fig. 17.

So far, only every second data file has been analyzed, and the total estimated statistics of ≈ 120 k events for the final Dalitz plot corresponds to about five days of data taking. After initial calibration and trigger optimization the time available for the measurement was limited by longer breaks in data taking due to several exchanges of the pellet target nozzle towards the end of this first run. This continuous nozzle blocking was identified after summer with the help of the infrastructure established for glass nozzle manufacturing in the Central Department of Technology (ZAT) to be due to debris from sinter filters at the gas input side of the nozzle. This material problem was eventually solved prior to the production runs in the second half of 2007, with nozzles now showing lifetimes in the range of at least several months.

The ABC effect denotes an unexpected isoscalar enhancement at low $\pi\pi$ invariant masses observed in two pion production experiments leading to a bound nuclear system in the final state. The effect has been interpreted as $\Delta\Delta$ excitation, but conventional calculations giving a good description of inclusive data fail to reproduce the strength of the effect seen in recent exclusive data obtained at the CELSIUS/WASA facility. In inclusive data, the ABC effect appears to be largest in the double-pionic fusion of deuterium to ^{4}He.

In December 2007, the reaction $dd \to {}^4\mathrm{He}\,\pi\pi$ has been measured exclusively with the WASA-at-COSY setup at nine different kinetic beam energies between $T_d = 800\,\mathrm{MeV}$ and $T_d = 1400\,\mathrm{MeV}$ corresponding to excess energies between 135 and 400 MeV with respect to the $2\pi^0$ threshold. As an example, Fig. 18 shows the clear identification of He nuclei at $T_d = 1117\,\mathrm{MeV}$ by the ΔE-E technique using the information from the first two layers of the Forward Range Hodoscope FRHa (ΔE) and

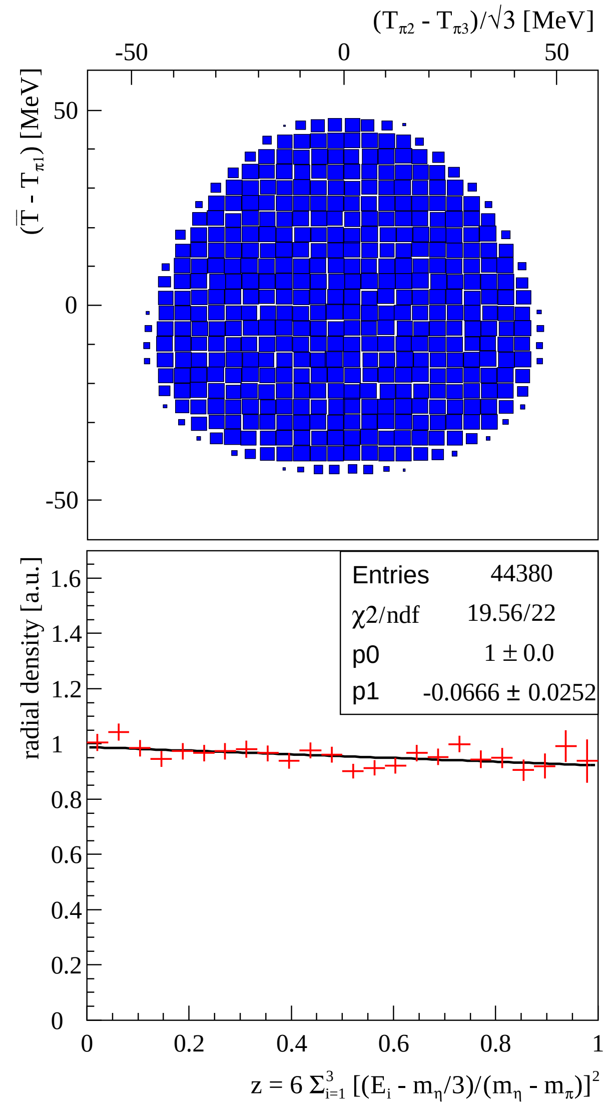

Fig. 17: Efficiency corrected symmetrized Dalitz plot of the $\eta \to 3\pi^0$ decay from WASA-at-COSY data (top) and radial density distribution for the extraction of the slope parameter α (bottom).

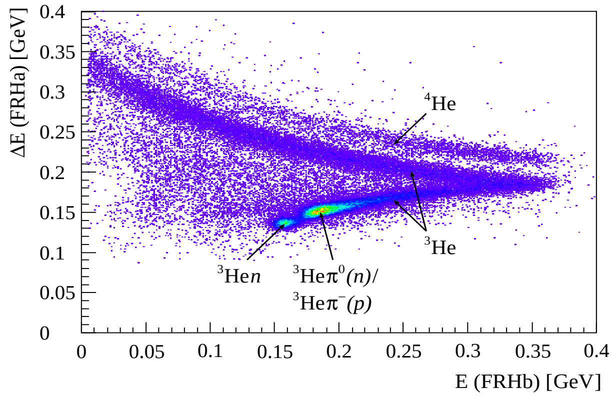

Fig. 18: ΔE-E plot from the first two FRH layers FRHa and FRHb at $T_d = 1117$ MeV. Bands for ^{3}He and ^{4}He are clearly separated. Structures for fast ^{3}He correspond to the binary $dd \to {}^3\mathrm{He}\,n$ breakup channel and quasi-free single pion production.

FRHb (E). Background from fast breakup protons and other minimum ionizing particles is completely removed already at trigger level by choosing appropriate thresholds for the upgraded FWC and the first FRH layer. For most of the energy range covered within this experiment, this allows to trigger on the He tagging system only, avoiding any trigger condition on the 2π system in the Central Detector and thus any trigger systematical effects on a direct comparison of $\pi^0\pi^0$ and $\pi^+\pi^-$ final states.

In Fig. 18 bands for ^{3}He and ^{4}He are clearly separated. For fast ^{3}He nuclei that are not stopped in FRHb, the two distinct enhancements can be identified with the breakup reaction $dd \to {}^3\mathrm{He}\,n$ and quasi-free single pion production via $nd\,(p)_{spec} \to {}^3\mathrm{He}\,\pi^-\,(p)_{spec}$ and $pd\,(n)_{spec} \to {}^3\mathrm{He}\,\pi^0\,(n)_{spec}$, respectively. Qualitatively, the ABC effect can already be read off the density variation along the ^{4}He band: The increase in events towards fast ^{4}He stopped in FRHb implies an enhancement for events with small $\pi\pi$ invariant masses. Slow ^{4}He nuclei — corresponding to large $\pi\pi$ masses — that are stopped already in FRHa are not contained in Fig. 18, but can be identified using the ΔE and E signals from the upgraded FWC and FRHa, respectively.

From the integrated running time of ≈ 36 hours at $T_d = 1117$ MeV a total statistics of roughly 4k fully identified $^4\mathrm{He}\,\pi^0\,\pi^0 \to {}^4\mathrm{He}\,(\gamma\gamma)\,(\gamma\gamma)$ events is expected for this beam energy, and statistics for the other beam energy settings are estimated to be similar.

One of the flagship experiments for WASA-at-COSY is a measurement of the reaction $dd \to {}^4\mathrm{He}\,\pi^0$ to extract the p-wave contribution to the Charge Symmetry (CS) breaking amplitude. The p-wave contribution being sensitive to the charge dependence of the πNN coupling constant has been identified as one of the crucial input parameters for a further consistent effective field theory analysis of the CS breaking mechanism both in the $dd \to {}^4\mathrm{He}\,\pi^0$ signal and in the $np \to d\,\pi^0$ forward-backward asymmetry, and can presently only be measured at COSY. The dd initial state interaction is the most uncertain part in theoretical calculations and can be constrained from measurements of CS conserving breakup reactions like $dd \to {}^3\mathrm{He}\,n\,\pi^0$ or $dd \to {}^3\mathrm{He}\,p\,\pi^-$, where the transition operator can be calculated from known amplitudes within Chiral Perturbation Theory (ChPT).

At the WASA facility, in a first step the breakup reaction $dd \to {}^3\mathrm{He}\,n\,\pi^0$ has been measured at a beam momentum of $p_d = 1.2$ GeV/c ($T_d = 351$ MeV) to provide information on the initial state interaction and to study the experimental (background) conditions for a later production run on the CS breaking channel with a cross section in the range of ≈ 100 pb. Experimentally, the reactions $dd \to {}^3\mathrm{He}\,n\,\pi^0$ and $dd \to {}^4\mathrm{He}\,\pi^0$ are identified by detecting recoil He nuclei from the energy loss informa-

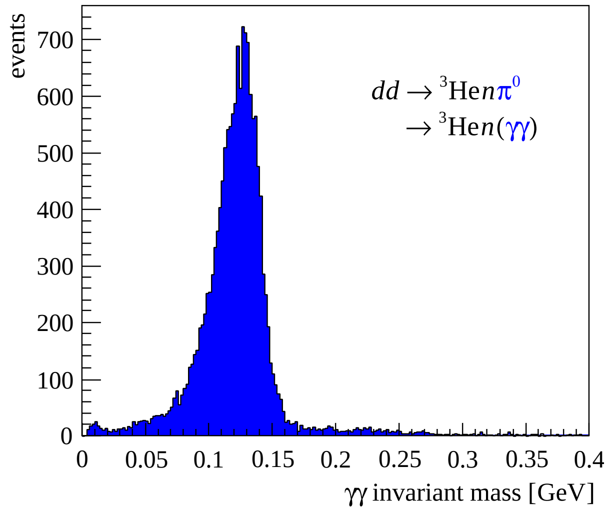

Fig. 19: $\gamma\gamma$ invariant mass for events with ^{3}He nuclei identified from the energy loss information in the WASA Forward Detector from approximately seven hours of data taking at $T_d = 351$ MeV, corresponding to the reaction $dd \to {}^3\text{He}\, n\, \pi^0$.

tion in the Forward Detector (as shown for higher energies in Fig. 18) in coincidence with the $\pi^0 \to \gamma\gamma$ decay. After He identification, eliminating contributions from $dd \to t\, p\, \pi^0$, the reaction $dd \to {}^3\text{He}\, n\, \pi^0$ is — with CS violating π^0 production suppressed by four orders of magnitude — the only source of π^0 in this energy range and the reconstructed $\gamma\gamma$ invariant mass (Fig. 19) shows the unambiguous background free identification of the CS conserving channel.

During the first half of 2008, a dedicated experiment to study η decays involving the anomalies of the QCD Lagrangian, *i.e.* decays with either two (virtual) photons ($\eta \to \gamma^*\gamma^* \to e^+e^-e^+e^-$) or one (virtual) photon and a $\pi^+\pi^-$ pair ($\eta \to \pi^+\pi^-\gamma^* \to \pi^+\pi^-e^+e^-$), has already been scheduled. The experiment aims at extracting precise branching ratios and γ^* invariant mass distributions from an anticipated statistics of few times 10^2 and 10^4 events, respectively, which can be compared to ChPT predictions.

Based on the experience from the measurement of the CS conserving $dd \to {}^3\text{He}\, n\, \pi^0$ channel, a first production run on $dd \to {}^4\text{He}\, \pi^0$ at high luminosities in the order of $10^{32}\,\text{cm}^{-2}\text{s}^{-1}$ is being prepared for a later stage in 2008.

1.3.4 Preparations for Spin-Filtering Studies at COSY and AD

The high physics potential of experiments with stored high-energy polarized antiprotons led to the PAX proposal for the High Energy Storage Ring (HESR) of the FAIR facility. It is proposed to polarize a stored antiproton beam by spin filtering with a polarized hydrogen (deuterium) gas target. The feasibility of spin filtering has been demonstrated in the FILTEX experiment at TSR (Heidelberg) in the 1990's but the theoretical understanding is controversial. In order to clarify this situation several experimental studies with protons (at COSY) as well as with antiprotons (at AD/CERN) have to be carried out. These investigations require an experimental set-up of a polarized internal gas target (PIT) with a system of Silicon detectors implemented into a large acceptance section of the magnetic lattice (Fig. 20).

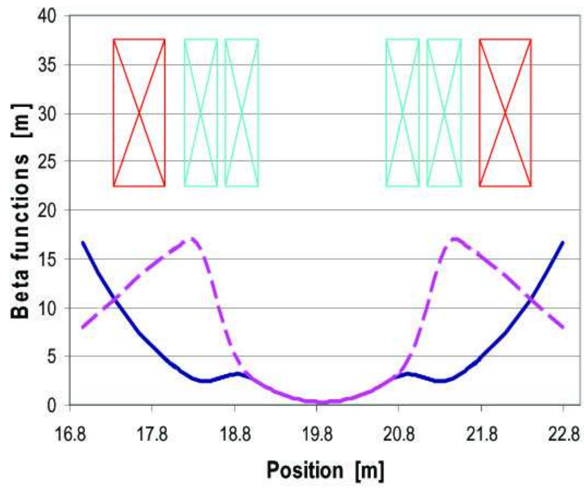

Fig. 20: The geometry of the low-β (large acceptance) section around the target at COSY. The storage cell (see below) will be located in the center between the four additionally needed magnets. The lines denote the vertical (dashed line) and horizontal (solid line) beta function, proportional to the size of the beam.

For longitudinal spin filtering at COSY the solenoids of WASA and the electron cooler can be used as a Siberian snake, but for the AD, an additional snake is required.

The former HERMES polarized atomic beam source was set up in Jülich with a modified vacuum system, mounted on a new support (Fig. 21). It was completely refurbished to allow a fast assembly and disassembly at COSY and AD. Making use of the earlier experience in the development of the control system for the polarized internal gas target for ANKE/COSY, the control system was renewed to allow for a full remote control via computer. The vacuum system with the microwave dissociator is operating well.

The HERMES Breit-Rabi polarimeter was rebuilt on a new support structure (Fig. 22). The sextupole magnet configuration was modified and a new strong field transition "Dual Cavity" was designed and built in order to measure the polarization of hydrogen and deuterium.

To reach the necessary areal densities for spin filtering, the use of a storage cell is mandatory. The present cell design (Fig. 23) consists of 5 μm Teflon walls supported by an aluminum frame. Thin walls allow low energy recoil particles to pass through and be detected by the Silicon Tracking Telescopes. The Teflon coating suppresses

Fig. 21: The reassembled polarized atomic beam source on a new support with the analysis chamber (mounted on the lower end) in the laboratory.

Fig. 22: The reassembled Breit-Rabi polarimeter on the new support.

depolarization and recombination of the target gas inside the cell. The vacuum system of the target section comprises two turbo molecular pumps, backed with smaller turbo molecular pumps and a dry fore-vacuum pump. This will ensure that most of the target gas exiting the storage cell is already pumped away in the target chamber. The adjacent chambers containing the magnets of the large acceptance section will be pumped by ion getter pumps. In addition, the cold surfaces of the superconducting magnets are covered with charcoal to use them as cryogenic pumps.

A first set of measurements is planned to be carried out at COSY. They include spin-filtering measurements with an initially unpolarized proton beam and a pure electron-polarized hydrogen target or a pure nuclear-polarized target in a strong holding field to determine the individual polarization buildup effect due to the electrons and nuclei. A second set of measurements is planned at AD/CERN. These will directly investigate the mechanism of the spin filtering process with an antiproton beam.

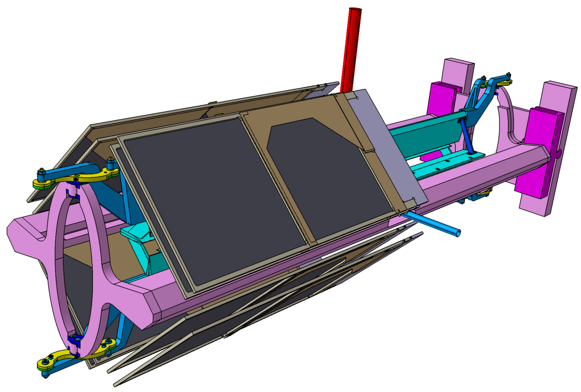

Fig. 23: The openable storage cell with the surrounding silicon detectors.

2 External Experiments

2.1 The ATRAP Experiment at CERN (Physics with Cold Anti-hydrogen)

A long-term goal of the ATRAP experiment at the CERN anti-proton decelerator AD is to confine ground-state $\bar{\mathrm{H}}$ atoms for a test of the CPT invariance by a comparison of hydrogen (H^0) to anti-hydrogen ($\bar{\mathrm{H}}^0$) atom spectroscopy and a measurement of the gravitational force on antimatter atoms. For the confinement of neutral antihydrogen atoms magnetic gradient fields have to be used like a Ioffe trap consisting of a magnetic quadrupole for radial and solenoids for axial trapping. The challenge is that the radial Ioffe field, overlaying the nested Penning trap (see Fig. 24) destroys the symmetry that guarantees stable confinement of the charged particle clouds $\bar{p}$ and e^+ needed to produce $\bar{\mathrm{H}}$ atoms.

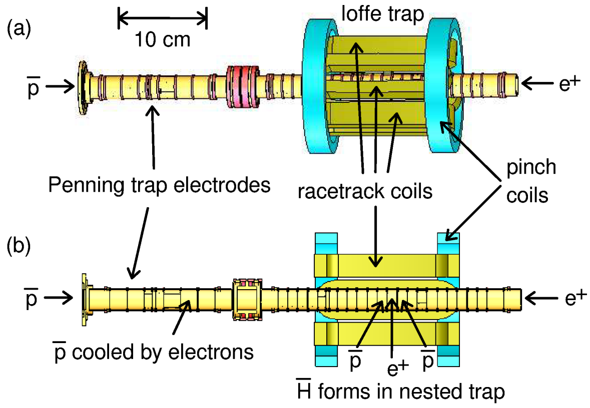

Fig. 24: Outside (a) and cross section (b) view of the ring electrodes from the Penning trap, overlayed by the quadrupole Ioffe trap.

ATRAP settled the controversial discussion whether charged particle clouds would remain confined long enough to form $\bar{\mathrm{H}}$ atoms by demonstrating long-time confinement of $\bar{p}$, e^- and e^+ within a quadrupole Ioffe trap. The production of antihydrogen atoms within this combined Penning-Ioffe trap was achieved. In fact even more $\bar{\mathrm{H}}$ atoms were detected with than without a Ioffe field. Figure 25 shows the potential structure created by the black ring electrodes (E2…E9) with the well depth contours (a) for ground-state $\bar{\mathrm{H}}$ atoms in the Ioffe trap. On-axis Potential wells seen by charged particles during (red) and after (green) $\bar{\mathrm{H}}$ production are displayed in part (b) of the figure together (d)–(f) with the corresponding equipotentials for these two cases. Magnetic field lines (blue) which are parallel to the trap axis with no Ioffe field (e) are significantly redirected (c) when the Ioffe field is added (d) and (f). Currents of 80 A in the pinch coils and 69 A in the bars of the racetrack coils increase the bias field to $B_0 = 2.2$ T, producing 375 mK radial and axial well depths for ground-state $\bar{\mathrm{H}}$ atoms, an axial gradient of $\beta = 93$ T/m, and a radial-to axial ratio $\beta R/B_0 = 0.78$ at the trap electrodes. The superconducting trap was realized with multi-strand NbTi wire wound on Ti forms, with close-fitting Ti parts and Al bands containing strong outward forces. The Ioffe trap has been designed by the ZAT of the FZJ and constructed in cooperation with the ZAT and ACCEL.

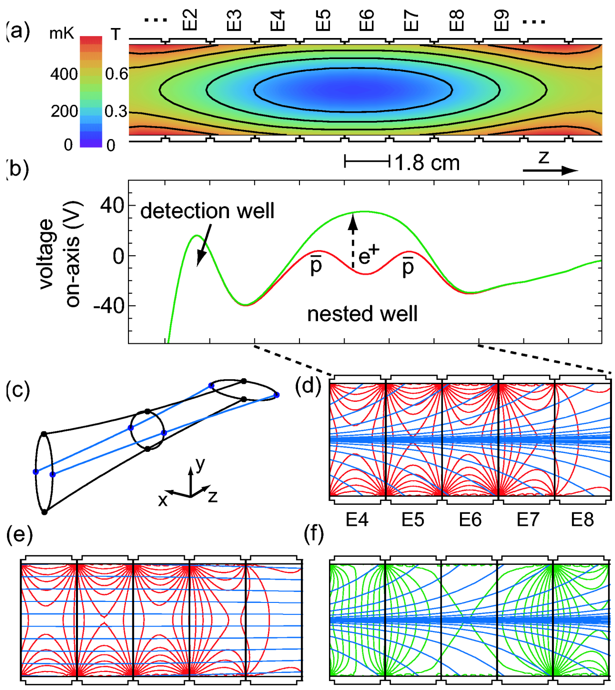

Fig. 25: Well depth and field distributions in the electrodes.

A typical measurement started with 10 min for calibrating the number of e^+ captured in the trap, followed by 10 min for accumulating and cooling 150 million e^- to be used for efficiently capturing e^+, and 400 million e^- for cooling $\bar{p}$. During the next 15 min simultaneously about 0.5 million $\bar{p}$ and 60 million e^+ are trapped and cooled. The $\bar{p}$ and e^+ are transferred adiabatically from the place where they are initially captured and cooled to the electrodes near the center of the de-energized quadrupole Ioffe trap. The $\bar{p}$ are injected into the nested trap, the $\bar{\mathrm{H}}$ atoms that form as the e^+ initially cool the $\bar{p}$ are discarded, and the scintillating detectors record how many $\bar{p}$ are lost. After the Ioffe trap is now ramped up in 14 min, a detection well (see Fig. 25b) is created. The $\bar{p}$ and e^+ interact during the next 10 min where the depth of the central e^+ well in the nested Penning trap is lowered to form $\bar{\mathrm{H}}$ atoms. Thereafter the Ioffe field is ramped down in 1 min. The $\bar{p}$ in the interaction region leave now as the depth of the green well in Fig. 25b is reduced and finally the detection well depth is zeroed so that the $\bar{p}$ within leave to annihilate and be counted. Figure 26a shows the normalized number of $\bar{\mathrm{H}}$ atoms ionized in the detection well as a function of the depth of the Ioffe trap. This number initially decreases with increasing Ioffe trap depth, but is actually enhanced when the quadrupole Ioffe trap gets deeper than 300 mK.

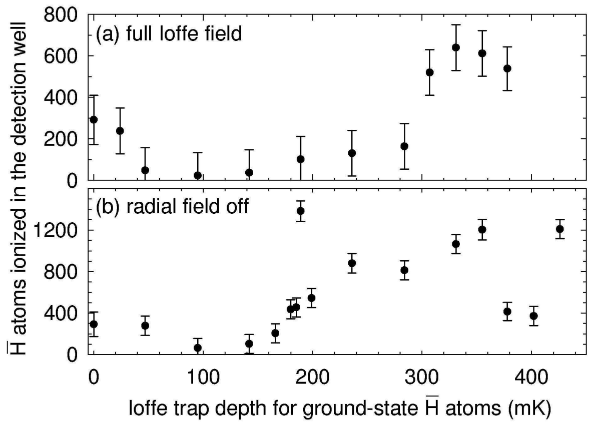

Fig. 26: Detected H̄ atoms *vs.* its depth, for (a) a complete Ioffe trap and (b) only pinch coils being energized.

To probe the effect of an adiabatic increase in the bias field the measurements were repeated without a radial Ioffe field. The H̄ production is overall larger as is demonstrated in Fig. 26b. The reproducible spiking features at 200 mK and near 400 mK require further studies, perhaps being due to collective excitations of an adiabatically heated e^+ plasma that enhance or inhibit $\bar{p}$ loss and the H̄ number that is detected. Summarizing, $\bar{\mathrm{H}}^0$ atoms were produced within a quadrupole Ioffe trap that is superimposed upon a short nested Penning trap. More atoms were detected within a strong Ioffe field, assuaging fears that the Ioffe field would prevent the production of $\bar{\mathrm{H}}^0$ atoms. As a next step it should be possible to determine $\bar{\mathrm{H}}^0$ atoms that are trapped within the magnetic quadrupole field and to optimize the production of cold, lowfield-seeking, ground-state $\bar{\mathrm{H}}^0$ atoms for further antimatter investigations.

3 Theoretical Investigations

The IKP theory group studies the strong interactions in their various settings — spanning topics in hadron structure and dynamics, the nuclear many-body problem and high-energy Quantum Chromodynamics (QCD). The main focus is on the formulation and application of effective field theories for precision hadron and nuclear physics based on the symmetries of QCD. Within the virtual institute on “Spin and strong QCD” work focuses on applications for physics at COSY and FAIR phase II. Some of the high-lights of these activities are discussed in the following.

3.1 The neutron-neutron scattering length from the reaction $\gamma d \to \pi^+$nn

A precise knowledge of the neutron-neutron (nn) scattering length a_{nn}, a quantity that characterizes scattering at low energies, is rather important for the understanding of the effects of charge symmetry breaking in nucleon-nucleon forces. Since a direct determination of a_{nn} in a scattering experiment is extremely difficult due to the absence of a free neutron target, the value for a_{nn} can be only extracted from analyses of reactions where there are three particles in the final state, *e.g.* $\pi^- d \to \gamma nn$ or $nd \to pnn$. There is some spread in the results for a_{nn} obtained by the various groups. In particular, two independent analyses of the reaction $nd \to pnn$ yielded significantly different values for a_{nn}, namely $a_{nn} = -16.1 \pm 0.4$ fm and $a_{nn} = -18.7 \pm 0.6$ fm, whereas the latest value obtained from the reaction $\pi^- d \to \gamma nn$ is $a_{nn} = -18.5 \pm 0.3$ fm. At the same time, for the proton-proton scattering length, which is directly accessible, a very recent analysis reports $a_{pp} = -17.3 \pm 0.4$ fm, after appropriately correcting for electromagnetic effects. This means that even the sign of $\Delta_a = a_{pp} - a_{nn}$ is not fixed. We examined the possibility to determine a_{nn} from yet another reaction, namely $\gamma d \to \pi^+ nn$. Thereby we utilize the tools provided by chiral perturbation theory. We showed that one can extract the value of a_{nn} reliably from this reaction by fitting the shape of a properly chosen momentum spectrum. In this case the main source of inaccuracies, caused by uncertainties in the single-nucleon photoproduction multipole E_{0+}, is largely suppressed. Furthermore, there is a suppression of the quasi-free pion production at specific angles where then the extraction of a_{nn} can be done with minimal theoretical uncertainty. Indeed we found that this uncertainty can be as low as 0.1 fm. Specific results are presented in Fig. 27 where we display the five-fold differential cross section for $\gamma d \to \pi^+ nn$ at the excess energy $Q = 4.65$ MeV ($\Delta E_\gamma = 5$ MeV) as a function of the relative momentum between the two neutrons, p_r. The dashed lines correspond to a polar angle θ_r of the two neutrons of 0°. Obviously in this configuration the quasi-free peak (at the upper end of the spectrum) is rather pronounced. On the other hand for $\theta_r = 90°$ (solid lines) the contribution from the quasi-free production is practically

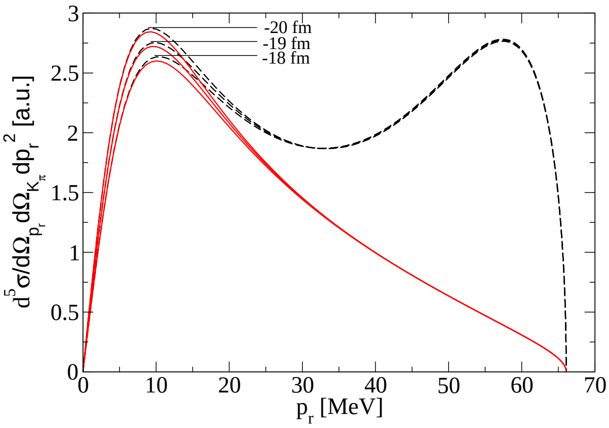

Fig. 27: Sensitivity of the differential cross section for the reaction $\gamma d \to \pi^+ nn$ to the nn scattering length a_{nn}. The solid and dashed lines correspond to the angular configurations with $\theta_r = 90°$ and $\theta_r = 0°$, respectively. The different values of a_{nn} used are specified in the figure.

absent. From the variations in a_{nn} one can see the sensitivity of the considered observable to the nn scattering lengths.

3.2 Delta isobar contribution to the two-nucleon force

Much work has been devoted over the last decade to understand the structure of the nuclear force within the framework of chiral effective field theory (EFT). Most of the studies are carried out based on effective Lagrangian for pions and nucleons chirally coupled to external sources. The resulting chiral expansion for e.g. the two-nucleon force exhibits a somewhat unnatural convergence pattern. For example, by far the most important two-pion exchange (TPE) contribution is the subleading one which arises at next-to-next-to-leading order (N^{2}LO) in the chiral expansion. A similar pattern is also observed for three-pion exchange and the charge-symmetry-breaking TPE potentials. This can be traced back to the large values of the dimension-two low-energy constants (LECs) $c_{3,4}$ which are well understood in terms of resonance saturation. In particular, the Δ-isobar provides the dominant (significant) contribution to c_3 (c_4). Given its low excitation energy, $m_\Delta - m_N = 293$ MeV, and strong coupling to the πN system, one can expect that the explicit inclusion of Δ in EFT utilizing the so-called small scale expansion (SSE) will allow to resum a certain class of important contributions and improve the convergence as compared to the delta-less theory. The dominant contribution to the TPE nucleon-nucleon (NN) potential due to intermediate Δ excitation arises at next-to-leading order in the SSE and was already considered in the literature. We worked out the first corrections which arise at N^{2}LO from triangle, box and crossed-box diagrams with one insertion of the subleading $\pi\pi NN$ or $\pi N\Delta$ interactions proportional to LECs c_i and the combination $b_3 + b_8$, respectively. Notice that the Δ contribution to the one-pion exchange (OPE) potential and contact interactions up to N^{2}LO can be absorbed into redefinition of the corresponding LECs. The values of the LECs c_i are different in the delta-less and delta-full theories and can be naturally extracted from πN scattering. At subleading order, the determination of c_i from the πN S- and P-wave threshold coefficients yields in the delta-less theory $c_1 = -0.57, c_2 = 2.84, c_3 = -3.87, c_4 = 2.89$, where only central values are given and the units are GeV^{-1}. Including the Δ contributions and utilizing the SU(4)/large-N_c relation between the $\pi N\Delta$ and πNN axial-vector coupling, $h_A = 3g_A/(2\sqrt{2})$, leads to $b_3 + b_8 = 1.40$ GeV^{-1} and $c_1 = -0.57, c_2 = -0.25, c_3 = -0.79, c_4 = 1.33$. As expected, the LECs $c_{2,3,4}$ are strongly reduced in magnitude which results in a much more natural convergence pattern for the TPE potential in the delta-full theory. Contrary to the delta-less theory, the numerically dominant contributions to the central, tensor and spin-spin components of the TPE potential are now generated at NLO with the N^{2}LO contributions yielding typically only modest corrections to the NLO result. The improved convergence is also clearly visible in peripheral NN partial waves which were calculated using the Born approximation and, at this order, are only sensitive to the OPE and TPE potentials, see Fig. 28 for a representative example. On the other hand, the N^{2}LO TPE potential in the delta-less theory is found to provide a surprisingly good approximation to the potential resulting at the same order in the delta-full theory. This indicates that the saturation of the LECs $c_{3,4}$ is the most important effect of the Δ-isobar at the considered order.

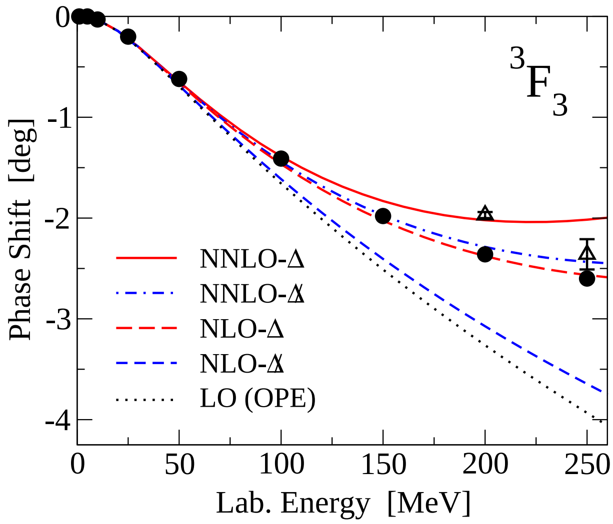

Fig. 28: $^3F_3$ NN phase shift in EFT with and without explicit Δ's calculated in first Born approximation using the spectral-function cutoff 700 MeV. The filled circles (open triangles) depict the results from the Nijmegen (Virginia Tech) PWA.

3.3 Nuclear lattice simulations: From nucleon-nucleon scattering to neutron matter

Lattice QCD has made considerable progress in describing the properties of nucleons and their interactions from first principles. However, so far only two-baryons system could be studied at limited precision. Thus, to explore systematically the influence of the QCD symmetries on the nuclear few- and many-body problem, we have started a long term effort in nuclear lattice simulations. After first simulations of nuclei with $A = 2,3,4$ based on the leading order (LO) effective potential derived from chiral effective field theory gave some promising results, we developed a new method to measure phase shifts in lattice simulations. For doing that, we impose a hard spherical well boundary on the relative separation between the two nucleons at some chosen radius $R_{\rm val}$. The hard spherical well removes extra copies of two-particle interactions due to the periodic boundaries on the lattice. This method is particularly suited to study higher angular momenta and phase shift mixing. It is applicable to any non-relativistic theory of point particles on the lattice and has been proven to work to high accuracy for a toy potential consisting of a central and a tensor interaction. Using the same approach, we have implemented the next-to-leading order chiral EFT two-nucleon potential for momenta up to the pion mass. To assess the model-independence of the simulations, we use two different lattice actions, one with instantaneous one-pion exchange and same-site contact interactions at LO (LO$_1$) and the other with Gaussian-smeared contact interactions (LO$_2$). The contributions from next-to-leading order contact interactions and two-pion exchange are treated perturbatively. For both lattice actions at NLO we find results for the NN phase shifts that are accurate up to corrections expected at higher order. We note that in general the Gaussian-smeared actions LO$_2$ and NLO$_2$ converge faster. In Fig. 29, the phase shifts for singlet and triplet S-waves are shown for the smeared action.

The same lattice action has been used to simulate the ground state of up to 12 neutrons in a periodic cube using Monte Carlo. We have explored the density range of 2% to 8% of normal nuclear matter density. Neutron-rich matter at this density is likely present in the inner crust of neutron stars. Furthermore, the Pauli suppression of three-body forces in dilute neutron matter makes it a good testing ground for chiral EFT applied to many-nucleon systems. Since only isospin $I = 1$ combinations contribute to neutron-neutron scattering, the corresponding 5 low-energy constants have been fixed from the $^1S_0$ and the three triplet P-waves. We have simulated 8, 10, and 12 neutrons on periodic cube lattices with spatial length $L_s = 5,6,7$ lattice units and $L_t \geq 10$ in the temporal direction. The results have converged at $L_s = 7$. In the lower panel of Fig. 29 we show the ground state en-

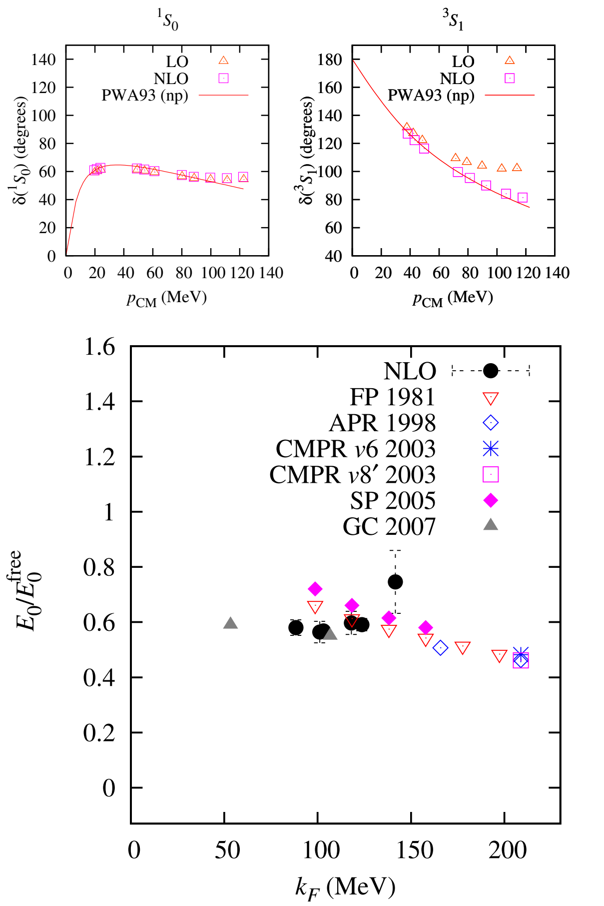

Fig. 29: Upper panel: S-wave phase shifts versus center-of-mass momentum for LO_2 (triangles) and NLO_2 (squares) compared to the Nijmegen partial wave analysis (solid lines). Lower panel: Results for the ground state energy E_0 at NLO (normalized to the free energy $E_o^{\rm free}$) versus the Fermi momentum k_F (black circles with error bars). For comparison, we show results available in the literature based on different methods.

ergy at NLO compared to the energy of a free Fermi gas. The Fermi momentum k_F is related to the neutron density via $k_F = (3\pi^2 N)^{1/3}/L$, with N the number of neutrons and L the length of the box. We find good agreement with earlier calculations based on different methods near $k_F = 120\,\text{MeV}$ but there is disagreement whether the slope is positive or negative. We have also analyzed the expansion about the unitary limit and find significant cancellations between the various triplet P-wave contributions. In the future, we intend to study larger systems of dilute neutron matter and investigate different lattice actions.

3.4 Baryon resonances and Regge phenomenology

Pion photoproduction is one of the premier tools to excite nucleon resonances and to analyze their properties by measuring the final state particles generated through the resonance decay. Especially in the second and third

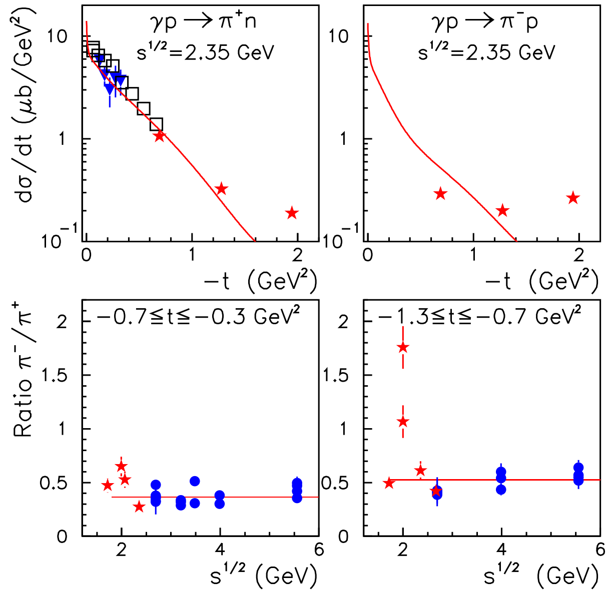

Fig. 30: Differential cross sections for charged pion photoproduction for center-of-mass energy 2.35 GeV as a function of the momentum transfer squared (upper panels) and the ratio of π^- to π^+ production (lower panels) as a function of the center-of mass energy. The squares and crosses show the world data obtained before 1980. The recent Hall A data are given by stars. The solid line represents the new Regge approach.

resonance region, the separation of the often overlapping resonances from the background is a difficult task. As a major step to allow for this separation, a Regge approach to charged pion photoproduction for photon energies above 3 GeV has been developed. The inclusion of both Regge poles and cuts allows to extend the analysis to polarization observables. A global fit of the world data on positive and negative single pion photoproduction at center-of-mass energies $2.6<\sqrt{s}<5.6$ GeV and at four-momentum transfer squared $-t \leq 2$ GeV^2 has been performed and checked by applying the approach to older data at 11 GeV and 16 GeV. The Regge amplitude is then extrapolated to lower energies, where it is expected to fail because of the presence of baryon resonances with narrow widths. Differential cross sections for charged pion photoproduction in the energy range between 1 GeV and 5 GeV have recently been obtained by the Hall A Collaboration at JLab, see the upper panels of Fig. 30.

We find that the Regge extrapolation starts to show deviations from the new data for $-t \leq 2$ GeV^2 at center-of-mass energies below 2.5 GeV. The deviations for π^- production are larger than the ones for π^+ production. The ratio of the differential cross sections of π^- and π^+ production are shown in the lower part of Fig. 30. For small momentum transfers (left panel) the experimental π^- to π^+ ratio remains constant and close to the value found at larger excitation energies. For larger momentum transfers (right

panel), however, a strong deviation of the experimental ratio from the high energy value $1/2$ is observed in the energy range between 1.7 GeV and 2.5 GeV.
Dedicated experiments on photon nucleon reactions in this energy interval may help to decide whether the observed resonance-like structure can be interpreted as a nucleon resonance.

3.5 Towards an understanding of the X(3872) and the X(3875)

In recent years a large number of open and closed charm states above the $\bar{D}D$ threshold, baptized X, Y, Z, were discovered at various accelerators. They all share two features: their properties are in large conflict with the quark model that works very successfully below the $\bar{D}D$ threshold and they are located close to a two-body threshold. Amongst those states the $X(3872)$ plays a special role. Not only because it is seen in many experiments (Belle, Babar, CDF, D0, CLEO-c), reactions (B decays, $\bar{p}p$), and with different decay channels ($J/\Psi\pi\pi$, $J/\Psi\pi\pi\pi$ (only seen at Belle; not confirmed), $\bar{D}D\pi$, and $\bar{D}D\gamma$), but also because for this state the most differential data exists. The established pole position of the $X(3872)$ is only 0.4 MeV below the $\bar{D}^0D^0$ threshold, but lies 50 to 100 MeV below the corresponding quark state. Therefore very early after its discovery, a molecular nature was proposed for the X, although no consensus exists so far. The situation became even more puzzling, when the data on the decay of the $X(3872)$ into $\bar{D}D\pi$ (and in $\bar{D}D\gamma$) showed a peak at significantly higher energies. The central question is, if this structure is yet another realization of the $X(3872)$, or a new state $X(3875)$. In our work, sketched in Fig. 31, we show that both structures, the one in $J/\psi\pi\pi$ and the one in $\bar{D}D\pi$, can only originate from the $X(3872)$ if it is a virtual state. We also show that the issue on the nature of the $X(3872)$ can be settled unambiguously once data with sufficient resolution and statistics is available — a challenge that can be taken by PANDA, once in operation.
In our analysis we use a generalized Flatté formula that allowed for an inclusion of all near-by thresholds. The data in the $J/\Psi\pi\pi\pi$ channel (so far only seen at Belle) is not of high quality. Thus in our fits we only use the data sets in $J/\Psi\pi\pi$ and $\bar{D}D\pi$. A straightforward combined χ^2 fit to the data always leads to a very bad description of the latter data set. However, since we want to investigate the consequence of taking the enhancement in the $\bar{D}D\pi$ channel seriously, we by hand require in the fit a good description of this channel and then optimized for the other. The best fit result that emerges from this procedure is shown as the solid, red line in Fig. 31. We find that it is only possible to describe both data sets simultaneously, if there is only a single pole that is located on the unphysical sheet, or, said differently, the $X(3872)$ is a virtual state. It is interesting to ask for the possible best fit for a bound state. If we take our best solution and by hand change the parameters such that the singularity moves

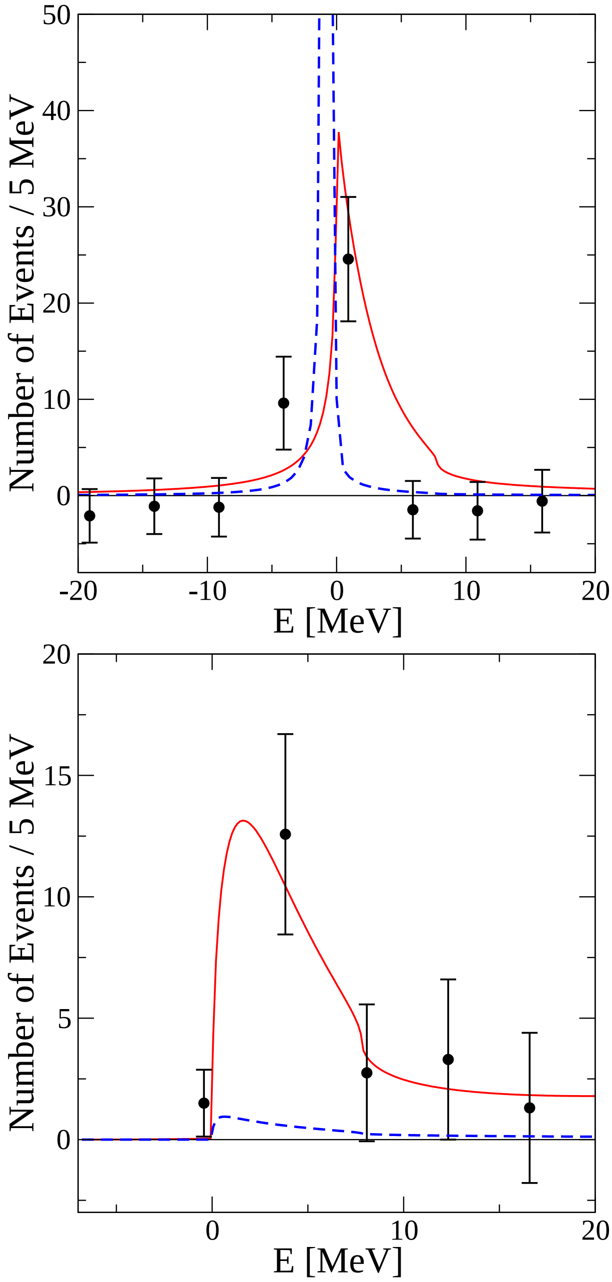

Fig. 31: Upper panel: comparison of our best fit (solid, red curve) to the data in the $J\Psi\pi^+\pi^-$ channel. The data are from Belle. The dashed, blue line is the result, when the pole is moved on the physical sheet. integrated over the given bins. Lower panel: Belle data in the $\bar{D}D\pi$ channel. Lines as above.

from the second to the first sheet while keeping the count rate in the $J/\Psi\pi\pi$ channel fixed, our curves change from the solid, red ones to the dashed, blue ones. Note that, once integrated over the experimental bins, the description of the data in the $J/\Psi\pi\pi$ channel is quite good also for this result, however, there is almost no signal in the $\bar{D}D\pi$ channel. Currently neither statistics nor resolution of the available data allows for a firm conclusion on the nature of the X. However, if the signal in the $\bar{D}D\pi$ channel were confirmed with higher statistics and the $J/\Psi\pi\pi$ signal is measured with higher resolution, an unambiguous determination of the nature of both the $X(3872)$ and the $X(3875)$ will be possible.

3.6 E0 emission in ^{12}C + α fusion at astrophysical energies

The ^{12}C + $\alpha \rightarrow ^{16}$O capture reaction, sometimes called the "Holy Grail" of nuclear astrophysics, determines the ratio of ^{16}O to ^{12}C at the end of helium burning in stars, which is very important for stellar evolution and nucleosynthesis. Nucleosynthesis requires a total S-factor for this reaction of about 170 keV b at a center-of-mass energy $E_{\mathrm{c.m.}} = 0.3$ MeV, the center of the Gamow window. The results of many experiments over more than 3 decades, extrapolated to the Gamow window, show that single-photon emission is dominated by E1 and E2 decay to the ^{16}O ground-state, with approximately equal intensity and a combined S-factor S(0.3) approaching the value quoted above. The corresponding cross sections are $\sigma_{E1}(0.3) \approx \sigma_{E2}(0.3) \approx 1.4 \cdot 10^{-17}$ b.
We examine the possible role of E0 emission, which has not, to our knowledge, been addressed previously. We note that if E0 emission were important, it would have escaped observation in prior ^{12}C + $\alpha \rightarrow ^{16}$O capture measurements, since they were made by detecting the emitted γ-rays, and the e^+e^- pairs produced by E0 emission would not result in a sharp gamma line near the transition energy. In the fusion reaction ^{12}C + $\alpha \rightarrow ^{16}$O$_{\mathrm{g.s.}}$ there are several factors that enhance the relative importance of E0 emission: 1) E0 emission occurs by s-wave capture, whereas E1 and E2 emission arise from p-wave and d-wave capture, respectively; 2) E1 emission is isospin-inhibited; and 3) the rather high transition energy results in larger E0/E1 and E0/E2 phase-space factor ratios. The radial matrix elements are different for E0 and E2 emission since the initial states are different. We have $\sigma_{E0}/\sigma_{E2} = (4\pi/5)(f_{E0}/f_{E2})(|R_{00}^2|/|R_{02}^2|)$, where $R_{l_f l_i}$ is the radial integral of r^2 between the initial continuum state with orbital angular momentum l_i and the final bound state with $l_f = 0$. The functions f_{E0} and f_{E2} are known from QED. We carried out potential model calculations of E0 and E2 emission in ^{12}C + $\alpha \rightarrow ^{16}$O$_{\mathrm{g.s.}}$. Using a Woods-Saxon potential with realistic parameters we obtain the E2 S-factor shown in Fig. 32. This curve is within a factor of 2 of the measured E2 S-factors below E$_{\mathrm{c.m.}} = 2$ MeV, and has $S_{E2}(0.3) = 85$ keV b, in agreement with the value 81 $\pm$ 22 keV b obtained by Hammer *et al.* from an extrapolated R-matrix fit to E2 data (other modern E2 fits that we are aware of yield $S_{E2}(0.3)$ values within a factor of two of these values). Our potential model results for R_{00}^2/R_{02}^2 are also shown in Fig. 32. We obtain a value of 1.1 for the ratio at 0.3 MeV. This may be compared to the value 3.2 calculated with a pure l_i = 0 Coulomb scattering wave, indicating that the interior and exterior contributions to the E0 matrix element interfere destructively. A calculation with $V(l_i = 0)$ = 122.03 MeV, which artificially enhances the contribution of the subthreshold 0_2^+ state by moving it 0.2 MeV closer to threshold, yields a ratio of 2.0 at 0.3 MeV. With R_{00}^2/R_{02}^2 = 1.1, our calculated E0/E2 cross section ratio is 2.6 x 10^{-4}. Taking S$_{E2}$(0.3) = 80 keV b, this corresponds to

$$S_{E0}(0.3) = 0.02 \text{ keV b}. \tag{2}$$

E0 emission to excited final states in ^{16}O is negligible due to the small phase space factor. Hence our best estimate for the E0 contribution to the astrophysical S-factor for ^{12}C + α capture is given by Eq. (2) above. Two-photon emission is also negligible, based on the measured branching ratio for this process in the decay of the 6.05 MeV 0^+ state. We conclude that electromagnetic processes other than single-photon E1 and E2 emission do not contribute significantly to the astrophysical rate for ^{12}C + α fusion.

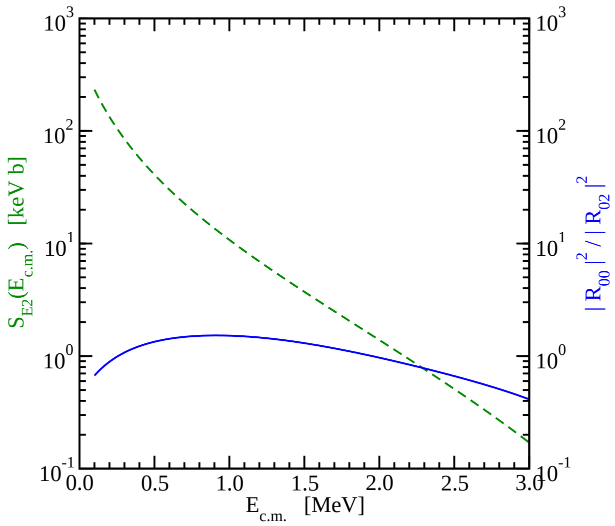

Fig. 32: Dashed curve and left scale: E2 S-factor; solid curve and right scale: E0/E2 radial matrix element ratio, *vs.* $E_{\mathrm{c.m.}}$.

3.7 Central production of the Higgs at the LHC from the nonlinear k-factorization perspective

The central exclusive diffractive production by emission from an exchanged pomeron is being considered as the most promising channel for the experimental observation of a light Higgs particle at LHC. The principal uncertainty in the expected counting rate stems from the poorly understood absorption corrections from multipomeron exchanges. Up to now these corrections were evaluated within phenomenological eikonal absorption models or Reggeon field theory models under ad hoc assumptions on multipomeron couplings. In the latter case, the truncated leading $\log(1/x)$ expansions often run into conflict with the unitarity constraints.
Recently the Cracow-ITEP-Jülich-Landau collaboration has developed a consistent QCD approach to the calcula-

tion of multipomeron effects in which the unitarity constraints are manifestly satisfied at each step of the leading $\log(1/x)$ evolution. The testing ground is an interaction with heavy nuclei. The underlying quantity is a nuclear gluon density defined in terms of a coherent nuclear gluon which is an expansion in the in-vacuum multigluon states. The nonlinear terms in the leading $\log(1/x)$ evolution equation, referred to as the BK equation, do naturally fall into two classes. The multiplication of nuclear pomerons is described by a diffractive triple-pomeron vertex which has the same basic structure as for the in-vacuum pomerons. There is a nice correspondence to Gribov's conjecture on diffraction dissociation as an origin of nuclear shadowing effects. The nonlinear terms of the second class can be viewed as a renormalization of the effective Regge trajectory of the collective nuclear gluon, their specific form is entirely of QCD origin.

The new development is a an extension of this nonlinear equation to the exclusive diffractive production of the Higgs in proton-nucleus collisions. Here the Higgs particle can be emitted from each and every exchanged pomeron. In close analogy to the case collective nuclear gluon density defined through the nuclear color dipole S-matrix, upon the resummation of multiple pomeron exchanges one can define the S-matrix for an emission of the Higgs by a collective nuclear pomeron. What emerges is a linear evolution equation for this S-matrix with the kernel which is a functional of the collective nuclear glue. A manifest unitarity property of this evolution equation is noteworthy. A solution of this equation in conjunction with the BK equation would allow for the first time the QCD based evaluation of the multipomeron exchanges with an explicit inclusion of multiplication of pomerons, the renormalization of the intercepts of the collective nuclear pomeron and the pomeron which emits the Higgs particle. The numerical analysis is in progress.

4 COSY: Operation and Developments

4.1 Overview

As in the years before COSY delivered beam with more than 90% reliability. With 6400 scheduled hours of operation the scheduled beam time could be increased compared to the two years before. The installation and commissioning of the WASA detector after its move from Uppsala to COSY was performed successfully.
SPIN@COSY continued to study the polarization behavior of stored beams of spin-1/2 fermions and spin-1 bosons and how to best accelerate polarized protons to higher energy.
COSY also contributed its expertise in the context of EU projects and assisted the research of outside users for instance by performing irradiations at the cyclotron.
Further details for the High Energy Storage Ring (HESR) have been worked out. The efforts aimed to advance the design of proposed systems and to increase the knowledge base through beam dynamic simulations and investigations. A new normal conducting lattice has been designed and detailed stochastic cooling simulations have been carried out to demonstrate the cooling capabilities in the new lattice.

4.2 Operation of COSY

The overall beam-time statistics is shown in Fig. 33 up to the end of the year 2007. After the two years 2005 and 2006 with long shutdown periods for the disassembly of WASA in Uppsala and its installation at COSY the beam time of COSY could again be increased to more than 6400 hours.

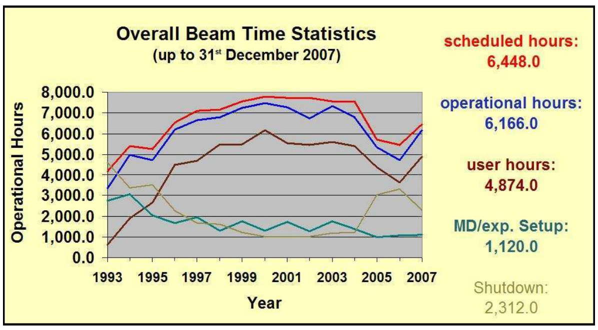

Fig. 33: Beam time statistics over the years since COSY start.

The distribution of required ion species is shown in Fig. 34. More than 40% of the time unpolarized protons were required for the experiments, nearly one third of the beam time were carried out with polarized ions. In this year COSY suffered from a low degree of polarization for protons. The origin of this problem has not been identified within the year 2007 and will be a major topic of investigations in the coming year.

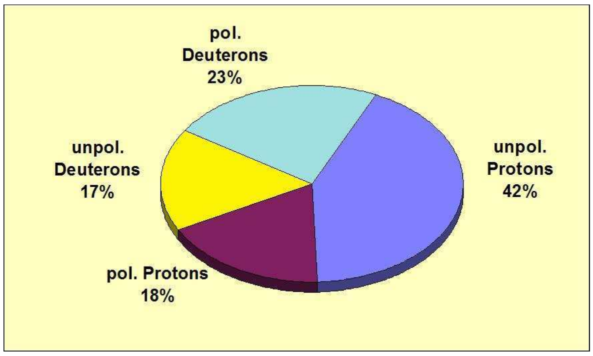

Fig. 34: Ion specific beam-time distribution in 2007.

4.3 Investigation of Spin Manipulation

In the framework of the SPIN@COSY collaboration detailed studies of spin manipulation of stored protons and deuterons have continued during the year 2007. To manipulate the polarization, an rf field is used to excite artificial spin resonances. By changing the frequency of the rf field in a controlled way, partial or full polarization reversals can be achieved. In the past few years, a discrepancy was found between the resonance strength $\varepsilon_{\mathrm{Bdl}}$ calculated from $\int$Bdl of the rf field and that extracted from measurements of the polarization ($\varepsilon_{\mathrm{FS}}$). One possible explanation of these observations is the interference of the induced spin resonance with some nearby intrinsic resonances. To further investigate this effect, a vertically polarized proton beam at 2.1 GeV/c was stored in COSY, and a spin resonance was induced with the transverse rf field of an rf dipole. The rf dipole was operated at an rf voltage, such as 1 kV rms, near a frequency $f_r = 902.6$ kHz giving an rf $\int \mathrm{Bdl} = 0.19 \pm 0.01$ T mm (rms). For different vertical betatron tune (ν_y) values, measurements were made of the vector polarization versus the ramp time; then the dependence of polarization on ramp time was fit to the "Froissart-Stora" formula to extract the resonance strength $\varepsilon_{\mathrm{FS}}$. In Fig. 35 the ratio of $\varepsilon_{\mathrm{FS}}$ to $\varepsilon_{\mathrm{Bdl}}$ is plotted versus the vertical tune ν_y.

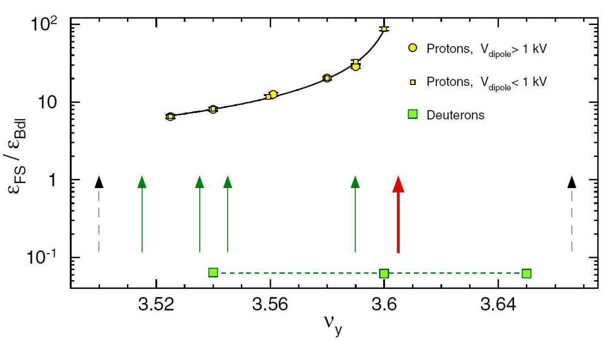

Fig. 35: Ratio of $\varepsilon_{\mathrm{FS}}$ to $\varepsilon_{\mathrm{Bdl}}$ is plotted *vs.* vertical betatron tune ν_y. The betatron beam resonances are shown by the black dashed arrows; the 1st and 3rd order proton spin resonances are shown by the red and green arrows, respectively.

The measured resonance strength strongly depends on the vertical betatron tune of an accelerator. A very large enhancement of the measured resonance strength $\varepsilon_{\rm FS}$ of almost a factor 100 was observed at $\nu_y = 3.605$ near the strongest intrinsic resonance $G\gamma = 8 - \nu_y$. This can be explained by large coherent betatron oscillations, induced by the rf dipole, near the intrinsic resonance. The equation $\varepsilon_{\rm FS}/\varepsilon_{\rm Bdl} = A + B/|\nu_y - Q_{\rm r}|$ was fit to the data to explain the resonance's behavior. This fit yielded the values: $A = 0.44 \pm 0.46$, $B = 0.5 \pm 0.03$ and $Q_{\rm r} = 3.6060 \pm 0.0005$. The measured resonance position $Q_{\rm r}$ is in good agreement with the expected resonance position at $\nu_y = 3.605$. The A value gives the ratio of $\varepsilon_{\rm FS}/\varepsilon_{\rm Bdl}$ at ν_y values far from the intrinsic resonance; however, A had a large uncertainty. The parameter B depends on the detailed properties of the accelerator.

To carry out similar investigations for polarized deuteron beams, a beam with a momentum of 1.85 GeV/c was stored in COSY. The rf dipole was operated at $f_{\rm rf} = 917$ kHz and $V_{\rm rf} = 3.1$ kV rms giving an rms $\int {\rm Bdl} = 0.60 \pm 0.03$ T mm. For COSY's normal vertical betatron tune ν_y around 3.6, no intrinsic resonance was encountered for deuterons (see data in Fig. 35. To investigate the interference between the induced spin resonance and an intrinsic spin resonance for deuterons, the vertical tune was varied over a much larger range. Figure 36b shows a measurement of polarization versus vertical tune ny with the rf dipole off. The intrinsic resonance was located at $\nu_y = 3.795$. Apparently, this was one of the first observations of an intrinsic deuteron resonance in this energy range.

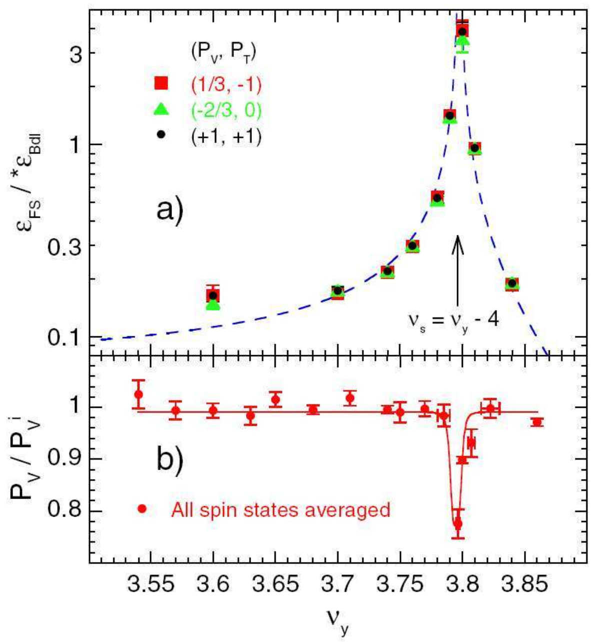

Fig. 36: (a) Ratio of $\varepsilon_{\rm FS}$ to $\star\varepsilon_{\rm Bdl}$ is plotted *vs.* the vertical betatron tune ν_y; Δf was 300 Hz; the cooling was off. (b) Measured deuteron vector polarization ratio at 1.85 GeV/c is plotted *vs.* ν_y; the rf dipole was off, the cooling was on. The red curve is a fit to a 2nd order Lorentzian.

Next the rf dipole was turned on and the resonance strength was measured at different ν_y values; Fig. 36a shows the resulting $\varepsilon_{\rm FS}/\varepsilon_{\rm Bdl}$ ratios plotted versus ν_y. The measured resonance strength ratio increases by almost a factor of 30 close to the intrinsic resonance.

These results show clearly the dependence of the measured resonance strength on the distance from the intrinsic depolarizing resonances in COSY and demonstrate the strong dependence of the rf spin resonance strength on coherent betatron oscillations.

4.4 RF Solenoid

In past years the radial magnetic field of an rf dipole was used to induce artificial spin resonances. In 2007 the rf dipole was replaced by an rf solenoid, which has a longitudinal rf magnetic field. This allowed studies of the previously-discovered deviation of the $\varepsilon_{\rm FS}/\varepsilon_{\rm Bdl}$ ratio from 1 for polarized deuteron beams. This newly installed rf-solenoid magnet was successfully used to spin manipulate polarized deuterons to experimentally test the Chao Matrix Formalism. The data are presented in the next subsection. Figure 37 shows a photo of the rf solenoid after its installation in COSY. It consists of a single-layer water-cooled copper coil wound on two Plexiglas half-pipes. To transfer its rf field to the beam, it was installed around one of COSY's ceramic vacuum pipes, replacing the rf dipole and using its rf power supply. The solenoid's maximum longitudinal rf magnetic field integral is $\int {\rm Bdl}_{\rm rms} = 0.67$ T mm.

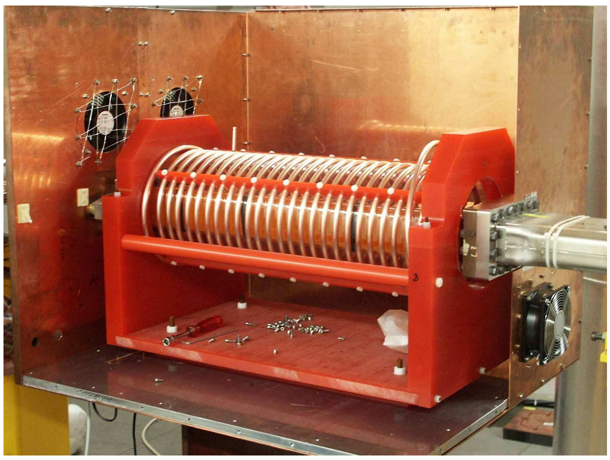

Fig. 37: The water-cooled rf solenoid; its longitudinal rf magnetic field integral is 1.95 T mm peak-to-peak.

4.5 Chao Matrix Formalism

The goal of this experiment was to precisely test a new analytic matrix formalism developed by a theoretical member of the SPIN@COSY team, Alexander Chao of SLAC. The Chao formalism is the first generalization of the famed 1960 Froissart-Stora formula, which al-

lows one to calculate the beam polarization after passing through a spin resonance. However, as Froissart and Stora correctly wrote, their formula is only valid if one measures the initial beam polarization long before crossing the spin resonance and the final beam polarization long after crossing it. As polarized beam hardware and the understanding of spin dynamics improved, polarized beam enthusiasts became eager to learn what happens very near or even inside a spin resonance.
Thus, Michigan PostDoc Vasily Morozov used the Chao formalism to calculate in detail what might happen in a new type of experiment, where a 1 MHz rf magnet's frequency is swept by a fixed range of 400 Hz, while its end-frequency fend is stepped through many different values near and inside spin resonance.
The Chao-Morozov calculations predicted that, if the magnet's resonance strength was not strong enough to fully flip the spin, then there would be large oscillations in the final polarization. These oscillations seem very sensitive to the resonance strength and other parameters, such as the beam's momentum spread $\Delta p/p$, and the resonance's central frequency f_r; thus, the oscillations might provide a new way to precisely measure such parameters.
The data from this new type of experiment showed striking oscillations that agreed very well with these calculations (see Fig. 38). The experiment's data also verified the polarization's extreme sensitivity to the resonance's strength, the resonance's frequency spread (due to the beam-momentum spread), and the resonance's central frequency f_r. Moreover, the data clearly demonstrated that the oscillations' size increased rapidly as the beam-momentum spread decreased.

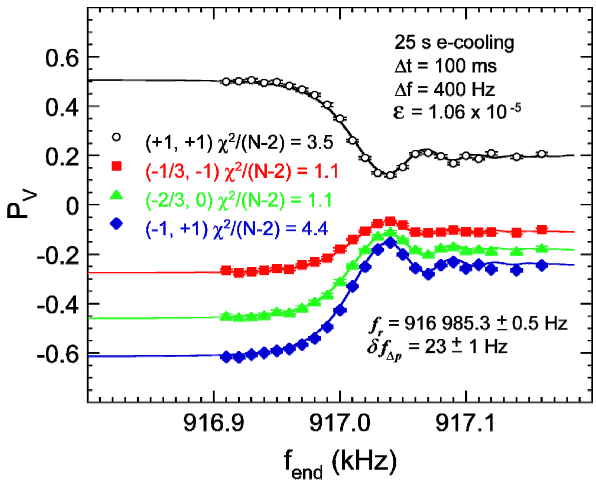

Fig. 38: Vertical vector polarization (P_V) of 1.85 GeV/c stored deuterons plotted vs the end-frequency of the 400 Hz sweep; this and other fits give precise measured values of: resonance strength ($\pm$0.5%), frequency spread ($\pm$1 Hz), and f_r ($\pm$0.00005%).

These new experimental results also confirm the validity of the Chao matrix formalism. Thus, it may now be used to better understand the behaviour of the 100–250 GeV polarized protons stored in Brookhaven's RHIC and perhaps someday polarized antiprotons in FAIR's 15 GeV HESR at GSI, or polarized protons stored in Japan's 30–50 GeV J-PARC or even in CERN's 7 TeV Large Hadron Collider.

4.6 Beam-Energy Calibration

An application of the rf solenoid for the accurate determination of the momentum or kinetic energy of the circulating beam was tested in the last year. The mapping of an induced spin resonance can be used for very accurate determination of the energy of the particle beam. The frequency of the depolarizing resonances induced by an rf solenoid or dipole field solely depend on the kinematical γ factor, *i.e.* the momentum (or kinetic energy) of the particle beam via the resonance condition $f_r = f_c(k \pm G\gamma)$, where f_r is the rf solenoid frequency, f_c the circulation frequency, k an integer, and G the gyromagnetic anomaly of the particle. The position of the resonance can be accurately determined by operating the rf-solenoid with fixed amplitude at fixed frequencies around the induced depolarizing resonance for a certain time and measuring the remaining polarization afterwards. Figure 39 shows an example of such a resonance map. The polarization normalized to the initial polarization is plotted versus the frequency of the rf-solenoid, depolarization occurs at the resonance. The mean frequency and its error can be determined from the measured curve via a Gaussian fit and yields a resonance frequency $f_r = (1011.831 \pm 0.001)$ kHz.
In a test experiment in conjunction with an ANKE beam time with deuterons of momentum $p = 3.118$ GeV/c the feasibility of this method was shown. The final analysis of the measured data is under progress and the result will be published soon. The achievable accuracy in momentum will be better than $\Delta p/p = 5 \cdot 10^{-5}$ and is superior to the usual momentum determination from the nominal orbit length and revolution frequency.

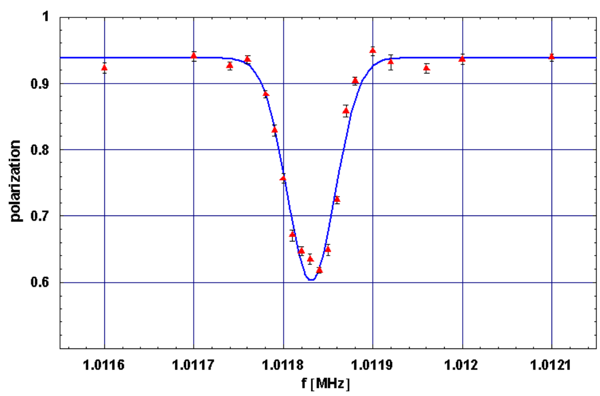

Fig. 39: Example of a measured resonance curve. The plot shows the measured vector polarization versus frequency of the rf-solenoid.

4.7 Beam-Lifetime Studies

Together with the activities for the PAX experiments, an extensive study of beam lifetimes was carried out. The PAX experimental program aims at measurements of polarization build up in an unpolarized proton beam by interaction with a polarized internal storage cell target. As one of the first step in this direction, the depolarization of a polarized proton beam in the presence of an unpolarized internal target, or even only in the presence of the electron beam of the electron cooler, slightly detuned in energy will be studied. All these experimental objectives are expected to work most efficiently at the lowest COSY momenta, where the beam lifetime of the COSY beams will be relatively short. In the past, no experiments where carried through at these low energies, such that the beam lifetime was no subject of optimization. In a first step towards the PAX experimental program, an extensive study of beam lifetimes at injection energy (45 MeV p) was carried out.

Before beam optimization the maximum displacement of the orbit from the reference orbit was ± 18 mm in the horizontal, and ± 7 mm in vertical direction. As the largest transversal acceptance is achieved with minimal displacement of the orbit, the orbit was corrected to ± 5 mm in both planes. After turn on of the electron cooler magnets, where the toroid magnets induce a large deflection of more than 50 mrad, the achievable orbit deviation was ± 12 mm. The transversal acceptance under these conditions was measured to be approximately 30 π mm mrad using a horizontal kicker magnet in COSY with and without storage cell. The storage cell is under these condition not the acceptance limiting aperture in COSY. This agrees with simulation results that for beam displacements of less than 6 mm the storage cell is the limiting aperture, but for larger displacements the COSY vacuum pipe will be the limiting aperture (see Fig. 40). The expected single scattering beam lifetime under these conditions is 5400 seconds.

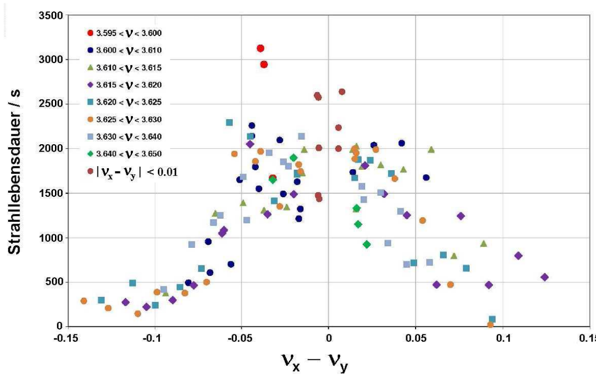

Fig. 40: Measured beam lifetime in seconds versus tune.

To utilize the full transversal acceptance of the accelerator the transversal working point of the machine needs to be optimized. For this purpose a systematic mapping of beam lifetime versus betatron tunes ν_x and ν_y was carried out.

The beam lifetime was determined from the measured beam current. The importance of betatron tunes ν_x and ν_y of the accelerator was shown during these measurements. Figure 40 shows the measured lifetimes versus the difference in tunes $\nu_x - \nu_y$. As the tunes approach the difference resonance, the largest beam lifetimes are observed. Because of remnant coupling between the transversal phase spaces, settings with equal ν_x and ν_y could not be reached (gap at $\nu_x - \nu_y = 0$ in Fig. 35). The difference resonance does not lead to beam losses, however the distance to nearby sum resonances is maximized, and therefore the beam lifetime reaches here its largest values. The observed maximum beam lifetimes are with approximately 2000 seconds still below the expected values of 5400 seconds, assuming single coulomb scattering losses in the residual gas. This discrepancy is not yet understood and further studies are planed.

4.8 Determination of Target Thickness and Luminosity from Beam-Energy Losses

In order to measure absolute cross sections in experiments at a storage ring, it is necessary to know the luminosity. A calibration reaction, such as proton-proton elastic scattering, is often used for this purpose. However, as an alternative, the energy loss of the beam particles due to the interaction with the target can be applied to determine the target thickness. When this is multiplied by the particle current, it directly yields the luminosity.

The energy loss of a coasting beam passing through a thin target in a storage ring is related to a shift in the revolution frequency, which can be measured by analyzing the longitudinal Schottky noise spectrum. This effect has been investigated during a long-term experiment at COSY using the ANKE spectrometer with a 2.65 GeV proton beam and a hydrogen cluster-jet target. The lattice setting for ANKE experiments with zero dispersion at the target provides an important prerequisite for the applicability of the energy loss technique because, under such conditions, the beam does not move away when its energy decreases. The accelerator was operated with 10-minute machine cycles in order that the energy loss of the beam particles stayed sufficiently small to guarantee that the beam remained within the momentum acceptance.

Figure 41 shows a selection of longitudinal Schottky noise spectra measured every minute through a single cycle. Here, as in all other cycles, a linear time dependence of the mean frequency was found. Such a dependence is a consequence of the constant beam-target overlap during the whole cycle due to zero dispersion and negligible emittance growth. Parasitic contributions, caused by residual gas in the ring and hydrogen contamination in the region around the target, were carefully studied by measurements without target and by steering the proton beam to positions left and right of the target. The resulting systematic corrections were $(8 \pm 3)\%$, which have to be subtracted from the primarily measured frequency shift. Based on the relevant machine parameters (beam momentum p, revolution frequency f, and frequency slip parameter $\eta = (\mathrm{d}f/f)/(\mathrm{d}p/p)$, and the stopping power $\mathrm{d}E/\mathrm{d}x$, the target thickness $n_{mathrmT}$ is calculated for each cycle. p and f are known to the order of 10^{-3}. The parameter η, a characteristic constant parameter for the lattice setting, was separately measured through the relative change of the revolution frequency when varying the magnetic field in the ring dipoles. The overall accuracy of the value obtained for the target thickness, which was in the range of a few times 10^{14} cm^2, was estimated as $\pm5\%$. The frequency measurements, which are also involved in the evaluation of η , are the dominating error source. The beam particle current was measured with a high-precision beam-current transformer in parallel in each cycle and this leads to a negligible error. The luminosity is therefore known with the same accuracy as the target thickness.

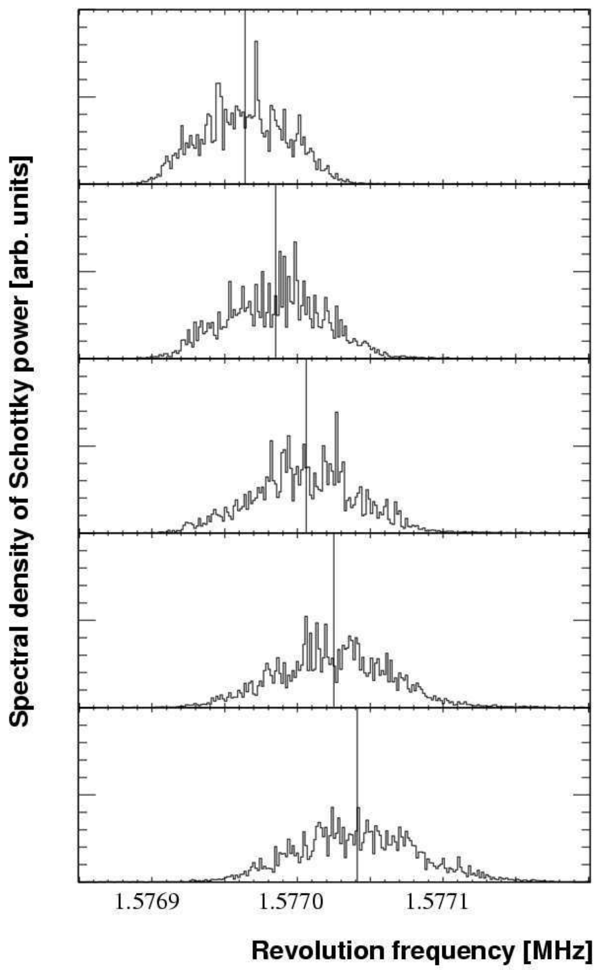

Fig. 41: Frequency distributions of the Schottky noise power measured during one ten-minutes cycle. The frequency shift is positive because these data were taken above the transition energy of the accelerator. Each spectrum is generated within 2 s. The time difference between consecutive spectra shown here is two minutes. The time dependence of the shift of the mean frequency over the cycle is a measure for the target thickness.

In conclusion, it is clear that, under the given experimental conditions with the cluster-jet target, the energy-loss technique is a simple and accurate tool for luminosity determination at the COSY storage ring. This can be of special interest for cases where there is a lack of reliable scattering data that can be used to calibrate the luminosity.

5 Preparations for FAIR

5.1 HESR Lattice Options

The magnet lattice of the HESR needs to fulfill several different requirements. The straight section of the ring should be dispersion free. The betatron amplitude functions (beta functions) at the interaction point with the target as well as at the electron cooler need to be adjustable over a large range, to allow best overlap with target and electron beam, respectively.

At the target this range of beta functions is in the range of 1 – 10 m, at the electron cooler 25 – 100 m. As the HESR should be operated as Synchrotron ring with a fixed injection momentum of 3.9 GeV/c and acceleration and deceleration to momenta between 1.5 and 15 GeV/c, the transition energy in the ring should be adjusted to values outside that range, because crossing of transition energy would lead to unwanted beam losses and emittance growth (without applying additional measures!). In addition, beta functions and phase advance between pickups and kickers of the stochastic cooling system has to be adjusted. Several different lattice options have been investigated that satisfy these requirements.

A magnet configuration with superconducting magnets was studied first. For this case a special lattice design with imaginary transition energy was developed for the HESR. The parameters of two of such solutions are shown in the left two columns in Table 1.

Table 1: Lattice options for the HESR.

Lattice type	6-fold	4-fold	"FODO"
magnet type	SC	SC	NC
Dipole number	48	32	44
length of dipole, type	1.82 m, (straight)	3.0 m, (bent)	4.2 m, (bent)
dipole field	3.6 T	3.6 T	1.7 T
deflection angle, sagitta	7.5 deg., 0.0297 m	11.25 deg., 0.0669 m	8.2 deg., 0.0705 m
Quad length	0.5 m	0.5 m	0.5 m
max. gradient	45 T/m	60 T/m	25 T/m
sextupole length	0.5 m	0.5 m	0.3 m
sextupole field	460 T/m^2	460 T/m^2	50 T/m^2
min. distance	0.6 m	0.6 m	0.3 m
working point	12.16	9.16	7.61
arc $\beta_{xy}^{max.}$	20 m	30 m	24- 0 m
$D_x^{max.}$	9 m	12 m	2-5.2 m
straight $\beta_{xy}^{max.}$	606 m - 150 m	585m -176 m	490 m -110 m
target β_{xy}	1-15 m	1-15 m	1-10 m
cooler β_{xy}	25 - 200 m	25- 200 m	25-200 m
chromaticity ξ_{xy}	-28 to -16	-28 to -16	-20 to -10
transition γ_{tr}	6i	6i	6.2 - 30
arc length	155 m	155 m	157 m
ring length	574 m	574 m	576 m

After review of many parts of the FAIR project, we were asked by the FAIR technical advisory committee to also consider a solution based on standard normal conducting magnets. In this case the decision was made to choose a regular focusing design known as FODO cell design. The value of transition energy would be located inside the energy range of the ring. However, this can be overcome by dividing the focusing and defocusing quadrupole families in the arcs into several sections with different focusing. The transition energy can then be moved above the HESR energy range. To still be able to reach zero dispersion in the straights a well known dispersion suppression scheme can be applied. In the last FODO cell of each arc, one dipole is removed, and the missing bending power is distributed to the rest of the dipole magnets in the arc. The right column in Table 1 summarizes the properties of the normal conducting version for HESR. All investigated lattice structures fulfill the requirements of the experiment. In Fig. 42 the optical functions for the two lattice versions are shown.

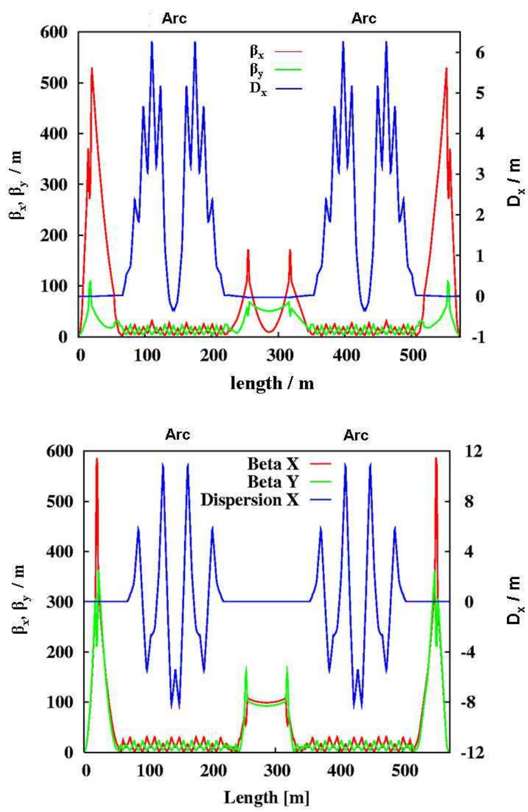

Fig. 42: Optical functions for the HESR superconducting 4 fold symmetry (bottom) and normal conducting (top) magnet lattice from Table 1. Shown are the horizontal betatron amplitude β_x (red), the vertical betatron amplitude β_y (green), and the horizontal dispersion D_x (blue) along the ring.

The normal conducting version of the lattice as presented above is presently subject to detailed studies. The studies of higher order multipole fields, orbit and chromaticity correction are in progress. Electron cooling and stochastic cooling are also studied in detail to ensure optimum ion-optical conditions. Preliminary investigations already indicated, that the normal conducting lattice will be able to fulfill all requirements, and will be the new reference design. An update of the technical report is in preparation.

5.2 Prototype Barrier Bucket Cavity for the HESR

A barrier bucket is not only used to improve the antiproton lifetime by building a 10% – 20% time gap but also to compensate the mean energy loss provoked by the pellet target. Starting from the broadband COSY cavity the design of the barrier bucket cavity was finished using one COSY tank with minor changes.

The asymmetric layout of the cavity with one gap results in a very compact design (length of cavity without gap: 28 cm). The length from flange to flange including the gap is in the order of 50 cm. The basic parameters are summarized in Table 2. The cavity was built at the central workshop of the FZJ. After measuring each individual core we installed four cores into the cavity and measured the impedances of the whole cavity with and without cooling water (Figure 43). The filling factor of the cavity can be further increased with two additional cores if needed.

Table 2: Basic parameters and requirements.

Frequency range	1..20 harmonics (0.5 - 10 MHz)
Gap voltage	10 < 600 V (max, depending on number of harmonic)
Mode of Operation	cw
Cooling	Water-cooled (if higher shunt impedance needed, forced airflow cooling possible)
Material	VitroPerm 500F

The influence of the cooling water is rather high, thus detailed calculation will be done to decide whether a water cooling is really needed or a forced air-flow cooling would be sufficient.

Additionally first RF power test have been carried out with an ENI300 power amplifier. The results are presented in Fig. 44. A gap-voltage of 300 V (peak-peak) could be easily reached over a very wide frequency range with the limited power of 300 W including a capacitor to simulate the gap-capacity.

5.3 Signal Synthesis for Barrier Bucket Operation

The revolution frequency at injection energy in COSY corresponds nearly to the HESR revolution frequency. Many Barrier Bucket tests have been done at COSY in

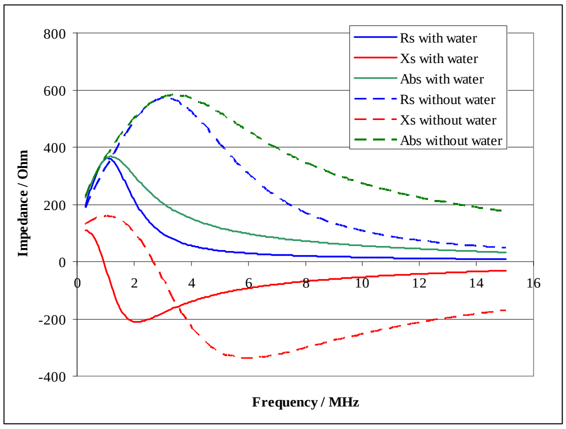

Fig. 43: Measurements of the cavity impedance with and without water cooling showing the resistive (Rs) and the reactance (Xs) components as well as the magnitude of the impedance (Abs).

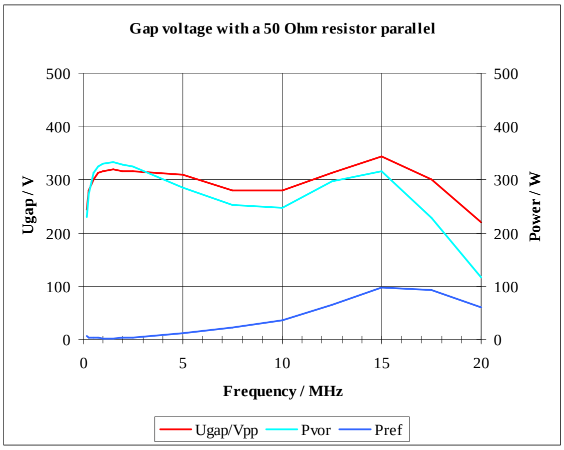

Fig. 44: First high power tests at the barrier bucket cavity showing the nearly frequency independent peak to peak gap voltage (red) together with the forward power (light blue) and the reflected power (dark blue).

advance to test and optimize the signal synthesis which is necessary to generate a single sinus gap voltage. An arbitrary waveform generator (AWG) has been used to generate a barrier bucket signal which was applied to the multi-harmonic COSY cavity. After measuring the corresponding gap voltage the Fourier series of the transfer function was calculated and a pre-distorted barrier bucket signal has been determined which gives the desired sinusoidal gap voltage (Fig. 45).

Figure 46 shows the starting barrier bucket input signal for the tube amplifier, the corresponding gap-voltage (trace 2) and the resulting beam shape measured with the phase pickup.

A nearly clean pulse shape was obtained at the gap with the use of 16 harmonics as shown in Fig. 47. Even this nearly clean gap-voltage is not sufficient to get a flat beam distribution. A wider broadband RF system (amplifier

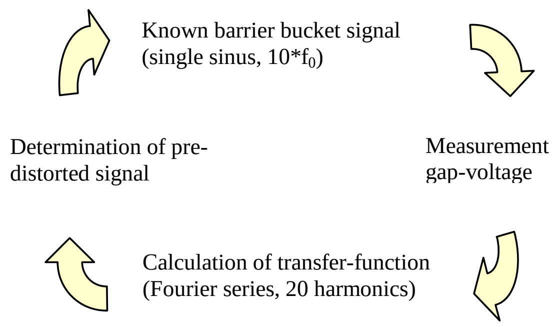

Fig. 45: Schematics of signal synthesis.

and cavity) is planned for HESR. It will be possible to use a larger number of harmonics and to minimize the rest of ripple further more. Up to now a commercial arbitrary function generator is in operation to generate the barrier bucket signal. At the HESR it is sufficient to create predefined wave forms in this way since it is not foreseen to use a moving barrier bucket.

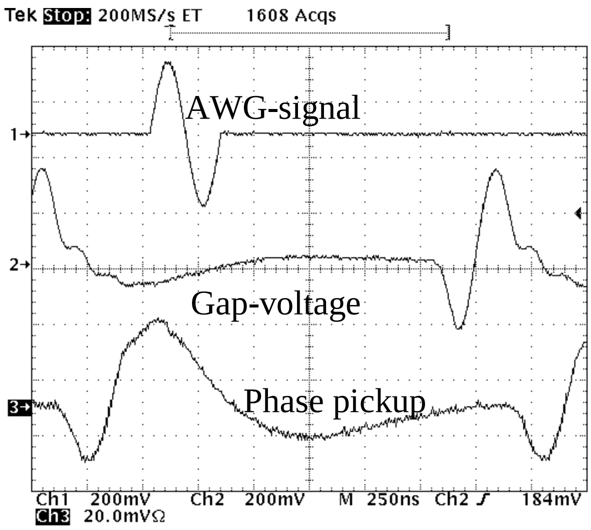

Fig. 46: Single sinusoidal starting signal, corresponding gap voltage and beam distribution measured with a phase pickup.

5.4 Barrier Bucket at COSY

The revolution frequency of COSY at most experiments differs compared to the HESR requirements to nearly a factor of three. At this higher frequency the effective signal generation for a barrier bucket is not only limit by the cavity but also by the arbitrary waveform generator. Nevertheless the first barrier bucket tests were promising and can help to improve not only the HESR experiments but as well the running experiments at COSY namely the WASA experiment with the thick pellet-target.
After the installation of the HESR barrier bucket prototype cavity first RF measurements started with a broad-

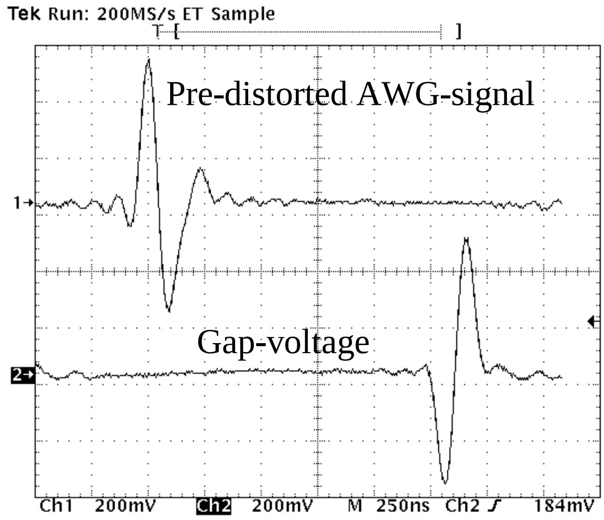

Fig. 47: Pre-distorted barrier bucket signal and the corresponding gap-voltage.

band 1 kW solid state amplifier. Because of the higher revolution frequency $f_0 \gg 1.3$ MHz for 2.69 GeV/c deuterons and the limitations by the existing arbitrary waveform generator we used a second method of signal preparation to get a single sinus barrier bucket signal at the gap. An additional DC pulse added to the single sinus waveform minimised the "ringing" of the cavity. Both the input signal at the solid state amplifier and the corresponding gap voltage are presented in Fig. 48.

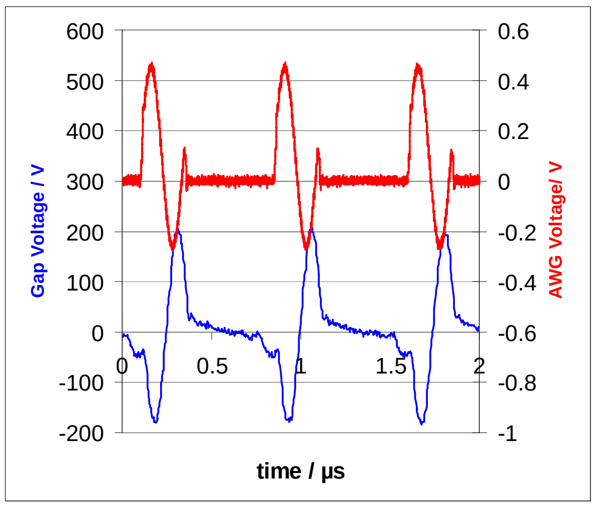

Fig. 48: Solid state amplifier input signal (dc plus single sinus) and corresponding gap-voltage.

The periodic bunch in the COSY ring within a barrier bucket is shown in Fig. 49 (blue curve) exhibiting the typical, nearly rectangular bunch shape together with a periodic bunch for a single sinusoidal voltage at harmonic one (red curve). Note that due to different cable lengths the two wave forms are shifted against each other by about one half of the revolution time.

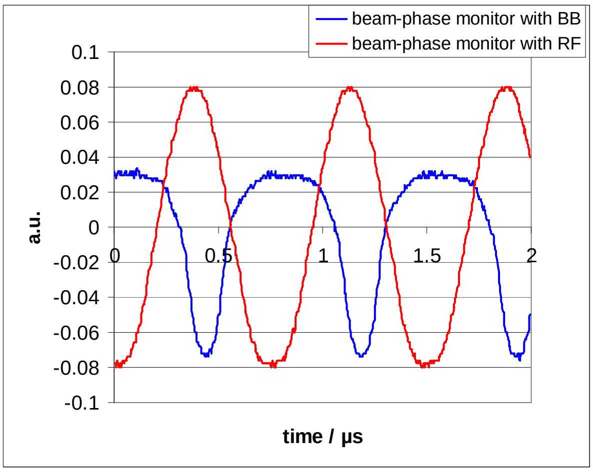

Fig. 49: Barrier bucket bunch (blue) in comparison with a bunch in a single harmonic cavity (red).

As compared to the bunch formed by a single harmonic cavity the barrier bucket bunch has reduced peak bunch intensity. The time gap between consecutive barrier-bucket bunches is smaller as wanted. In both cases the number of stored deuterons in the bunch is the same. The prototype barrier bucket cavity located in one of COSY's arc is exhibited in Fig. 49 where the asymmetric layout of the cavity with one gap resulting in a very compact design (length of cavity core without gap 28 cm) is clearly visible. The length from flange to flange including the gap is in the order of 50 cm.

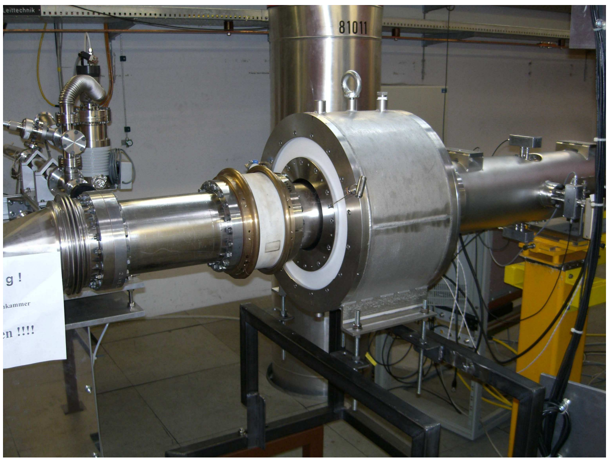

Fig. 50: The barrier bucket cavity with its asymmetric layout is installed in one arc of COSY. In this figure the shielding of the gap is dismounted to make it visible.

5.5 The PANDA Experiment

5.5.1 Introduction

One major component of the approved **F**acility for **A**ntiproton and **I**on **R**esearch (FAIR) at the GSI in Darmstadt is the **H**igh **E**nergy **S**torage **R**ing (HESR) with the "Anti**P**roton **AN**nihilations at **DA**rmstadt" - experiment ($\overline{\rm P}$ANDA). The HESR will provide a phase space cooled antiproton beam of unsurpassed quality and precision. A momentum range up to 15 GeV/c together with an average interaction rate of 10 MHz will allow the detailed study of a wide variety of topics, like the structure of hadrons in the charmonium mass range, the spectroscopy of double hypernuclei and electromagnetic processes. To serve this wide physics program the general purpose experiment $\overline{\rm P}$ANDA is currently planned.
The basic concept of the detector is given by its division into two main parts, the central or target spectrometer and the forward spectrometer. This combines a nearly 4π coverage in the target region together with high acceptance of particles emitted at small polar angles in this fixed target kinematics.
The heart of the central spectrometer is a micro vertex detector located direct around the target for extremely precise tracking information. It is surrounded by the central tracker built either of straw tubes (STT) or a time projection chamber (TPC) in the barrel part, and a set of micro pattern gas detectors, so called triple gas electron multiplier detectors (GEM) in the forward direction. Particle identification is done by two ring imaging Cherenkov counters surrounded by a compact electromagnetic calorimeter made out of $PbWO_4$ crystals. The entire system is situated in a 2 T solenoidal magnet which is covered outside with detectors for muon identification and tracking.
The forward spectrometer consists of a 2 T m dipole magnet with a set of multiwire drift chambers (MuDC) for tracking, a RICH detector for particle identification, calorimeters for charged and neutral particles and a layer of muon counters.
The ongoing activities of the IKP for the $\overline{\rm P}$ANDA detector are focused in three parts: the micro vertex detector, the straw tube tracker and the simulation of the tracking detectors. Furthermore an effort was started dealing with an evaluation of the physics potential of the baryon spectroscopy with the $\overline{\rm P}$ANDA experiment

5.5.2 Micro vertex detector

The Micro Vertex Detector (MVD) plays a key role in the PANDA experiment to identify open charm and strangeness by detecting secondary decays of particles displaced from the primary interaction point. These decay lengths range from a few 100 μm for charmed mesons and baryons up to several cm for strange hadrons. One of the most important issues for the design of the pixel part of the MVD is the data handling and transfer. In order to allow an open charm trigger based on secondary vertex tagging a quasi online data processing in the DAQ chain is envisaged. This requires a complete data transfer from the MVD to a certain DAQ stage and therefore the MVD itself must be readout without any trigger. Based on extensive hit rate simulations a VHDL model of the readout scheme of the pixel front-end electronics have been developed and tested.

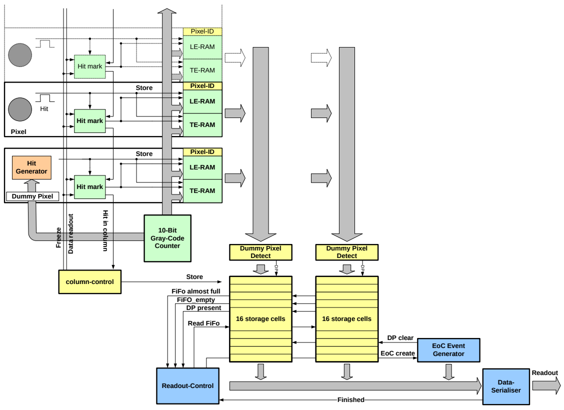

Fig. 51: Readout scheme for the front-end electronics of the pixel part of the MVD.

The tested readout scheme can be seen in Fig. 51. The basic concept of the pixel readout is a time-stamp architecture. In each pixel the leading and the trailing edge of the discriminator signal will be stored using a 10-bit Grey counter. A fast asynchronous scan will transfer the hit data together with the pixel-ID column wise to the end-of-column buffer. These buffers work like a FiFo storing the hit data until the readout control decides to transfer the data from the EoC buffers depending on their filling state to the serialiser and the LVDS output lines of the front-end chip. The shown scheme was successfully tested with the simulated hit rates.
Furthermore, a versatile digital readout system, whose main purpose is prototype testing of $\overline{\rm P}$ANDA MVD front-end chip candidates, featuring a modular design of hardware, firmware and the corresponding software framework was developed.

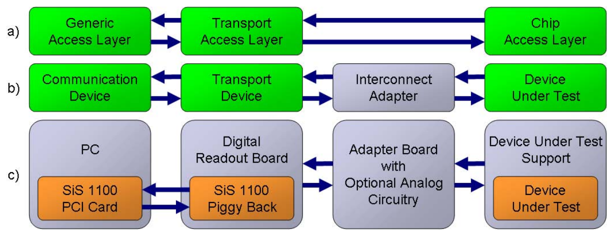

Fig. 52: Readout chain. a) shows the abstract model of the software modules, b) the abstract model of the hardware devices and c) shows the actual setup.

The software framework, in the following referred to as MRF, follows a modular design approach by implement-

ing an abstract communication model which defines a hierarchy of communication layers, each layer corresponding to a single module in the software framework (compare Figure 52a respectively a single hardware device within the readout chain (Figure 52b. Another module of the MRF is a special data storage class which provides a common interface for transfer, storage and display of both configuration data and data returned by the device.
The readout hardware strictly separates analog and digital parts of the readout. The classification of the hardware components closely follows the communication layer concept of the software, as shown in Figure 52b. While the digital readout board itself (developed by IKP in close cooperation with ZEL) contains purely digital components, any (optional) analog circuitry is implemented on an additional adapter board which connects the front-end support with the digital readout board. Its embedded FPGA can be reconfigured to support arbitrary communication protocols and I/O pinouts for front-end connection, while the connection to the PC is realized via a SiS 1100 optical gigabit link PCI card. Compare Figure 52c for an overview on the setup.
The performance tests of the readout system are very promising. The current FPGA design runs stably at the desired internal clock rate of 40 MHz. Furthermore, even without any optimizations of signal timings, the system could handle more than twice this speed. Clock generation for the connected Atlas FE-I3 front-end chip yields stable frequencies of 5 MHz and 40 MHz on two independent external clock lines with signal rise and fall times well below 2 ns. The same results were obtained for the data lines. Data transmission is performed using access functions of the MRF. It also features a full digital representation of all of the front-end's configuration registers which is used for chip setup. Future plans include deploying the digital readout system as a test stand for prototypes of the Topix front-end chip for silicon pixel sensors which is currently under development at INFN Torino.

5.5.3 MVD simulations in pandaRoot

On the $\overline{\text{P}}$ANDA collaboration meeting in Vienna in September 2006 it was decided to change the simulation framework to a Root based system used already by CBM, another big experiment within FAIR. The new basic framework is called FairRoot with the two specializations cbmRoot and pandaRoot. With this decision it was the task of the various subdetectors to implement their detector in the new framework. For the micro-vertex-detector this work was split into two parts: The responsibility for the strip part were taken over by the Dresden group, and for the pixel part were taken over by the IKP group.
At the beginning of the work a CAD converter was written, which allows to convert CAD files in the STEP format into Root geometries which can be directly used in the simulation software. This approach has the advantage that even complex geometries can be simulated and

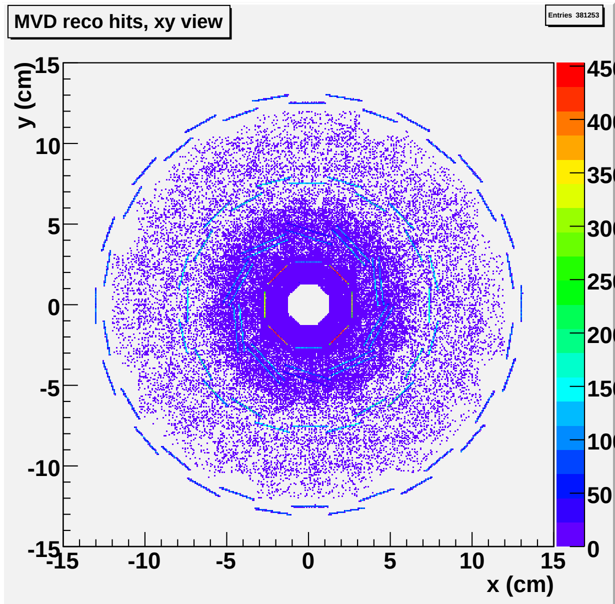

Fig. 53: Position of the reconstructed points projected onto the xy-plane

the best possible matching between real detector and simulation model can be achieved.

Until the end of the year 2007 the chain of geometry description, Monte-Carlo hit generation, digitization of the hits and the back calculation of the hit position out of the digitized data was achieved.

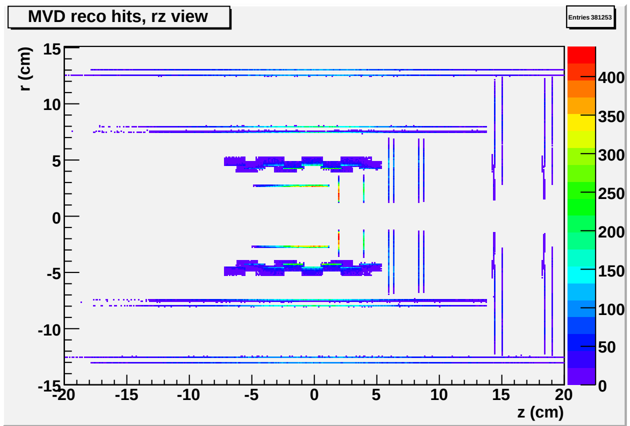

Fig. 54: Position of the reconstructed points projected onto the rz-plane

In Figures 53 and 54 the position of the reconstructed points projected onto the xy-plane and rz-plane are shown. The geometry of the micro-vertex-detector is clearly visible with its four barrel layers and six disks in forward direction.

5.5.4 Aging Tests of Straw Tubes

High rate tests of straws for the proposed central straw tube tracker (STT) of the future $\overline{\text{P}}$ANDA detector were carried out with a total exposure time of 199 hours to the COSY beam. The goal was to check the influence of the beam exposure and charge deposition on the straw efficiency and to verify that all assembled materials including the gas system do not create harmful pollution, *e.g.* by outgassing. Within the short time of about 10 days beam irradiation, it was possible to collect a charge load in the single tubes corresponds to at least three years of $\overline{\text{P}}$ANDA operation at the desired luminosity with an expected 50 % live-time of data-taking time per year.
The straw design and all materials were the same used for the COSY-TOF straw tracker assembly. For the $\overline{\text{P}}$ANDA detector the same straw tube design had been proposed, only the exact length is still open and may vary between about 120 cm to 150 cm. The straw setup consisted of a double-layer of 32 tubes, installed behind the COSY-TOF apparatus and exposed to the residual proton beam with a momentum of about 3 GeV/c. Due to the horizontal layout and a beam spot of about 2×2 cm^2 the particle rate through all tubes was almost the same.
The gas supply of the 32 straws was divided into four individual gas circuits. Thus, it was possible to test at the same time four different gas mixtures and gas gains with the same particle rates. The chosen gas mixtures were Argon based, with different fractions of CO_2 (10 % and 30 %) and one mixture with 10 % Ethane. The gas pressure for all mixtures was 1650 mbar. The typical gas flow was one volume exchange per hour. In total, 16 high voltage supply channels (one channel per two straws) allowed to operate the straws at different voltage levels and gas gains. The current of every voltage channel was monitored with a resolution of 2 nA.
The expected particle rates for the individual tubes in the $\overline{\text{P}}$ANDA central tracker volume were derived from a simulation of $\bar{p}p$ interactions and assuming an event rate of 10^7 s^{-1}. The mean particle flux for straws in the innermost layer was $\simeq$400 kHz per 1500 mm long tube. The maximum flux of $\simeq$7 kHz/cm in the tube was concentrated within $z = 2 \pm 2$ cm (target position at $z = 0$ cm) coming from $\bar{p}p$ elastic interactions with a laboratory scattering angle $\theta \simeq 90°$ and relatively low momentum. These particles are highly ionising and produced a high charge load of $\simeq$0.4 C/cm/year, if one assumed a typical gas gain inside the tubes of $5 \cdot 10^4$.
During the beam time no high voltage failures, dark currents or broken wires due to the high charge load were observed. Possible efficiency losses were checked after the beam time by exposing all tubes to a ^{55}Fe radioactive source with 5.9 keV γ-emission. The amplitude heights, which are direct measure of the gas gain, were checked for each straw at different longitudinal positions around the beam irradiation spot (see Fig. 55)
It can be seen that some straws (no. 9−16) showed an efficiency drop of about 3–8 % where the beam hit the tubes. For other straws no change in amplitude height

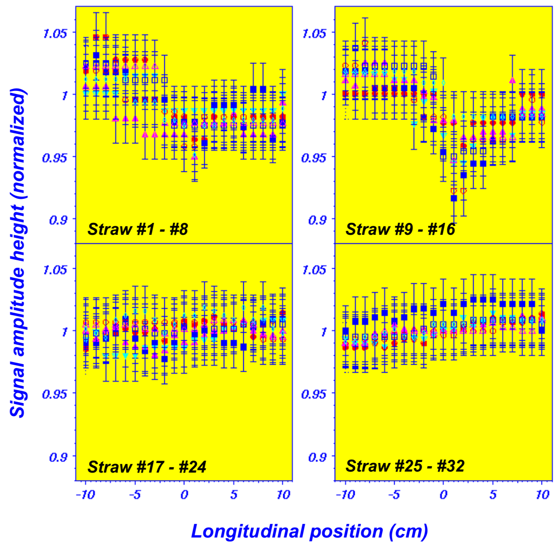

Fig. 55: Measured efficiency along the tube for all 32 straws. The beam hit all tubes around 0 cm.

was measured. The sensitivity of the measurement was about 2 % of the amplitude height, so that the observed effect for most of the straws was only slightly above resolution. The absence of any efficiency changes for more than half of all straws could be explained by better material quality and properties, but needs further investigations.
The results confirmed that the straw design and used materials are suited and will not limit the life time of the STT detector to a remarkable extent. For a robust STT operation a gas mixture and pressure which allows lower high voltage operation should be preferred, *e.g.* an Argon-based gas mixture with a CO_2 fraction of about 10 % and gas gain of about $5 \cdot 10^4$ at a pressure of about 1600 mbar.

5.5.5 Baryon spectroscopy with $\overline{\text{P}}$ANDA

The understanding of baryon excitation spectra is one of the prime goals of non-perturbative QCD. Consequently, baryon spectroscopy has been introduced as a new topic in the PANDA physics program. A physics working group on this subject has been formed in the PANDA Collaboration, in order to determine the most relevant physics questions to be investigated, and to assess the experimental feasibility.
So far, apart from planned studies of double hypernuclei, the physics program of PANDA was mainly focused on annihilation channels in $\bar{p}p$ and $\bar{p}A$ collisions, like for charmonium spectroscopy, for searches for exotic hadrons with gluonic excitations, or for the measurement of the charmonium-nucleon cross section. A large fraction of the total $\bar{p}p$ cross section, in particular at higher energies, is however associated with inelastic channels having a baryon antibaryon pair in the final state. Since inelastic reactions resulting in final states of the type ”baryon + antibaryon + meson(s)” to a significant fraction

proceed through excited states, this offers the opportunity for spectroscopic studies of various baryon species. The discovery potential is considered to be particularly high for Ξ hyperons with double strangeness. The measured $\bar{p}p \rightarrow \bar{\Xi}\Xi$ cross section is up to $2\,\mu$b, and the cross section for the population of excited Ξ^* states is estimated to be of the same order of magnitude, allowing for large production rates. On the other hand, with only two excited states having still not firmly established spin-parity assignments above the octet and decuplet ground states, very little is known on the Ξ excitation spectrum. Even less is known on the triple-strange Ω spectrum, however the predicted production cross section is by more than two orders of magnitude smaller. Spectroscopy of charmed baryons at PANDA is limited to excitation energies below 0.93 GeV for Λ_c and below 0.76 GeV for Σ_c by the maximum $\bar{p}$ momentum of 15 GeV/c.
First simulations indicate that for reactions possibly populating Ξ or Ω resonances like $\bar{p}p \rightarrow \bar{\Xi}^+\Xi^-\pi^0$, $\bar{p}p \rightarrow \bar{\Xi}^+\Lambda K^-(+\text{c.c.})$, or $\bar{p}p \rightarrow \bar{\Omega}^+\Xi^-K^0(+\text{c.c.})$ almost the full phase space is covered by PANDA detector components. It is also concluded that the tracking capability of the target spectrometer at smaller angles and at larger distances downstream of the target will be essential for the reconstruction of delayed Ξ and Λ decay vertices. The planned replacement of the MDC detectors by GEM chambers and additional MVD discs further downstream as compared to the current design will improve reconstruction efficiency and resolution in reaction channels populating strange and multi-strange hyperon resonances.

A Councils

A.1 HGF Midterm Review Council

Prof. J. Bisplinghoff	Universität Bonn	
Prof. C. Guaraldo	INFN Frascati, I	
Prof. M. Harakeh	KVI Groningen, NL	
Prof. A. Merschenz-Quack	FH Aachen	
Prof. V. Metag	Universität Gießen	
Prof. E. Moulinari	Universita de Modena, I	
Dr. D. Müller	BMBF/GSI Darmstadt	
Dr. R. Opitz	Helmholtz Gemeinschaft	
Prof. St. Paul	TU München	Chairperson
Prof. K. Peters	GSI Darmstadt	
Prof. D.O. Riska	Helsinki Institute of Physics, FI	
Prof. A. Schäfer	Universität Regensburg	
Dr. S. Schmidt	Helmholtz Gemeinschaft	
Prof. J. Stachel	Universität Heidelberg	
Prof. W.T.H. van Oers	University of Manitoba, CA	
Dr. M. Wappelhorst	Ministerium IWFT/NRW, Düsseldorf	

A.2 COSY Program Advisory Committee

Prof. D. Barber	DESY, DE	
Prof. J. Bijnens	Lund University, SE	
Prof. H. Freiesleben	TU Dresden, DE	
Prof. B. Friman	GSI Darmstadt, DE	
Prof. N. Herrmann	Universität Heidelberg, DE	
Prof. T. Johansson	Uppsala Universitet, SE	
Prof. H. Löhner	KVI Groningen, NL	
Prof. A. Magiera	Jagellonian University Cracow, PL	
Prof. W. Meyer	Universität Bochum, DE	
Prof. W.T.H. van Oers	University of Manitoba, CA	Chairperson
Prof. E. Oset	Universitat de Valencia, ES	
Prof. C. Schaerf	INFN Roma II, IT	

B Publications 2007

1. Experiment

1. Abdel-Bary, M.; Abdel-Samad, S.; Brinkmann, K. T.; Castelijns, R.; Clement, H.; Dietrich, J.; Doroshkevich, E.; Dshemuchadse, S.; Ehrhardt, K.; Erhardt, A; Eyrich, W.; Freiesleben, H.; Gast, W.; Georgi, J.; Gillitzer, A.; Karsch, L.; Kilian, K.; Krapp, M.; Kuhlmann, E.; Lehmann, A.; Morsch, H.-P.; Paul, N.; Pinna, L.; Pizzolotto, C.; Ritman, J.; Roderburg, E.; Schadmand, S.; Schönmeier, P.; Schröder, W.; Schulte-Wissermann, M.; Sefzick, T.; Teufel, A.; Ucar, A.; Wüstner, P.; Zupranski, P.
   Improved study of a possible Θ^+ production in the $pp \to pK^0\Sigma^+$ reaction with the COSY-TOF spectrometer
   Physics Letters B **649** (2007) 252.

2. Abdel-Bary, M.; Abdel-Samad, S.; Brinkmann, K.-T.; Clement, H.; Dietrich, J.; Doroshkevich, E.; Dshemuchadse, S.; Ehrhart, K.; Erhardt, A.; Eyrich, W.; Filippi, A.; Freiesleben, H.; Fritsch, M.; Gillitzer, A.; Hesselbarth, D.; Jä, R.; Karsch, L.; Kilian, K.; Kuhlmann, E.; Marcello, S.; Michel, P.; Mö, K.; Morsch, H. P.; Pizzolotto, C.; Plettner, C.; Ritman, J.; Roderburg, E.; Schö, P.; Schroeder, W.; Schulte-Wissermann, M.; Steinke, M.; Sun, G. J.; Ullrich, W.; Wenzel, R.; Wintz, P.; Wagner, M.; Wilms, A.; Wirth, S.; Zupranski, P.;
   Comparison of isoscalar vector meson production cross sections in proton-proton collisions
   Physics Letters B **647** (2007) 351.

3. Abdel-Bary, M.; Abdel-Samad, S.; Kilian, K.; Ritman, J.
   Performance measurements of a 7 mm-diameter hydrogen heat pipe
   Cryogenics **47** (2007) 158.

4. Adam, H.-H.; Geck, I.; Khoukaz, A.; Lister, T.; Santo, R.; Steltenkamp, S.; Täschner, A.; Czerwinski, E.; Czyzykiewicz, R.; Janusz, M.; Jarczyk, L.; Kamys, B.; Klaja, P.; Moskal, P.; Piskor-Ignatowicz, B.; Przerwa, J.; Smyrski, J.; Grzonka, D.; Kilian, K.; Oelert, W.; Sefzick, T.; Winter, P.; Wolke, M.; Wüstner, P.; Budzanowski, A.; Rozek, T.; Siemaszko, M.; Zipper, W.
   Hadronic ^{3}He eta production near threshold
   Physical Review C **75** (2007) 14004.

5. Agakichiev, B.; Agodi, C.; Alvarez-Pol, H.; Balanda, A.; Bertini, D.; Bielcik, J.; Bellia, G.; Bohmer, M.; Bokemeyer, H.; Boyard, J. L.; Braun-Munzinger, P.; Cabanelas, P.; Chernenko, S.; Christ, T.; Coniglione, R.; Cosentino, L.; Diaz, J.; Dohrmann, F.; Duran, I.; Eberl, T.; Enghardt, W.; Fabbietti, L.; Fateev, O.; Fernandez, C.; Finocchiaro, P.; Friese, J.; Frohlich, I.; Fuentes, B.; Garabatos, C.; Garzon, J. A.; Gernhauser, R.; Golubeva, M.; Gonzalez-Diaz, D.; Grosse, E.; Guber, F.; Hennino, T.; Hlavac, S.; Holzmann, R.; Homolka, J.; Ierusalimov, A.; Iori, I.; Ivashkin, A.; Jaskula, M.; Jurkovic, M.; Kagarlis, M.; Kajetanowicz, M.; Kampfer, B.; Kanaki, K.; Karavicheva, T.; Kastenmuller, A.; Kidon, L.; Kienle, P.; Koenig, I.; Koenig, W.; Korner, H. J.; Kolb, B. W.; Kotte, R.; Krucken, R.; Kugler, A.; Kuhn, W.; Kulessa, R.; Kurepin, A.; Lang, S.; Lange, S.; Lehnert, J.; Lins, E.; Magestro, D.; Maiolino, C.; Malarz, A.; Markert, J.; Metag, V.; Mousa, J.; Munch, M.; Muntz, C.; Naumann, L.; Nekhaev, A.; Novotny, J.; Otwinowski, J.; Pachmayer, Y.C.; Pechenov, V.; Perez, T.; Piattelli, P.; Pietraszko, J.; Pleskac, R.; Ploskon, M.; Pospisil, V.; Prokopowicz, W.; Przygoda, W.; Ramstein, B.; Reshetin, A.; Ritman, J.; Roy-Stephan, M.; Rustamov, A.; Sadovsky, A.; Sailer, B.; Salabura, P.; Sanchez, M.; Sapienza, P.; Schmah, A.; Schon, H.; Schon, W.; Schroder, C.; Schwab, E.; Simon, R. S.; Smolyankin, V.; Smykov, L.; Spataro, S.; Spruck, B.; Strobele, H.; Stroth, J.; Sturm, C.; Sudol, M.; Suk, M.; Taranenko, A.; Tlusty, P.; Toia, A.; Traxler, M.; Tsertos, H.; Vassiliev, D.; Vazquez, A.; Wagner, V.; Walus, W.; Wisniowski, W.; Wojcik, T.; Wustenfeld, J.; Zanevsky, Y.; Zeitelhack, K.; Zovinec, D.; Zumbruch, P.
   Dielectron production in ^{12}C+^{12}C collisions at 2-AGeV with HADES
   Physical Review Letters **98** (2007) 052302.

6. Bargholtz, C.; Bashkanov, M.; Bogoslawsky, D.; Calen, H.; Cappellaro, F.; Clement, H.; Demirörs, L.; Ekström, C.; Fransson, K.; Geren, L.; Gustafsson, L.; Höistad, B.; Ivanov, G.; Jacewicz, M.; Jiganov, E.; Johansson, T.; Keleta, S.; Koch, I.; Kullander, S.; Kupsc, A.; Kuznetsov, A.; Laukhin, I. V.; Lindberg, K.; Marciniewski, P.; Meier, R.; Morosov, B.; Oelert, W.; Pauly, C.; Pettersson, H.; Petukhov, Y.; Povtorejko, A.; Ruber, R.J.M.Y.; Schönning, K.; Scobel, W.; Shafigullin, R.; Shwartz, B.; Skorodko, T.; Sopov, V.; Stepaniak, J.; Tchernyshev, V.; Tegner, P. E.; Thörngren-Engblom, P.; Tikhomirov, V.; Turowiecki, A.; Wagner, G. J.; Wolke, M.; Yamamoto, A.; Zabierowski, J.; Zartova, I.; Zlomanczuk, J.
   Measurement of the $\eta \to \pi^+\pi^-e^+e^-$ decay branching ratio
   Physics Letters B **644** (2007) 299.

7. Barsov, S.; Büscher, M.; Hartmann, M.; Hejny, V.; Kacharava, A.; Keshelashvili, I.; Khoukaz, A.; Koptev, V.; Kulessa, P.; Kulikov, A.; Lehmann, I.; Leontyev, V.; Macharashvili, G.; Maeda, Y.; Mersmann, T.; Merzliakov, S.;

Mikirtichyants, S.; Mussgiller, A.; Oellers, D.; Ohm, H.; Rathmann, F.; Schleichert, R.; Seyfarth, H.; Ströher, H.; Trusov, S.; Valdau, Yu.; Wüstner, P.; Yaschenko, S.; Wilkin, C.
Study of omega-meson production in *pp* collisions at ANKE
European Physical Journal A **31** (2007) 95.

8. Bashkanov, M.; Bogoslawsky, D.; Calen, H.; Capellaro, F.; Clement, H.; Demirörs, L.; Ekström, C.; Fransson, K.; Gustafsson, L.; Höistad, B.; Ivanov, G.; Jacewicz, M.; Jiganov, E.; Johansson, T.; Keleta, S.; Koch, I.; Kullander, S.; Kupsc, A.; Kuznetsov, A.; Marciniewski, P.; Meier, R.; Morosov, B.; Oelert, W.; Pauly, C.; Petukhov, Y.; Pettersson, H.; Povtorejko, A.; Ruber, R.J.M.Y.; Schönning, K.; Scobel, W.; Skorodko, T.; Shwartz, B.; Sopov, V.; Stepaniak, J.; Tchernyshev, V.; Thörngren Engblom, P.; Tikhomirov, V.; Turowiecki, A.; Wagner, G. J.; Wiedner, U.; Wolke, M.; Yamamoto, A.; Zabierowski, J.; Zlomanczuk, J.
Measurement of the slope parameter for the $\eta \to 3\pi^0$ decay in the $pp \to pp\eta$ reaction
Physical Review C **76** (2007) 048201.

9. Bellemann, F.; Berg, A.; Bisplinghoff, J.; Bohlscheid, G.; Ernst, J.; Henrich, C.; Hinterberger, F.; Ibald, R.; Jahn, R.; Joosten, R.; Kilian, K.; Kozela, A.; Machner, H.; Magiera, A.; Munkel, J.; von Neumann-Cosel, P.; von Rossen, P.; Schnitker, H.; Scho, K.; Smyrski, J.; Tölle, R.; Wilkin, C.
Experimental study of the $pd \to {}^3\mathrm{He}K^+K^-$ and $pd \to {}^3\mathrm{He}\phi$ reactions close to threshold
Physical Review C **75** (2007) 015204.

10. Betigeri, M. G.; Biswas, P. K.; Budzanowski, A.; Chatterjee, A.; Jahn, R.; Guha, S.; Hawranek, P.; Jain, B. K.; Jha, V.; Kilian, K.; Kliczewski, S.; Kirillov, Da.; Kirillov, Di.; Kolev, D.; Kravcikova, M.; Kutsarova, T.; Lesiak, M.; Lieb, J.; Machner, H.; Magiera, A.; Maier, R.; Martinska, G.; Nedev, S.; Piskunov, N.; Prasuhn, D.; Protic, D.; Ritman, J.; von Rossen, P.; Roy, B. J.; Shukla, P.; Sitnik, I.; Siudak, R.; Tsenov, R.; Ulicny, M.; Urban, J.; Vankova, G.
A large acceptance scintillator detector with wavelength shifting fibre readout for search of η-nucleus bound states
Nuclear Instruments and Methods in Physics Research Section A **578** (2007) 198.

11. Bubak, A.; Budzanowski, A.; Filges, D.; Goldenbaum, F.; Heczko, A.; Hodde, H.; Jarczyk, L.; Kamys, B.; Kistryn, M.; Kistryn, St.; Kliczewski, St.; Kowalczyk, A.; Kozik, E.; Kulessa, P.; Machner, H.; Magiera, A.; Migdal, W.; Paul, N.; Piskor-Ignatowicz, B.; Puchala, M.; Pysz, K.; Rudy, Z.; Siudak, R.; Wojciechowski, M.; Wüstner, P.
Non-equilibrium emission of complex fragments from *p*+Au collisions at 2.5 GeV proton beam energy
Physical Review C **76** (2007) 014618.

12. Czyzcykiewicz, R.; Moskal, P.; Adam, H.-H.; Budzanowski, A.; Czerwinski, E.; Gil, D.; Grzonka, D.; Hodana, M.; Janusz, M.; Jarczyk, L.; Kamys, B.; Khoukaz, A.; Kilian, K.; Klaja, P.; Lorentz, B.; Oelert, W.; Piskor-Ignatowicz, B.; Przerwa, J.; Rejdych, B.; Ritman, J.; Sefzick, T.; Siemaszko, M.; Smyrski, J.; Täschner, A.; Ulbrich, K.; Winter, P.; Wolke, M.; Wüstner, P.; Zipper, W.
Mechanism of Near-Threshold Production of the η Meson
Physical Review Letters **98** (2007) 122003.

13. Czyzykiewicz, R.; Moskal, P.; Adam, H.-H.; Budzanowski, A.; Czerwinski, E.; Gil, D.; Grzonka, D.; Janusz, M.; Jarczyk, L.; Kamys, B.; Khoukaz, A.; Klaja, P.; Majewski, J.; Oelert, W.; Piskor-Ignatowicz, C.; Przerwa, J.; Ritman, J.; Rohdjess, H.; Rozek, T.; Sefzick, T.; Siemasko, M.; Smyrski, J.; Täschner, A.; Ulbrich, K.; Winter, P.; Wolke, M.; Wüstner, P.; Zipper, W.
Study of the production mechanism of the η meson by means of analysing power measurements International *Journal of Modern Physics A* **22** (2007) 518.

14. Gabrielse, G.; Larochelle, P.; Le Sage, D.; Levitt, B.; Kolthammer, W. S.; Kultjanishvili, I.; McConnell, R.; Wrubel, J.; Esser, F. M.; Glückler, H.; Grzonka, D.; Hansen, G.; Martin, S.; Oelert, W.; Schillings, J.; Schmitt, M.; Sefzick, T.; Soltner, H.; Zhang, Z.; Comeau, D.; George, M. C.; Hessels, E. A.; Storry, C. H.; Weel, M.; Speck, A.; Nillius, F.; Walz, J.; Hänsch, T. W.
Antiproton Confinement in a Penning-Ioffe Trap for Antihydrogen
Physical Review Letters **98** (2007) 113002.

15. Herskind, B.; Hagemann, G. B.; Dossing, Th.; Ronn Hansen, C.; Schunk, N.; Sletten, G.; Oedegard, S.; Hübel, H.; Bringel, P.; Bürger, A.; Neusser, A.; Singh, A. K.; Al-Khatib, A.; Patel, S. B.; Nyako, B. M.; Algora, A.; Dombradi, Z.; Gal, J.; Kalinka, G.; Sohler, D.; Molnar, J.; Timar, J.; Zolnai, L.; Juhasz, K.; Bracco, A.; Leoni, S.; Camera, F.; Benzoni, G.; Mason, P.; Paleni, A.; Million, B.; Wieland, O.; Bednarczyk, P.; Azaiez, F.; Byrski, Th.; Curien, D.; Dakov, O.; Duchene, G.; Khalfallah, F.; Gall, B.; Piqeras, L.; Robin, J.; Dudek, J.; Rowley, N.;

Redon, N.; Hannachi, F.; Scheurer, J. N.; Wilson, J. N.; Lopez-Martens, A.; Korichi, A.; Hauschild, K.; Roccaz, J.; Siem, S.; Fallon, P.; Lee, I. Y.; Görgen, A.; Maj, A.; Kmiecik, M.; Brekiesz, M.; Styczen, J.; Zuber, K.; Lisle, J. C.; Cederwall, B.; Lagergren, K.; Evans, A. O.; Rainovski, G.; De Angelis, G.; La Rana, G.; Moro, R.; Lieder, R. M.; Lieder, E. O.; Gast, W.; Jäger, H.; Pasternak, A. A.; Petrache, C. M.; Petrache, D.
Light Charged Particles as Gateway to Hyperdeformation
Acta Physica Polonica B **38** (2007) 1421.

16. Indelicato, P.; Boucard, S.; Covita, D. S.; Gotta, D.; Gruber, A.; Hirtl, A.; Fuhrmann, H.; Le Bigot, E.-O.; Schlesser, S.; dos Santos, J. M. F.; Simons, L. M.; Stingelin, L.; Trassinelli, M.; Veloso, J.; Wasser, A.; Zmeskal, J.
Highly charged ion X-rays from Electron-Cyclotron Resonance Ion Sources
Nuclear Instruments and Methods in Physics Research Section A **580** (2007) 8.

17. Indelicato, P.; Trassinelli, M.; Anagnostopoulos, D. F.; Boucard, S.; Covita, D. S.; Borchert, G.; Dax, A.; Egger, J. P.; Gotta, D.; Gruber, A.; Hirtl, A.; Hennebach, M.; Fuhrmann, H.; Le Bigot, E.-O.; Liu, Y.-W.; Manil, B.; Nelms, N.; Schlesser, S.; dos Santos, J. M. F.; Simons, L. M.; Stingelin, L.; Veloso, J.; Wasser, A.; Wells, A.; Zmeskal, J.
Experiments on Highly Charged Heavy Ions in Conjunction with Exotic Atoms
Advances in Quantum Chemistry **53** (2007) 217.

18. Levitt, B.; Gabrielse, G.; Larochelle, P.; Le Sage, D.; Kolthammer, W. S.; McConnell, R.; Wrubel, J.; Speck, A.; Grzonka, D.; Oelert, W.; Sefzick, T.; Zhang, Z.; Comeau, D.; George, M. C.; Hessels, E. A.; Storry, C. H.; Weel, M.; Walz, J.
Single-Component Plasma of Photoelectons
Physics Letters B **656** (2007) 25.

19. Maeda, Y.; Sakai, H.; Fujita, K.; Greenfield, M. B.; Hatanaka, K.; Hatano, M.; Kamiya, J.; Kawabata, T.; Kuboki, H.; Okamura, H.; Rapaport, J.; Saito, T.; Sakemi, Y.; Sasano, M.; Sekiguchi, K.; Shimizu, Y.; Suda, K.; Tameshige, Y.; Tamii, A.; Wakasa, T.; Yako, K.; Blomgren, J.; Mermod, P.; Öhrn, A.; Österlund, M.; Witala, H.; Deltuva, A.; Fonseca, A. C.; Sauer, P. U.; Glöckle, W.; Golak, J.; Kamada, H.; Nogga, A.; Skibinski, R.
Differential cross section and analyzing power measurements for $\vec{n}$ elastic scattering at 248 MeV
Physical Review C **76** (2007) 014004.

20. Mersmann, T.; Khoukaz, A.; Büscher, M.; D. Chiladze, D.; Dymov, S.; Hartmann, M.; Hejny, V.; Kacharava, A.; Keshelashvili, I.; Kulessa, P.; Maeda, Y.; Mielke, M.; Mikirtychiants, S.; Ohm, H.; Papenbrock, M.; Prasuhn, D.; Rathmann, F.; Rausmann, T.; Schleichert, R.; Serdyuk, V.; Stein, H.-J.; Ströher, H.; Täschner, A.; Valdau, Yu.; Wilkin, C.; Wronska, A.
Precision Study of the η^3He System Using the $dp \to {}^3$Heη Reaction
Physical Review Letters **98** (2007) 242301.

21. Moskal, P.; Adam, H.-H.; Budzanowski, A.; Czerwinski, E.; Czyzykiewicz, R.; Gil, D.; Grzonka, D.; Janusz, M.; Jarczyk, L.; Kamys, B.; Khoukaz, A.; Klaja, P.; Majewski, J.; Oelert, W.; Piskor-Ignatowicz, C.; Przerwa, J.; Ritman, J.; Rejdych, B.; Rozek, T.; Sefzick, T.; Siemasko, M.; Smyrski, J.; Täschner, A.; Winter, P.; Wolke, M.; Wüstner, P.; Zipper, W.
η and η' meson production at COSY-11
International Journal of Modern Physics A **22** (2007) 305.

22. Nekipelov, M.; Büscher, M.; Hartmann, M.; Keshelashvili, I.; Kleber, V.; Koptev, V.; Maeda, Y.; Mikirtychiants, S.; Schleichert, R.; Sibirtsev, A.; Ströher, H.; Valdau, Yu.
Investigation of the reaction $pp \to pK^0\pi^+\Lambda$ in search of the pentaquark
Journal of Physics G **34** (2007) 627.

23. Oelert, W.; Adam, H.-H.; Budzanowski, A.; Czerwinski, E.; Czyzykiewicz, R.; Gil, D.; Grzonka, D.; Janusz, M.; Jarczyk, L.; Kamys, B.; Khoukaz, A.; Klaja, P.; Moskal, P.; Piskor-Ignatowicz, B.; Przerwa, J.; Rozek, T.; Santo, R.; Sefzick, T.; Siemaszko, M.; Smyrski, J.; Täschner, A.; Winter, P.; Wolke, M.; Wüstner, P.; Zipper, W.
General thoughts to the Kaon pair production in the threshold region
International Journal of Modern Physics A **22** (2007) 502.

24. Piskor-Ignatowicz, C.; Smyrski, J.; Moskal, P.; Adam, H.-H.; Budzanowski, A.; Czerwinski, E.; Czyzykiewicz, R.; Gil, D.; Grzonka, D.; Janusz, M.; Jarczyk, L.; Kamys, B.; Khoukaz, A.; Klaja, P.; Majewski, J.; Oelert, W.; Przerwa, J.; Ritman, J.; Rozek, T.; Sefzick, T.; Siemasko, M.; Täschner, A.; Winter, P.; Wolke, M.; Wüstner, P.; Zipper, W.
Near threshold η meson production in dp collisions
International Journal of Modern Physics A **22** (2007) 528.

25. Smyrski, J.; Adam, H.-H.; Budzanowski, A.; Czerwinski, E.; Czyzykiewicz, R.; Gil, D.; Grzonka, D.; Janusz, M.; Jarczyk, L.; Kamys, B.; Khoukaz, A.; Klaja, P.; Moskal, P.; Oelert, W.; Piskor-Ignatowicz, C.; Przerwa, J.; Ritman, J.; Rozek, T.; Sefzick, T.; Siemasko, M.; Täschner, A.; Winter, P.; Wolke, M.; Wüstner, P.; Zipper, W.
Study of the ^{3}He-η system in *dp* collisions
Nuclear Physics A **790** (2007) 438.

26. Smyrski, J.; Adam, H.-H.; Budzanowski, A.; Czerwinski, E.; Czyzykiewicz, R.; Gil, D.; Grzonka, D.; Janusz, M.; Jarczyk, L.; Kamys, B.; Khoukaz, A.; Klaja, P.; Moskal, P.; Oelert, W.; Piskor-Ignatowicz, C.; Przerwa, J.; Ritman, J.; Rozek, T.; Sefzick, T.; Siemaszko, M.; Täschner, A.; Winter, P.; Wolke, M.; Wüstner, P.; Zipper, W.
Measurement of the $dp \to {}^{3}\mathrm{He}\eta$ reaction near threshold
Physics Letters B **649** (2007) 258.

27. Sokolov, A.; Ritman, J.; Wintz, P.
Application of the time-dependent charge asymmetry method for longitudinal position determination in prototype proportional chambers for the PANDA experiment
Nuclear Instruments and Methods in Physics Research Section A **574** (2007) 50.

28. Speck, A.; Gabrielse, G.; Larochelle, P.; Le Sage, D.; Levitt, B.; Kolthammer, W. S.; McConnell, R.; Wrubel, J.; Grzonka, D.; Oelert, W.; Sefzick, T.; Zhang, Z.; Comeau, D.; George, M. C.; Hessels, E. A.; Storry, C. H.; Weel, M.; Walz, J.
Density and geometry of single component plasmas
Physics Letters B **650** (2007) 119.

29. Stephan, E.; Kistryn, St.; Sworst, R.; Biegun, A.; Bodek, K.; Ciepal, I.; Deltuva, A.; Epelbaum, E.; Fonseca, A.; Glöckle, W.; Golak, J.; Kalantar-Nayestanaki, N.; Kamada, H.; Kis, M.; Kozela, A.; Mahjour-Shafiei, M.; Micherdzinska, A.; Nogga, A.; Sauer, P.; Skibinski, R.; Witala, H.; Zejma, J.; Zipper, W.
Vector and tensor analyzing powers of elastic deuteron-proton scattering at 130 MeV deuteron beam energy
Physical Review C **76** (2007) 057001.

30. Thorngren Engblom, P.; Negasi Keleta, S.; Cappellaro, F.; Hoistad, B.; Jacewicz, M.; Johansson, T.; Koch, I.; Kullander, S.; Pettersson, H.; Schonning, K.; Zlomanczuk, J.; Calen, H.; Fransson, K.; Kupsc, A.; Marciniewski, P.; Wolke, M.; Pauly, C.; Demirors, L.; Scobel, W.; Stepaniak, J.; Zabierowski, J.; Bashkanov, M.; Clement, H.; Khakimova, O.; Kren, F.; Skorodko, T.
Anisotropy in the pion angular distribution of the reaction $pp \to pp\pi^{0}$ at 400 MeV
Physical Review C **76** (2007) 011602.

31. Trassinelli, M.; Boucard, S.; Covita, D. S.; Gotta, D.; Hirtl, A.; Indelicato, P.; Le Bigot, E.-O.; dos Santos, J. M. F.; Simons, L. M.; Stingelin, L.; Veloso, J.F.C.A.; Wasser, A.; Zmeskal, J.
He-like argon, chlorine and sulfur spectra measurement from an Electron Cyclotron Resonance Ion Trap
Journal of Physics, Conference Series **58** (2007) 129.

32. Ullrich, W.; Abdel-Bary, M.; Brinkmann, K. T.; Clement, H.; Dietrich, J.; Doroshkevich, E.; Dshemuchadse, S.; Ehrhardt, K.; Erhardt, A; Eyrich, W.; Freiesleben, H.; Gillitzer, A.; Jäkel, R.; Karsch, L.; Kilian, K.; Kuhlmann, E.; Marcello, S.; Morsch, H.-P.; Pizzolotto, C.; Ritman, J.; Roderburg, E.; Schröder, W.; Schulter-Wissermann, M.; Teufel, A.; Ucar, A.; Wenzel, R.; Wintz, P.; Wüstner, P.; Zupranski, P.
Omega meson production in proton proton collisions
International Journal of Modern Physics A **22** (2007) 621.

33. Valdau, Y.; Koptev, V.; Barsov, S.; Büscher, M.; Dymov, S.; Hartmann, M.; Kacharava, A.; Merzliakov, S.; Mikirtychyants, S.; Mussgiller, A.; Nekipelov, M.; Schleichert, R.; Ströher, H.; Wilkin, C.
The $pp \to K^{+}n\Sigma^{+}$ reaction near threshold
Physics Letters B **652** (2007) 245.

34. Vlasov, P.; Hinterberger, F.; Povtoreiko, A.; Ritman, J.; Siudak, R.
A Cherenkov detector for WASA at COSY
International Journal of Modern Physics A **22** (2007) 612.

35. Wilkin, C.; Büscher, M.; Chiladze, D.; Dymov, S.; Hanhart, C.; Hartmann, M.; Hejny, V.; Kacharava, A.; Keshelashvili, I.; Khoukaz, A.; Maeda, Y.; Mersmann, T.; Mielke, M.; Mikirtychiants, S.; Papenbrock, M.; Rathmann, F.; Rausmann, T.; Schleichert, R.; Ströher, H.; Täschner, A.; Valdau, Yu.; Wronska, A.
Is there an η^{3}He quasi-bound state?
Physics Letters B **654** (2007) 92.

2. Theory

36. Avdeenkov, A.; Grümmer, F.; Kamerdzhiev, S.; Krewald, S.; Lyutorovich, N.; Speth, J.
Self-consistent calculations within the extended theory of finite Fermi systems
Physics Letters B **653** (2007) 196.

37. Baur, G.; Hencken, K.; Trautmann, D.
Electron-positron pair production in ultrarelativistic heavy ion collisions
Physics Reports **453** (2007) 1.

38. Baur, G.; Snover, K. A.; Typel, S.
E0 emission in $\alpha +^{12}$ C fusion at astrophysical energies
Physical Review C **75** (2007) 058801.

39. Baur, G.; Typel, S.
Direct reactions with exotic nuclei, nuclear structure and astrophysics
Progress in Particle and Nuclear Physics **59** (2007) 122.

40. Belushkin, M. A.; Hammer, H.-W.; Meißner, U.-G.
Dispersion analysis of the nucleon form factors including meson continua
Physical Review C **75** (2007) 035202.

41. Bernard, V.; Meißner, Ulf-G.
Chiral perturbation theory
Annual Review of Nuclear and Particle Science **57** (2007) 33.

42. Borasoy, B.; Epelbaum, E.; Krebs, H.; Lee, D.; Meißner, U.-G.
Lattice simulations for light nuclei: Chiral effective field theory at leading order
European Physical Journal A **31** (2007) 105.

43. Borasoy, B.; Epelbaum, E.; Krebs, H.; Lee, D.; Meißner, U.-G.
Two-particle scattering on the lattice: Phase shifts, spin-orbit coupling, and mixing angles
European Physical Journal A **34** (2007) 185.

44. Borasoy, B.; Bruns, P. C.; Meißner, U.-G.; Nißler, R.
A gauge invariant chiral unitary framework for kaon photo- and electroproduction on the proton
European Physical Journal A **34** (2007) 161.

45. Borasoy, B.; Epelbaum, E.; Krebs, H.; Lee, D.; Meißner, U.-G.
Two-particle scattering on the lattice: Phase shifts, spin-orbit coupling and mixing angles
European Physical Journal A **34** (2007) 185.

46. Choudhury, D.; Nogga, A.; Phillips, D. R.
Investigating neutron polarizabilities through Compton scattering on ^{3}He
Physical Review Letters **98** (2007) 232303.

47. Döring, M.
Radiative decay of the Δ(1700)
Nuclear Physics A **786** (2007) 164.

48. Döring, M.; Geng, L.S.; Oset, E.
The Radiative decay of the Λ(1405) and its two-pole structure
European Physical Journal A **32** (2007) 201.

49. Döring, M.; Koch, V.
Charge Fluctuations and electric mass in a hot meson gas
Physical Review C **76** (2007) 054906.

50. Döring, M.; Oset, E.; Strottmann, D.
Chiral dynamics in the $\pi^0\eta$ photoproduction on the proton
International Journal of Modern Physics A **22** (2007) 537.

51. Gasparyan, A.; Haidenbauer, J.; Hanhart, C.; Miyagawa, K.
ΛN scattering length from the reaction $\gamma d \to K^+ \Lambda n$
European Physical Journal A **32** (2007) 61.

52. Golak, J.; Skinbinski, R.; Witala, H.; Glöckle, W.; Nogga, A.; Kamada, H.
Lorentz boosted nucleon-nucleon potential applied to the $^3\vec{\mathrm{He}}(\vec{e}, e'p)pn$ and $^3\vec{\mathrm{He}}(\vec{e}, e'n)pp$
Acta Physica Polonica B **38** (2007) 2143.

53. Grishina, V. Yu.; Büscher, M.; Kondratyuk, L. A.
$K^{-}\,{}^3$He and K^+K^- interactions in the $pd \to {}^3\mathrm{He}K^+K^-$ reaction
Physical Review C **75** (2007) 015208.

54. Hagen, G.; Papenbrock, T.; Dean, D. J.; Schwenk, A.; Nogga, A.; Wloch, M.; Piecuch, P.
Coupled-cluster theory for three-body Hamiltonians
Physical Review C **76** (2007) 034302.

55. Haidenbauer, J.
Meson exchange hyperon-nucleon interaction based on correlated $\pi\pi/K\bar{K}$ exchange
European Physical Journal A **33** (2007) 287.

56. Haidenbauer, J.
Meson-exchange description of hadronic systems: Recent developments
Nuclear Physics A 790 (2007) 457.

57. Haidenbauer, J.; Krein, G.; Meißner, U. G.; Sibirtsev, A.
Meson-exchange description of $\bar{D} - N$ interaction from meson-exchange and quark-gluon dynamics hadronic systems: Recent developments
European Physical Journal A **33** (2007) 107.

58. Hanhart, C.
Towards an understanding of the light scalar mesons
European Physical Journal A **31** (2007) 543.

59. Hanhart, C.; Kalashnikova, Yu. S.; Kudryavtsev, A. E.; Nefediev, A.
Two-photon decays of hadronic molecules
Physical Review D **75** (2007) 074015.

60. Hanhart, C.; Kalashnikova, Yu. S.; Kudryavtsev, A. E.; Nefediev, A. V.
Reconciling the $X(3872)$ with the near-threshold enhancement in the $D^0\bar{D}^0$ final state
Physical Review D **76** (2007) 034007.

61. Hanhart, C.; Kubis, B.; Pelaez, J. R.
Towards an understanding of $a_0 - f_0$ mixing
Physical Review D **76** (2007) 074028.

62. Hanhart, C.; Wirzba, A.
Remarks on $NN \to NN\pi$ beyond leading order
Physics Letters B **650** (2007) 354.

63. Kalantar-Nayestanaki, N.; Epelbaum, E.
The Three-nucleon system as a laboratory for nuclear physics: The need for 3N forces
Nuclear Physics News **17** (2007) 22.

64. Krebs, H.; Epelbaum, E.; Meißner, U.-G.
Nuclear forces with Δ excitations up to next-to-next-to-leading order, part I: Peripheral nucleon-nucleon waves
European Physical Journal A **32** (2007) 127.

65. Lacour, A.; Kubis, B.; Meißner, U.-G.
Hyperon decay form factors in chiral perturbation theory
Journal of High Energy Physics **10** (2007) 083.

66. Lensky, V.; Baru, V.; Epelbaum, E.; Hanhart, C.; Haidenbauer, J.; Kudryavtsev, A.; Meißner, U. G.
Neutron-neutron scattering length from the reaction $\gamma d \to \pi^+ nn$ employing chiral perturbation theory
European Physical Journal A **33** (2007) 339.

67. Lensky, V.; Baru, V.; Haidenbauer, J.; Hanhart, C.; Kudryavtsev, A.; Meißner, U.-G.
Dispersive and absorptive corrections to the pion-deuteron scattering length
Physics Letters B **648** (2007) 46.

68. Meißner, U.-G.
Modern theory of nuclear forces A.D. 2006
European Physical Journal A **31** (2007) 397.

69. Meißner, U.-G.; Rakhimov, A. M.; Wirzba, A.; Yakhshiev, U. T.
Neutron-proton mass difference in isospin-asymmetric nuclear matter
European Physical Journal A **32** (2007) 299.

70. Meißner, U.-G.; Rakhimov, A. M.; Wirzba, A.; Yakhshiev, U. T.
Neutron-proton mass difference in nuclear matter
European Physical Journal A **31** (2007) 357.

71. Nakayama, K.; Oh, Y.; Haidenbauer, J.; Lee, T.-S. H.
On the sign of the $\pi\rho\omega$ coupling constant
Physics Letters B **648** (2007) 351.

72. Navratil, P.; Gueorguiev, V. G.; Vary, J. P.; Ormand, W. E.; Nogga, A.
Structure of $A = 10 - 13$ nuclei with two plus three-nucleon interactions from chiral effective field theory
Physical Review Letters **99** (2007) 042501.

73. Nikolaev, N. N.; Schäfer, W.; Zakharov, B. G.; Zoller, V. R.
Unitarity constraints for deep-inelastic scattering on nuclei: Predictions for electron-ion colliders
JETP Letters **84** (2007) 537.

74. Polinder, H.; Haidenbauer, J.; Meißner, U.-G.
Strangeness $S = -2$ baryon-baryon interactions using chiral effective field theory
Physics Letters B **653** (2007) 29.

75. Sibirtsev, A.; Haidenbauer, J.; Hammer, H.-W.; Meißner, U.-G.
The $pp \to K^+\Sigma^+ n$ cross-section from missing-mass spectra
European Physical Journal A **32** (2007) 229.

76. Sibirtsev, A.; Haidenbauer, J.; Krewald, S.; Meißner, U.-G.; Thomas, A. W.
$K\bar{K}$ photoproduction from protons
European Physical Journal A **31** (2007) 221.

77. Sibirtsev, A.; Haidenbauer, J.; Krewald, S.; Lee, T. S.; Meißner, U.-G.; Thomas, A. W.
Regge approach to charged-pion photoproduction at invariant energies above 2 GeV
European Physical Journal A **34** (2007) 49.

78. Sibirtsev, A.; Haidenbauer, J.; Meißner, U. G.
Comment on "Mass and $K\Lambda$ Coupling of the $N(1535)$"
Physical Review Letters **98** (2007) 039101.

79. Tertychny, G.; Tselyaev, V.; Kamerdzhiev, S.; Grümmer, F.; Krewald, S.; Speth, J.; Avdeenkov, A.; Litvinova, E.
Microscopic description of the low lying and high lying electric dipole strength in stable Ca isotopes
Physics Letters B **647** (2007) 104.

80. Tertychny, G.; Tselyaev, V.; Kamerdzhiev, S.; Grümmer, F.; Krewald, S.; Speth, J.; Litvinova, E.; Avdeenkov, A.
Pygmy dipole resonance in stable Ca isotopes
Nuclear Physics A **788** (2007) 159.

81. Tselyaev, V.; Speth, J.; Grümmer, F.; Krewald, S.; Avdeenkov, A.; Litvinova, E.; Tertychny, G.
Extended theory of finite Fermi systems: Application to the collective and noncollective E1 strength in ^{208}Pb
Physical Review C **75** (2007) 014315.

82. Uzikov, Yu. N.; Haidenbauer, J.
Spin observables of the reactions $NN \to \Delta N$ and $pd \to \Delta pp(^1S_0)$ in collinear kinematics
Physics of Atomic Nuclei **70** (2007) 2138.

83. Uzikov, Yu. N.; Haidenbauer, J.; Wilkin, C.
Dynamics of $^1S_0$ diproton formation in the $pd \to (pp)_s n$ and $pN \to (pp)_s \pi$ reactions in the GeV region
Physical Review C **75** (2007) 014008.

3. Accelerator (including conference proceedings)

84. Chechenin, A.; Senichev, Y.; Vasyukhin, N.
The Optimum Chromacity Scheme Correction for Monochromatic and Non-Monochromatic Beam in HESR
Proceedings of the 22nd Particle Accelerator Conference 2007 (PAC 2007), p. 3286.

85. Chechenin, A.; Senichev, Y.; Vasyukhin, N.
The Regular and Random Multi-pole Errors Influence on the HESR Dynamic Aperture
Proceedings of the 22nd Particle Accelerator Conference 2007 (PAC 2007), p. 3949.

86. Conradie, J.L.; Celliers, P.J.; Villiers, J.G.; Delsink, J.L.G.; du Plessis, H.; du Toit, J.H.; Fenemore, R.E.F.; Fourie, D.T.; Kohler, I.H.; Lussi, C.; Mansfield, P.T.; Mostert, H.; Muller, G.S.; Price, G.S.; Rohwer, P.F.; Sakildien, M.; Thomae, R.W.; Â van Niekerk, M.J.; van Schalkwyk, P.A.; Kormany, Z.; Dietrich, J.; Weis, T.; Adam, S.; Goetz, D.; Schmelzbach, P.A.
Improvements to the iThemba LABS Cyclotron Facilities
Proceedings of the 18th Int. Conference on Cyclotrons and their Applications.

87. Dietrich, J.; Boehme, C.; Weis, T.; Botha, A. H.; Conradie, J. L.; Rohwer, P. F.
Beam Profile Measurements Based on Light Radiation of Atoms Excited by the Particle Beam
Proceedings of the 22nd Particle Accelerator Conference 2007 (PAC 2007), p. 3955.

88. Dietrich, J.; Boehme, C.; Kamerdzhiev, V.
Beam Profile Measurements Based onBeam Interaction with Residual Gas
Proceedings of the 8th Int. Topical Meeting on Nuclear Applications and Utilization of Accelerators (ACCAPP'07), p. 138.

89. Dietrich, J.; Boehme, C.; Weis, T.; Botha, A.H.; Conradie, J.L.; Rohwer, P.F.
Beam Profile Measurements Based on Light Radiation of Atoms Excited by the Particle Beam
CARE-Report-2007-029-HIPPI.

90. Esser, F.; Eichhorn, R.; Laatsch, B.; Singer, H.; Stassen, R.
Results of the first cool down of the Juelich accelerator module
Proceedings of the International Cryogenic Engineering Conference (ICEC21), p. 51.

91. Gebel, R.; Felden, O.; Maier, R.; von Rossen, P.
Tripling the total charge perpulse of the polarized light ion source at COSY/Jülich
Proceedings of the 11th International Symposium on the Production and Neutralization of Negative Ion Beams (PNNIB 2006); AIP Conference Proceedings **925** p. 105.

92. Krisch, A. D.; Leonova, M. A.; Morozov, V. S.; Raymond, R. S.; Sivers, D. W.; Wong, V. K.; Gebel, R.; Lehrach, A.; Lorentz, B.; Maier, R.; Prasuhn, D.; Schnase, A.; Stockhorst, H.; Hinterberger, F.; Ulrich, K.
Unexpected reduction of rf spin resonance strength for stored deuteron beams
Physical Review Special Topics, Accelerators and Beams **10** (2007) 071001.

93. Krisch, A. D.; Leonova, M. A.; Morozov, V. S.; Raymond, R. S.; Sivers, D. W.; Wong, V. K.; Gebel, R.; Lehrach, A.; Lorentz, B.; Maier, R.; Prasuhn, D.; Schnase, A.; Stockhorst, H.; Hinterberger, F.; Ulrich, K.
Experimental test of the new analytic matrix formalism for spin dynamics
Physical Review Special Topics, Accelerators and Beams **10** (2007) 041001.

94. Senichev, Y.
HESR Lattice with Non-Similar Arcs for Stochastic Cooling
Proceedings of the 22nd Particle Accelerator Conference 2007 (PAC 2007), p. 3289.

95. Smirnov, A.V.; Meshkov, I.N.; Sidorin, A.O.; Dietrich, J.; Noda, A.; Shirai, T.; Souda, H.; Tongu, H.; Noda, K.
Necessary Condition for Beam Ordering
Proceedings of the Workshop on Beam Cooling and Related Topics (COOL07), p. 87.

96. Stockhorst, H.; Stassen, R.; Katayama, T.; Thorndahl, L.
Experimental Test of Momentum Cooling Model Predictions at COSY and Conclusions for WASA and HESR
Proceedings of the Symposium on Meson Physics at COSY-11 and WASA at COSY. (AIP Conference Proceedings **950**) p. 239.

97. Stockhorst, H.; Stassen, R.; Maier, R.; Prasuhn, D.; Katayama, T.; Thorndahl, L.
Stochastic Cooling for the HESR at FAIR
Proceedings of COOL 2007, p. 30.

98. Toelle, R.; Bongardt, K.; Dietrich, J.; Esser, F.; Felden, O.; Greven, R.; Hansen, G.; Klehr, F.; Lehrach, A.; Lorentz, B.; Maier, R.; Prasuhn, D.; Raccanelli, A.; Schmitt, M.; Senichev, Y.; Senicheva, E.; Stassen, R.; Stockhorst, H.; Steck, M.; Bergmark, T.; Galnander, B.; Johnson, S.; Johnson, T.; Lofnes, T.; Norman, G.; Peterson, T.; Rathsman, K.; Reistad, D.; Hinterberger, F.
HESR at FAIR: Status of Technical Planning
Proceedings of the 22nd Particle Accelerator Conference (PAC 2007), p. 1442.

4. Miscellaneous

99. Schult, O. W. B.
Die Tatsachen und der Glaube
Die Neue Ordnung **61** (2007) 275.

100. Schult, O. W. B., Feinendegen, L.E.; Shreeve, W.W.; Pierson, R.N.
Optimal use of weight and height for evaluation of obesity and other disorders
International Journal of Body Composition Research **5** (2007) 153.

C Diploma and Ph.D. Theses 2007

1. Diploma

1. F. Ballout,
   Pion-Nucleus Scattering in Chiral Perturbation Theory,
   Universität Bonn
2. M. Freunek,
   Nucleon-Nucleon Interaction in Chiral Effective Field Theory in Configuration Space,
   Universität Bonn
3. M. Mittag,
   Messung zur Ortsabhängigkeit der Energiedeposition geladener Teilchen in Szintillationszählern am Beispiel des WASA-Zentraldetektors,
   Hochschule Merseburg (FH)
4. S. Reimann,
   Untersuchungen zum Energieverlust im Startdetektor des Flugzeitspektrometers TOF und Analyse der Reaktion $pp \to d\pi^+$ bei 3059 MeV/c,
   Technische Universität Dresden
5. E. Schlauch,
   Derivation of a chiral effective operator for the electromagnetic current coupling to a two-nucleon system,
   Universität Bonn
6. C. Weidemann,
   Messung der chemischen Verschiebung von $K\alpha$- und $K\beta$-Übergängen in Mangan,
   Universität zu Köln

2. Ph.D.

7. S. Dymov,
   Investigation of the deuteron breakup by protons of 0.6 – 0.9 GeV with emission of a forward proton pair,
   JINR Dubna, Russia
8. K. Grigoryev,
   A storage cell production for experiments with polarized internal gas target (PIT) at ANKE spectrometer at the COSY storage ring,
   Petersburg, Nuclear Physics Institute, Russia
9. A. Kowalczyk,
   Proton induced spallation reactions in the energy range 0.1 – 10 GeV,
   Jagellionian University Cracow, Poland
10. V. Lensky,
    Elastic and inelastic pion reactions an few nucleon systems,
    Universität Bonn
11. T.Mersmann,
    Untersuchung der η-^{3}He Endzustandswechselwirkung am Experimentaufbau ANKE,
    Universität Münster
12. V.S. Morozov,
    Using Spin Resonances to Manipulate the Polarization of Spin-1/2 and Spin-1 Particle Beams,
    University of Michigan, U.S.A.
13. C. Pizzolotto,
    Measurement of polarisation observables at the COSY-TOF spectrometer,
    Universität Erlangen
14. Z. Zhang,
    The Detection of Cold Antihydrogen Atoms,
    Universität Bochum

D Invited Talks and Colloquia

1. Baur, G.
   Strong electromagnetic fields in ultraperipheral heavy ion collisions: multiphoton processes
   ECT* Workshop on Photoproduction at Collider Energies: from RHIC and HERA to LHC
   Trento, Italy: 15.01.2007 – 19.01.2007

2. Baur, G.
   Direct reactions with exotic nuclei and nuclear astrophysics
   Nuclear Physics in Astrophysics III
   Dresden, Germany: 26.03.2007 – 31.03.2007

3. Baur, G.
   Introductory remarks on Ultraperipheral Heavy Ion Collisions (UPC)
   Session on Photon and Electroweak Boson Physics from HERA, RHIC and Tevatron to LHC, PHOTON 2007
   Paris, France: 09.07.2007 – 13.07.2007

4. Baur, G.
   Very strong electromagnetic fields for a very short time: pair production and ionization in relativistic heavy ion collisions
   Theory Group Meeting of the SPARC Collaboration Atomic Physics in Strong Fields
   Darmstadt, Germany: 17.07.2007 – 18.07.2007

5. Büscher, M.
   The Moscow-Jülich Pellet Target
   PANDA Collaboration Meeting, plenary talk
   Dubna, Russia: 02.07.2007 – 06.07.2007

6. Dietrich, J.
   HESR- Beam Diagnostics — Changes since 7/8 September 2005
   Review Meeting on Beam Diagnostics for the FAIR Project
   Darmstadt, Germany: 14.05.2007

7. Dietrich, J.
   Beam Profile Measurements Based on Light Radiation of Atoms Excited by the Particle Beam
   LANL, Los Alamos, USA: 02.07.2007

8. Dietrich, J.
   COSY — Status and Future
   LANL, Los Alamos, USA: 02.07.2007

9. Dietrich, J.
   Beam Profile Measurements Based on Beam Interaction with Residual Gas
   8th International Topical Meeting on Nuclear Applications and Utilization of Accelerators (ACCAPP'07)
   Pocatello, Id., USA: 29.07.2007 – 02.08.2007

10. Dietrich, J.
    Beam Profile Measurements Based on Light Radiation of Atoms Excited by the Particle Beam
    HIPPI 07
    Orsay, France: 26.09.2007 – 28.09.2007

11. Dietrich, J.
    Tune Measurements at COSY with Noise Excitation
    CARE-N3 networking for HHH
    Chamonix, France: 11.12.2007 – 13.12.2007

12. Dietrich, J.
    Beam Profile Measurements Based on Light Radiation of Atoms Excited by the Particle Beam
    COSY FFE Workshop
    Bad Honnef, Germany: 18.12.2007 – 19.12.2007

13. Dzyuba, A.
    Study of kaon anti-kaon pair production at the ANKE spectrometer (COSY)
    Seminar talk, PNPI
    Gatchina, Russia: 09.01.2007

14. Dzyuba, A.
    Kaon-Pair Production in Hadron-Induced Reactions at ANKE
    11th International Conference on Meson-Nucleon Physics and the Structure of the Nucleon (MENU2007)
    Jülich, Germany: 10.09.2007 – 14.09.2007

15. Dzyuba, A.
    $K\bar{K}$-pair production near threshold in nucleon-nucleon scattering at the ANKE spectrometer
    Seminar talk, PNPI
    Gatchina, Russia: 23.10.2007

16. Engels, R.
    The Lamb-shift Polarimeter for the polarized Fusion Experiment
    Workshop on Polarized Fusion
    Gatchina, Russia: 02.10.2007 – 06.10.2007

17. Engels, R.
    First Experiments with the Polarized Internal Gas Target (PIT) at ANKE/COSY
    12th International Workshop on Polarized Sources, Targets and Polarimeter (PSTP2007)
    Brookhaven, NY, USA: 10.09.2007 – 14.09.2007

18. Engels, R.
    A New Application of a Lamb-shift Polarimeter
    12th International Workshop on Polarized Sources, Targets and Polarimeter (PSTP2007)
    Brookhaven, NY, USA: 10.09.2007 – 14.09.2007

19. Epelbaum, E.
    Subleading $3N$ interactions in chiral EFT
    Workshop on Three-Nucleon Interactions from Few- to Many-Body Systems, TRIUMF
    Vancouver, Canada: 12.03.2007 – 16.03.2007

20. Epelbaum, E.
    Δ-resonance contributions to the nuclear force
    Workshop on Effective Field Theories and Few-Nucleon Systems
    Okayama, Japan: 01.06.2007 – 02.06.2007

21. Epelbaum, E.
    Effective Field Theories in Nuclear Physics
    Okayama University of Science, Invited lecture
    Okayama, Japan: 02.06.2007

22. Epelbaum, E.
    Chiral dynamics of two- and three-body systems
    ECT* Workshop on Advanced Many-body Methods for Nuclear Physics
    Trento, Italy: 02.06.2007 – 06.06.2007

23. Epelbaum, E.
    Chiral dynamics of few-nucleon system
    International Nuclear Physics Conference
    Tokyo, Japan: 03.06.2007 – 08.06.2007

24. Epelbaum, E.
    Chiral effective potential with Delta degrees of freedom
    20th European Conference on Few-Body Problems in Physics
    Pisa, Italy: 10.09.2007 – 14.09.2007

25. Epelbaum, E.
    Δ-resonance contributions to the nuclear force
    International Symposium on Meson-Nucleon Physics and the Structure of Hadrons
    Jülich, Germany: 10.09.2007 – 14.09.2007

26. Epelbaum, E.
    Few-nucleon forces and systems in chiral effective field theory
    20th European Conference on Few-Body Problems in Physics
    Pisa, Italy: 10.09.2007 – 14.09.2007

27. Epelbaum, E.
    Effective field theory and nuclear forces
    Jahrestagung des Komitees für Hadronen- und Kernphysik
    Darmstadt, Germany: 25.10.2007 – 26.10.2007

28. Epelbaum, E.
    Chiral dynamics in few-nucleon systems: current status and future perspectives
    Bonn, Germany: 08.11.2007

29. Fedorets, P.
    Droplet production from thin cryogenic jets with the Moscow-Jülich Pellet Target
    Frühjahrstagung der Deutschen Physikalischen Gesellschaft
    Gießen, Germany: 12.03.2007 – 16.03.2007

30. Fedorets, P.
    A Frozen Pellet Target for PANDA
    11th International Conference on Meson-Nucleon Physics and the Structure of the Nucleon (MENU2007)
    Jülich, Germany: 10.09.2007 – 14.09.2007

31. Fedorets, P.
    Presentation of MPEI and ITEP
    PANDA Coordination Board Meeting, XXII. Collaboration Meeting
    Darmstadt, Germany: 17.09.2007 – 19.09.2007

32. Fedorets, P.
    Development of a Pellet Target for Internal Experiments
    COSY-FFE Workshop and CANU Meeting
    Bad Honnef, Germany: 17.12.2007 – 19.12.2007

33. Fröhlich, I.
    Pluto: A Monte Carlo Simulation Tool for Hadronic Physics
    XI International Workshop on Advanced Computing and Analysis Techniques in Physics Research
    Amsterdam, The Netherlands: 23.04.2007 – 27.04.2007

34. Gebel, R.
    Operation of the injector cyclotron JULIC for the Cooler Synchrotron COSY/Jülich
    International Conference for Cyclotrons and their Applications, Cyclotrons 2007
    Giardini-Naxos: 01.10.2007 – 05.10.2007

35. Gebel, R.
    Polarized H^- and D^- Beams at COSY/Jülich
    Polarized Sources, Targets and Polarimetry (PSTP 2007)
    Brookhaven, NY, USA: 10.09.2007 – 14.09.2007

36. Goldenbaum, F.
    Cosmic Rays Nucleosynthesis and Spallation Processes in the Early Galaxy
    School on Pulsed Neutrons: Characterization of Materials
    Trieste, Italy: 17.10.2007

37. Goldenbaum, F.
    Spallation Physics and Computer Modeling
    School on pulsed neutrons: Characterization of Materials (lecture, Invited by IAEA)
    ICTP, Miramare, Trieste, Italy: 15.10.2007 – 26.10.2007

38. Goldenbaum, F.
    Evaporation and pre-equilibrium emission and fission time scale in GeV proton-induced spallation reactions
    International Conference on Nuclear Fragmentation; From basic Research to Applications (NUFRA2007)
    Kemer/Antalya, Turkey: 24.09.2007 – 01.10.2007

39. Goldenbaum, F.
Evaporation, fission and pre-equilibrium emission in GeV proton-induced spallation reactions
GSI-Colloquium Talk
Darmstadt, Germany: 23.05.2007

40. Goldenbaum, F.
Progress in nuclear data for accelerator applications in Europe
International Conference on Nuclear Data for Science and Technology (ND2007)
Nice, France: 22.04.2007 – 27.04.2007

41. Gotta, D.
Pionic *NN* interactions at Threshold πN and π Atoms
Workshop on Precision Measurements at Low Energy, Paul Scherrer Institut
Villigen, Switzerland: 17.01.2007 – 18.01.2007

42. Gotta, D.
Prospects of Exotic-Atom Bragg Spectroscopy
International Workshop SPARC
Paris, France: 12.02.2007 – 15.02.2007

43. Gotta, D.
X-rays from Pionic and Antiprotonic Atoms
Atomphysik-Seminar, GSI
Darmstadt: 13.06.2007

44. Grigoryev, K.
The Polarized Internal gas Target at ANKE: a first double-polarized experiment
Frühjahrstagung der Deutschen Physikalischen Gesellschaft
Gießen, Germany: 12.03.2007 – 16.03.2007

45. Grigoryev, K.
The Polarized Internal gas Target at ANKE: a first double-polarized experiment
ANKE/PAX Workshop on SPIN PHYSICS
Ferrara, Italy: 29.06.2007 – 01.06.2007

46. Haidenbauer, J.
Hyperon-nucleon interaction
Symposium on Meson Physics at COSY-11 and WASA-at-COSY
Cracow, Poland: 17.06.2007 – 22.06.2007

47. Haidenbauer, J.
Meson production in nucleon-nucleon collisions
The 20th European Conference on Few-Body Problems in Physics
Pisa, Italy: 10.09.2007 – 14.09.2007

48. Hanhart, C.
How and when can one identify hadronic molecules in the baryon spectrum
International Conference on Baryon Spectroscopy (NSTAR2007)
Bonn, Germany: 05.09.2007 - 08.09.2007

49. Hanhart, C.
How to identify hadronic molecules
Universität Bern, seminar talk
Bern, Switzerland: 04.04.2007

50. Hanhart, C.
How to identify hadronic molecules
Universita Autonoma de Barcelona, seminar talk
Barcelona, Spain: 09.05.2007

51. Hanhart, C.
On the nature of light scalar mesons
International Workshop on Production and Decay of η and η' Mesons (Eta07)
Peniscola, Spain: 10.05.2007

52. Hanhart, C.
Reconciling the X(3872) with the near-threshold enhancement in the $D_0 \bar{D}_0^*$ final state
International Workshop on Heavy Quarkonium 2007, DESY
Hamburg, Germany: 17.10.2007 – 20.10.2007

53. Hanhart, C.
The effect of isospin violation on scalar meson production
XII International Conference on Hadron Spectroscopy (HADRON07)
Frascati, Rome: 08.10.2007 – 13.10.2007

54. Hanhart, C.
Towards an understanding of the hadron spectrum
Universität Tübingen, seminar talk
Tübingen, Germany: 26.01.2007

55. Hanhart, C.
What we can learn from spectroscopy — and what not
BRAG2007
Bonn, Germany: 04.09.2007

56. Hügging, F.; Mertens, M.; Ritman, J.; Stockmanns, T.
Development of a Versatile Readout System for High Rate Detector Electronics 11th International Conference on Meson-Nucleon Physics and the Structure of the Nucleon (MENU2007)
Jülich, Germany: 10.09.2007 – 14.09.2007

57. Janusz, M.; Yurev, L.
From Charged tracks to the ChPT anomalies
11th International Conference on Meson-Nucleon Physics and the Structure of the Nucleon (MENU2007)
Jülich, Germany: 10.09.2007 – 14.09.2007

58. Jany, B.R.
η' Decays with WASA-at-COSY
11th International Conference on Meson-Nucleon Physics and the Structure of the Nucleon (MENU2007)
Jülich, Germany: 10.09.2007 – 14.09.2007

59. Kleines, H.; Zwoll, K.; Wüstner, P.; Erven, W.; Kämmerling, P.; Kemmerling, G.; Loevenich, H.; Ackens, A.; Wolke, M.; Hejny, V.; Ohm, H.; Sefzick, T.; Nellen, R.; Marciniewski, P.; Fransson, K.; Gustafsson, L.; Kupsc, A.; Calen, H.
Performance Issues of the New DAQ System for WASA at COSY
15th IEEE Real Time Conference 2007 (RT 07)
Batavia, Ill., USA: 29.04.2007 – 04.05.2007

60. Krewald, S.
Baryon resonance analysis with the Jülich meson exchange model
Workshop on the Physics of Excited Nucleons (NSTAR2007)
Bonn, Germany: 05.09.2007 – 08.09.2007

61. Krewald, S.
Extendend Theory of Finite Fermi Systems
The 3rd Japanese-German EFES(JSPS)-DFG/GSI Workshop on Nuclear Structure and Astrophysics
Frauenwoerth, Germany: 29.09.2007 – 02.10.2007

62. Lehrach, A.
General Design Criteria, Lattice Concepts and Structures for HESR
Review Meeting MiniTAC Lattice for the FAIR Project
Darmstadt, Germany: 5.6.2007

63. Lehrach, A.
HESR Design
Review Meeting TAC for the FAIR Project
Darmstadt, Germany: 11. – 13.06.2007

64. Lehrach, A.
    Fixed Target and Collider Options for HESR at FAIR
    Hard QCD with Antiprotons at GSI FAIR
    Trento, Italy: 16. – 20.07.2007

65. Lehrach, A.
    High-Energy Storage Ring (HESR)
    11th International Conference on Meson-Nucleon Physics and the Structure of the Nucleon (MENU2007)
    Jülich, Germany: 10.09.2007 – 14.09.2007

66. Lehrach, A.
    Relevant storage ring properties and limitations
    Workshop on Polarized Antiproton Beams — How?
    Daresbury, England: 29. – 31.08.2007

67. Meißner, U.-G.
    On the low-energy constants of the chiral effective pion-nucleon Lagrangian
    Workshop on Three-Nucleon Interactions from Few- to Many-Body Systems
    TRIUMF, Vancouver, Canada: 12.03.2007 – 16.03.2007

68. Meißner, U.-G.
    HadronTH: Structure and dynamics of hadrons
    I3HP Collaboration Committee Meeting
    Frascati, Italy: 20.05.2007

69. Meißner, U.-G.
    Nucleon from factors from dispersion theory
    Jefferson Lab User Group Meeting 2007
    Newport News, USA: 18.06.2007 – 20.06.2007

70. Meißner, U.-G.
    Hadronic atoms
    International Conference on Hadron Physics TROIA'07
    Canakkale, Spain: 30.08.2007 – 01.09.2007

71. Meißner, U.-G.
    QCDnet: Hadron physics with light and heavy quarks
    I3 HadronPhysics2 Opening Meeting
    Frascati, Italy: 28.09.2007 – 29.09.2007

72. Meißner, U.-G.
    Quark mass dependence of baryons
    HadronTHÂ´07 Workshop
    Barcelona, Spain: 01.10.2007 – 05.10.2007

73. Meißner, U.-G.
    Three-nucleon forces from effective field theory: Why Fujita and Miyazawa were not just lucky
    International Symposium on New Facet of Three Nucleon Force — 50 years of Fujita-Miyazawa Three Nucleon Force (FM50)
    Tokyo, Japan: 29.10.2007 – 31.10.2007

74. Nekipelov, M.
    Present Understanding of Spin-Filtering Experiments
    11th International Conference on Meson-Nucleon Physics and the Structure of the Nucleon (MENU2007)
    Jülich, Germany: 10.09.2007 – 14.09.2007

75. Nogga, A.
    Approaching light nuclei and hypernuclei based on chiral interactions
    20. European Conference on Few-Body Problems in Physics (EFB20)
    Pisa, Italy: 10.09.2007

76. Nogga, A.
Correlations in few-nucleon systems
Workshop on Dense and Cold Nuclear Matter and Hard Exclusive Processes
Ghent, Belgium: 20.08.2007 – 24.08.2007

77. Nogga, A.
Understanding light nuclei based on simulations
VSR-Seminar
Jülich, Germany: 12.12.2007

78. Oelert, W.
Antimaterie — 10 Jahre danach
Haus Overbach
Jülich, Germany: 19.01.2007

79. Oelert, W.
AD-Physics 2007 and Beyond
Workshop AB-Division, CERN
Geneva, Switzerland: 23.01.2007

80. Oelert, W.
Antimaterie — die gespiegelte Welt — die geheimnisvolle Materie aus Antiteilchen - I
Seminar für Schüler des Ansbachgymnasiums
Jülich, Germany: 13.03.2007

81. Oelert, W.
Antimaterie — die gespiegelte Welt — die geheimnisvolle Materie aus Antiteilchen - II Seminar für Schüler des Ansbachgymnasiums
Jülich, Germany: 15.03.2007

82. Oelert, W.
Antimatter — the mirrored world of matter
Polish Academy of Art and Sciences
Cracow, Poland: 29.05.2007

83. Oelert, W.
Production of Antihydrogen
Jagellonian University, Physics Institute
Cracow, Poland: 30.05.2007

84. Polinder, H.
Hyperon-nucleon interactions in effective field theory
Workshop on Hadron Physics with COSY-TOF
Jülich, Germany: 20.03.2007 – 21.03.2007

85. Polinder, H.
$S = -1, -2$ baryon-baryon interactions in chiral effective field theory
International Nuclear Physics Conference (INPC2007)
Tokyo, Japan: 03.06.2007 – 08.06.2007

86. Polinder, H.
Strange two-baryon interactions using chiral effective field theory
20th European Conference on Few-Body Problems in Physics (EFB20)
Pisa, Italy: 10.09.2007 – 14.09.2007

87. Redmer, C.F.
In search of the box anomaly with the WASA-at-COSY facility
Symposium on Meson Physics at COSY-11 and WASA-at-COSY
Cracow, Poland: 17.06.2007 – 22.06.2007

88. Redmer, C.F.
In search of the box anomaly with the WASA-at-COSY facility
11th International Conference on Meson-Nucleon Physics and the Structure of the Nucleon (MENU2007)
Jülich, Germany: 10.08.2007 – 14.08.2007

89. Ritman, J.
Investigations of fundamental Symmetries in Hadronic Systems — Start of WASA-at-COSY
International Workshop XXXV on Gross Properties of Nuclei and Nuclear Excitations
Hirschegg, Austria: 14.01.2007 – 20.01.2007

90. Ritman, J.
WASA-at-COSY
Internationales Graduierten-Kolleg, Universität Giessen
Giessen, Germany: 24.05.2007

91. Ritman, J.
FAIR: a Horizon for Future Charming Physics
Symposium on Meson Physics at COSY11 and WASA-at-COSY
Cracow, Poland: 19.06.2007 – 20.06.2007

92. Ritman, J.
Hadron Physics Experiments at the COSY Facility
XII International Conference on Hadron Spectroscopy (HADRON07)
Frascati, Italy: 08.10.2007 – 10.10.2007

93. Ritman, J.
Perspektiven Hadronischer Sonden
Jahrestreffen des Komittee Hadronen- und Kernphysik
Darmstadt, Germany: 25.10.2007 – 26.10.2007

94. Senichev, Y.
The advanced HESR lattice for improved stochastic cooling
COOL 2007
Bad Kreuznach, Germany: 10.09.2007 – 14.09.2007

95. Senichev, Y.
Possible lattices with imaginary gamma-transition for PS2: why and how?
BEAM 2007, CERN
Geneva, Switzerland: 01.10.2007 – 05.10.2007

96. Stockhorst, H.; Stassen, R.; Katayama, T.; Thorndahl, L.
Experimental Test of Momentum Cooling Model Predictions at COSY and Conclusions for WASA and HESR
Symposium on Meson Physics at COSY-11 and WASA-at-COSY
Cracow, Poland: 17.06.2007 – 22.06.2007

97. Stockhorst, H.; Stassen, R.; Katayama, T.; Thorndahl, L.
Theory of Stochastic Momentum Cooling
Symposium on Meson Physics at COSY-11 and WASA-at-COSY
Cracow, Poland: 17.06.2007 – 22.06.2007

98. Stockhorst, H.; Stassen, R.; Maier, R.; Prasuhn, D.; Katayama, T.; Thorndahl, L.
Stochastic Cooling for the HESR at FAIR
Workshop on Beam Cooling and Related Topics (COOL07)
Bad Kreuznach, Germany: 10.09.2007 – 14.09.2007

99. Stockmanns, T.; Hügging, F.; Mertens, M.; Ritman, J.
A high rate, high resolution Micro-Vertex-Detector for the PANDA-Experiment
11th International Conference on Meson-Nucleon Physics and the Structure of the Nucleon (MENU2007)
Jülich, Germany: 10.09.2007 – 14.09.2007

100. Stockmanns, T.
Open and hidden charm at PANDA
XII International Conference on Hadron Spectroscopy (HADRON07)
Frascati, Italy: 08.10.2007 – 13.10.2007

101. Strauch, T.
Pionic Deuterium
Frühjahrstagung der Deutschen Physikalischen Gesellschaft
Gießen, Germany: 12.03.2007 – 16.03.2007

102. Strauch, T.
Pionic Deuterium
11th International Conference on Meson-Nucleon Physics and the Structure of the Nucleon (MENU2007)
Jülich, Germany: 10.09.2007 – 14.09.2007

103. Ströher, H.
How to polarize antiprotons and what to do with it?
Hirschegg 2007: Structure and Dynamics of Hadrons
Hirschegg, Austria: 17.01.2007

104. Ströher, H.
Programm Physik der Hadronen
Helmholtz Forschungsbereich Struktur der Materie
Berlin, Germany: 03.04.2007

105. Ströher, H.
From ANKE/COSY to PAX/FAIR
ANKE-PAX Collaboration Meeting/Workshop on Spin Physics
Ferrara, Italy: 30.04.2007

106. Ströher, H.
Workshop Summary
ANKE-PAX Collaboration Meeting/Workshop on Spin Physics
Ferrara, Italy: 01.05.2007

107. Wirzba, A.
The Casimir effect as scattering problem
Workshop on Quantum Field Theory under the Influence of External Conditions (QFEXT07)
Leipzig, Germany: 16.09.2007 – 21.09.2007

108. Wolke, M.
WASA-at-COSY — Symmetries and Symmetry Breaking
Kernphysikalisches Kolloquium, Universität Bonn
Bonn, Germany: 25.01.2007

109. Wolke, M.
Status report on the experiments with WASA-at-COSY
2nd International EtaMesonNet Workshop (ETA07)
Peniscola, Spain: 10.05.2007 – 11.05.2007

110. Wolke, M.
From the candle COSY-11 to the flambeau (fackla) of WASA-at-COSY: a ship we entered to study symmetries in nature
Symposium on Meson Physics at COSY-11 and WASA-at-COSY
Cracow, Polen: 17.06.2007 – 22.06.2007

111. Wolke, M.
η Meson Decays with WASA-at-COSY
11th International Conference on Meson-Nucleon Physics and the Structure of the Nucleon (MENU2007)
Jülich, Germany: 10.09.2007 – 14.09.2007

112. Wolke, M.
Hadronenphysik an COSY
KHuK Jahrestreffen
Darmstadt, Germany: 26.10.2007 – 27.10.2007

113. Yuan, X.
Measurement of the reaction $dd \rightarrow \alpha K^+K^-$ with ANKE/COSY
Frühjahrstagung der Deutschen Physikalischen Gesellschaft
Gießen, Germany: 12.03.2007 – 16.03.2007

114. Yuan, X.
Measurement of the reaction $dd \rightarrow \alpha K^+K^-$ with ANKE/COSY
11th International Conference on Meson-Nucleon Physics and the Structure of the Nucleon (MENU2007)
Jülich, Germany: 10.09.2007 – 14.09.2007

115. Zychor, I.
Studies of $\Lambda(1405)$ in pp Collisions with ANKE at COSY-Jülich
11th International Conference on Meson-Nucleon Physics and the Structure of the Nucleon (MENU2007)
Jülich, Germany: 10.09.2007 – 14.09.2007

E Funded Projects

Project	Responsible	Partner Institute	Funded by
Virtual Institute Spin and Strong QCD	U.-G. Meißner	GSI, Univ.'s Bern, Bonn, Ferrara, Cracow, Torino	HGF
CARE	R. Tölle		EU/FP6
TA-COSY	D. Grzonka		EU/FP6
Hadron Physics Theory Netzwerk	U.-G. Meißner	Network	EU/FP6
EtaMesonNet	W. Oelert	Network	EU/FP6
Pellet Target	M. Büscher	ITEP, MPEI Moscow (Russia)	EU/FP6
EURONS/EXL	D. Grzonka		EU/FP6
EUROTRANS/NUDATRA	F. Goldenbaum		EU/FP6
DIRAC Secondary Beams	R. Tölle		EU/FP6
DIRAC Phase 1	R. Tölle		EU/FP6
DIRAC Secondary Beams PANDA-4	J. Ritman		EU/FP6
DIRAC Second. Beams PANDA-2	J. Ritman		EU/FP6
Advanced Residual Gas Profile Monitor	J. Dietrich	GSI	EU/FP6
Design Study for Pick-up Electronic Development	J. Dietrich	GSI	EU/FP6
Strange and Charmed Scalar Mesonss	M. Büscher	ITEP, INR Moscow (Russia)	DFG
Light Scalar Resonances $a_0/f_0(980)$	M. Büscher	ITEP, MPEI Moscow (Russia)	DFG
Scalar Mesons	M. Büscher	ITEP, INR Moscow (Russia)	DFG
Pellet Target	M. Büscher	ITEP, MPEI Moscow (Russia)	DFG
K^- Production in Nuclei	M. Hartmann	ITEP Moscow (Russia)	DFG
Isospin Violation	M. Büscher	IMP Lanzhou (China)	DFG
Jets in Hard Processes	N.N. Nikolaev	Landau Inst., ITEP Moscow (Russia)	DFG
Properties of Unstable Nuclei	S. Krewald	Petersburg State Univ., IPPE Obninsk (Russia)	DFG
Pion Reactions on Few Nucleon Systems	C. Hanhart	ITEP Moscow (Russia)	DFG
Quark-gluon degrees of freedom in the confinement region of QCD	J. Haidenbauer	UNESP Sao Paulo (Brasil)	DFG
ATRAP	W. Oelert	Univ. Mainz	DFG
Fundamental Research with Hadrons	W. Oelert	Jagellinian Univ. Cracow (Poland)	DFG
Broken Symmetries	H. Machner	Univ. Helsinki (Finland)	DAAD
PPP Poland	P.v. Rossen		DAAD
Rare Decays of η and η' Mesons	S. Schadmand	Indian Inst. of Technology Bombay	DAAD/DST India
Spin observables in $\vec{d}\vec{p}\to\{pN\}N$ at low transferred momenta	J. Haidenbauer	JINR Dubna (Russia)	Heisenberg-Landau Program
Eta-Meson Physics	H. Machner	BARC Mumbai (India)	Int. Büro BMBF
Target Development for nuclear physics experiments at COSY and AEA cyclotron	J. Ritman	AEA Cairo (Egypt)	Int. Büro BMBF
Medical Applications of Accelerators	J. Dietrich	iThemba LABS (South Africa)	Int. Büro BMBF
A Pellet Target for PANDA	M. Büscher	ITEP, MPEI Moscow (Russia) Uppsala Univ. (Sweden), GSI	INTAS
Advanced Beam Dynamic for Storage Rings	A. Lehrach		INTAS
EM-processes in the peripheral collisions of relativistic and ultrarelativistic heavy ions	G. Baur	Belfast, Tashkent, Arkhangelsk	GSI-INTAS
Projectile Electron Losses in the Collisions of Fast and Relativistic Low Charged Ions	G. Baur	GSI, Stockholm, Tashkent, Moscow, Arkhangelsk	GSI-INTAS
Polarized Target	F. Rathmann	PNPI Gatchina (Russia)	ISTC
Few Nucleon Systems in χEFT	E. Epelbaum	Univ. Bonn	HGF
Baryon Resonance Analysis	U.-G. Meißner	JLAB (U.S.A.)	JLAB

F COSY-FFE Projects

Project	Responsible	Institute
Θ^+ und Anti-decuplet	Prof. K. Goeke	Univ. Bochum
Frozen Spin Target	Prof. W. Meyer	Univ. Bochum
Entwicklung von Software zur Teilchenidentifikation und Erkennung von split-offs im el.-magn. Kalorimeter des WASA-Experiments	Prof. U. Wiedner	Univ. Bochum
Zusammenarbeit von HISKP-Bonn an internen Experimenten an COSY	Prof. J. Bisplinghoff	Univ. Bonn
Polarisiertes Target für TOF	Dr. H. Dutz	Univ. Bonn
Theorectical studies of strangeness and charm production at COSY and PANDA/FAIR	Prof. H.-W. Hammer	Univ. Bonn
Entwicklung eines Partialwellenprogrammes für die Analyse von Daten von WASA	Prof. E. Klempt	Univ. Bonn
Zusammenarbeit an COSY H-Strahl Laserdiagnose	Prof. T. Weis	Univ. Dortmund
COSY-TOF detector	Prof. H. Freiesleben	TU Dresden
Bau von Detektoren für ANKE und K^--Nachweis	Prof. B. Kämpfer	FZ Dresden-Rossendorf
Measurement of the degree of polarisation of laser accelerated protons	Prof. O. Willi	Univ. Düsseldorf
Theoretische Untersuchungen zur künftigen COSY-Physik	Prof. M. Dillig	Univ. Erlangen-Nürnberg
Bau eines Cherenkovdetektors für WASA at COSY	Prof. W. Eyrich	Univ. Erlangen-Nürnberg
Experimente mit COSY-TOF	Prof. W. Eyrich	Univ. Erlangen-Nürnberg
Polarization experiments with ANKE at COSY	Prof. E. Steffens	Univ. Erlangen-Nürnberg
Meson production and resonance properties in the coupled channel K-Matix approach	Prof. U. Mosel	Univ. Gießen
ANKE Experiment und Auswertung $pp \to dK^+\bar{K}^0$	Prof. H. Paetz gen. Schieck	Univ. Köln
Schwellenexperimente an COSY-11 und ANKE	Dr. A. Khoukaz	Univ. Münster
Installation und Inbetriebnahme des WASA-Detektors am COSY-Ring und Durchführung von Experimenten an WASA at COSY	Prof. H. Clement	Univ. Tübingen
Experimente an COSY-TOF	Prof. H. Clement	Univ. Tübingen
Polarized internal target for ANKE at COSY	Prof. M. Nioradze	Tbilisi State Univ. (Georgia)
Spin dependence in pd interactions	Prof. P. Dalpiaz	Univ. Ferrara (Italy)
Photonendetektor an ANKE	Prof. A. Magiera	Jagellinian Univ. Cracow (Poland)
WASA at COSY	Prof. M. Jezabek	INP Crakow (Poland)
Strange Baryon Produktion at ANKE	Prof. Z. Sujkowski	IPJ Otwock-Swierk (Poland)
Neutron tagging and strangeness production at ANKE	Dr. V. Koptev	PNPI Gatchina (Russia)
Set-up and research with the spectator/vertex detection system at ANKE-COSY	Prof. V. Kulikov	JINR Dubna (Russia)
Investigation of scalar meson production in pp, pd and dd collisions	Prof. L. Kondratyuk	ITEP Moscow (Russia)
Development of a frozen-pellet target	Dr. A. Gerasimov	ITEP Moscow (Russia)
Development, commissioning and operation of components for the COSY experiments WASA and ANKE and spin-filtering studies at COSY as preparation of the PAX experiment in the framework of the FAIR project at GSI	Dr. A. Vasilyev	PNPI Gatchina (Russia)
Development of online software tools for COSY-TOF	Prof. V.N. Afanasiev	MIEM Moscow (Russia)
Cooperation COSY-WASA for $pp \to pp\eta$ and $pp \to pp\eta\pi^0$	Prof. T. Johansson	Uppsala Univ. (Sweden)
Search for mixing between light mesons	Prof. A. Rudchik	INR Kiev (Ukraine)
Unified analysis of meson production in hadronic reactions	Prof. K. Nakayama	Univ. of Georgia (U.S.A.)
SPIN@COSY: Spin-Manipulating Polarized Deuterons and Protons	Prof. A. Krisch	Univ. of Michigan (U.S.A.)

G Conferences (co-)organized by the IKP

G.1 The 11th International Conference on Meson-Nucleon Physics and the Structure of the Nucleon, MENU2007

The common aspects in both the charmed quark sector and in the light quark sector were the major reason to bring together 354 experts from high-energy physics and nuclear physics to the 11th International Conference on Meson-Nucleon Physics and the Structure of the Nucleon, which took place on 10–14 September at the FZJ.

The plenary talks summarized the progress in light quark physics, such as in studies of η and η' decay, exotic atoms, three-nucleon forces, and lattice methods and recent discoveries of particles both with open and hidden charm, and the opportunities opened by studying the decays of those particles. The progress at the new Japanese facility JPARC, the European FAIR project, and the 12 GeV upgrade at the Thomas Jefferson Laboratory were presented in detail. There were five parallel sessions covering special topics such as spin physics, meson and baryon spectroscopy, lattice calculations and in-medium physics. Willem Van Oers, Manitoba University, spoke as the representative of the International Union of Pure and Applied Physics who together with FZJ, Deutsche Forschungsgemeinschaft, Jefferson Lab, and the Hadron Physics I3 FP6 European Community Programme made this conference possible. The next MENU conference will be held in Newport News, Virginia, in 2010. Reports about the conference can be found in the March issue of the CERN courier, http://cerncourier.com/cws/latest/cern, and in the Nuclear Physics News International, http://www.nupecc.org/nupecc. Proceedings are on the econf archive at SLAC. For slides of the talks, see www.fz-juelich.de/ikp/menu2007.

G.2 Symposium on Meson Physics at COSY-11 and WASA-at-COSY, Cracow (Poland)

The international Symposium on Meson Physics at COSY-11 and WASA-at-COSY was held in Cracow from June 17–22 on the occasion of the completion of the COSY-11 experiment. It also coincided with the beginning of the experimentation with the WASA apparatus which was successfully transferred from CELSIUS facility in Uppsala to the cooler synchrotron COSY.
Since the core of the COSY-11 group is based on an exemplary German-Polish collaboration, the main sessions took place in Libraria of the Collegium Maius at Jagellonian University. This location has great significance as it is where Nicolaus Copernicus learned astronomy.

Fig. 57: Participants of the symposium on Meson Physics at COSY-11 and WASA-at-COSY in the medieval courtyard of the Collegium Maius of the Jagellonian University.

In the first part of the meeting the scientific achievements of the COSY-11 group were summarized and the status on the ongoing data evaluation for more than ten projects was reported. The second part of the symposium was devoted to the prospects for studies of the fundamental symmetries by means of the η and η' decays with the newly commissioned WASA-at-COSY facility.

Fig. 56: MENU2007 participants in front of the lecture hall of FZJ

Fig. 58: Participants of the WASA-at-COSY analysis meeting in front of the main building of the Institute of Nuclear Physics in Cracow.

The physics of the η and η' mesons receives increasing interest with complementary experimental programmes planned at DAΦNE-2 and MAMI-C facilities. The plans were presented by invited guests from these laboratories. The symposium continued at the Institute of Nuclear Physics in Cracow where the participants met to discuss the status of the simulations and the data analysis from the first WASA-at-COSY production run in April 2007. Written contributions have been published in volume 950 of the International Conference Proceedings Series of the American Institute of Physics. The symposium was jointly organized by the Jagellonian University, Institute of Nuclear Physics PAN, IKP of the Research Center Jülich and the University of Silesia. More information regarding the meeting is available via http://confer.uj.edu.pl/COSY-11/07/.

G.3 INTAS Meeting Pellet Targets, Moscow (Russia)

The preparation of the pellet target for PANDA is supported by an INTAS project (06-1000012-8787). The consortium comprises the IKP/FZJ, ITEP and MPEI (both Moscow), Uppsala University and GSI-Darmstadt. On June 29 representatives of all institutes met at ITEP for a project kick-off meeting.

Fig. 59: Participants of the first INTAS consortium meeting on pellet targets at ITEP.

Within the INTAS consortium the IKP is in charge of the project coordination and of the tests with the target prototype which is located in the COSY accelerator hall.

G.4 The Workshop on the Physics of Excited Nucleon, NSTAR2007

The excitation spectrum of the nucleon promises to offer important insights into the non-perturbative regime of QCD. Dedicated experimental programs at various laboratories exist to perform accurate measurements of the meson photo- and electroproduction off the nucleon, studying the excitation of the nucleon. This workshop is the 6$^{\text{th}}$ in a series of meetings since 2000 (Co-organizer U.-G. Meißner).

H Teaching Positions

Institute	Name	University
IKP-1	PD Dr. A. Gillitzer	Bonn
	PD Dr. F. Goldenbaum	Wuppertal
	Prof. Dr. H. Machner	Duisburg-Essen
	Prof. Dr. W. Oelert	Bochum
	Prof. Dr. J. Ritman	Bochum
	PD Dr. S. Schadmand	Gießen
IKP-2	PD Dr. M. Büscher	Köln
	PD Dr. D. Gotta	Köln
	PD Dr. F. Rathmann	Erlangen-Nürnberg
	Prof. Dr. H. Ströher	Köln
	Dr. M. Wolke	Bochum
IKP-3	Prof. Dr. G. Baur	Basel
	Prof. Dr. E. Epelbaum	Bonn
	Univ. Doz. Dr. J. Haidenbauer	Graz
	PD Dr. C. Hanhart	Bonn
	Prof. Dr. S. Krewald	Bonn
	Prof. Dr. U.-G. Meißner	Bonn
	Prof. Dr. N.N. Nikolaev	Moscow
	Dr. A. Nogga	Bonn
	PD Dr. A. Wirzba	Bonn
IKP-4	Prof. Dr. Dr. h.c. J. Dietrich	Dortmund
	Dr. A. Lehrach	Bonn
	Prof. Dr. R. Maier	Bonn

I Beam Time at COSY 2007

Date	Experiment	Duration	Reaction
12.01.07–22.01.07	ANKE	1 week	pol.deuterons, 146.2+159
22.01.–29.01.	ANKE	1 week	$\vec{d}\vec{p} \to ppn$, 172
02.02.–12.02.	GEM	1 week	$\vec{d}p \to ppn$, 148.1
16.02.–21.03.	ANKE	5 weeks	$pA \to \alpha K^+K^-X$, 147.2
06.04.–07.05.	WASA	4 weeks	$pp \to pp\eta(\to 3\pi)$, 167
11.05.–21.05.	SPIN@COSY	1 week	$\vec{d}$ beam, 170
25.05.–04.06.	TOF	1 week	$\vec{p}p \to pp\omega$, 129.2
04.06.–11.06.	TOF	1 week	$\vec{p}p \to pK^0\Sigma^+$, 141.3
11.06.–18.06.	TOF	1 week	$\vec{p}d \to pK^0\Lambda p$,141.3
18.06.–02.07.	ANKE-PAX	2 weeks	$\vec{p}$ beam, 169
07.09.–17.09.	ANKE	1 week	$pp \to K^+\Sigma^+n$, 171.1
21.09.–08.10.	WASA	2 weeks	commissioning, 136.5
12.10.–22.10.	ANKE	1 week	$\vec{d}p \to {}^3\mathrm{He}\,\eta$, 157.1
26.10.–05.11.	ANKE	1 week	$\vec{p}p \to (pp)_s\pi^0$, 158.1
09.11.–19.11.	ANKE-PAX	1 week	pol.lifetime, 169.1
20.11.–26.11.	WASA	1 week	$pd \to Scalars$, 174
27.11.–04.12.	WASA	1 week	$dd \to {}^3\mathrm{He}\,n\pi^0$, 173
04.12.–19.12.	WASA	2 weeks	$dd \to \alpha 2\pi$, 174
Total '07		28 weeks	

J Personnel

J.1 Scientific Staff

F. Ballout (IKP-3) (until 31 May, 2007)

Prof. Dr. G. Baur (IKP-3)

Dr. U. Bechstedt (IKP-4)

Dr. K. Bongardt (IKP-4)

DI N. Bongers (IKP-4)

DI W. Borgs (IKP-2) (until 30 April, 2007)

DI R. Brings (IKP-4)

PD Dr. M. Büscher (IKP-2)

DP A. Chechenin (IKP-4)

DP A. Chechenin (IKP-4)

DP E. Czerwinski (IKP-1) (since 1 October, 2007)

DP D. Chiladze (IKP-2)

Prof. Dr.Dr.h.c. J. Dietrich (IKP-4)

Dr. A. Djalois (IKP-1)

Dr. M. Döring (IKP-3) (since 1 October, 2007)

Dr. R. Engels (IKP-2)

Prof. Dr. E. Epelbaum (IKP-3)

DI F.-J. Etzkorn (IKP-4)

Dr. P. Fedorets (IKP-2)

Dr. O. Felden (IKP-TA)

M. Freunek (IKP-3) (until 15 May, 2007)

Dr. W. Gast (IKP-1)

Dr. R. Gebel (IKP-4)

Dr. M. George (IKP-1) (since 1 April 2007)

PD Dr. A. Gillitzer (IKP-1)

PD Dr. F. Goldenbaum (IKP-1)

PD Dr. D. Gotta (IKP-2)

DI R. Greven (IKP-4) (since 1 January, 2007)

Dr. F. Grümmer (IKP-3)

Dr. D. Grzonka (IKP-1)

DI W. Günther (IKP-4)

Dr. F.-K. Guo (IKP-3) (since 1 October, 2007)

Univ. Doz. Dr. J. Haidenbauer (IKP-3)

PD Dr. C. Hanhart (IKP-3)

Dr. M. Hartmann (IKP-2)

M. Hausner (IKP-3) (since 1 August 2007)

Dr. V. Hejny (IKP-2)

DI K. Henn (IKP-4)

DP M. Hodana (IKP-1) (since 1 November, 2007)

Dr. F. Hügging (IKP-1)

Dr. V. Kamerdjiev (IKP-4)

D. Khaneft (IKP-2) (since 21 June 2007)

DP D. Kirillov (IKP-4) (until 18 December 2007)

DP P. Klaja (IKP-1)

A. Klingler (IKP-2)

St. Kölling (IKP-3) (since 16 April, 2007)

DP A. Kowalczyk (IKP-1) (until 28 February, 2007)

Dr. H. Krebs (IKP-3)

Prof. Dr. S. Krewald (IKP-3)

DI K. Kruck (IKP-4)

Dr. A. Lehrach (IKP-4)

DP V. Lensky (IKP-3) (until 7 June, 2007)

Dr. B. Lorentz (IKP-4)

Prof. Dr. H. Machner (IKP-1)

Prof. Dr. R. Maier (IKP-4)

Prof. Dr. U.-G. Meißner (IKP-3)

DP M. Mertens (IKP-1)

D. Minossi (IKP-3) (since 16 April, 2007)

DI I. Mohos (IKP-4)

Dr. M. Nekipelov (IKP-2)

Prof. Dr. N.N. Nikolaev (IKP-3)

Dr. A. Nogga (IKP-3)

Prof. Dr. W. Oelert (IKP-1)

DP D. Oellers (IKP-2)

Dr. H. Ohm (IKP-2)

DI N. Paul (IKP-1)

Dr. C. Pauly (IKP-1)

Dr. M. Pavon-Valderrama (IKP-3) (since 1 June 2007)

Dr. H. Polinder (IKP-3) (until 30 September, 2007)

Dr. D. Prasuhn (IKP-4)

DP D. Protic (IKP-TA)

DP J. Przerwa (IKP-1)

PD Dr. F. Rathmann (IKP-2)

DP Ch.F. Redmer (IKP-1)

DI A. Richert (IKP-4)

Prof. Dr. J. Ritman (IKP-1)

Dr. E. Roderburg (IKP-1)

DI J. Sarkadi (IKP-TA)

DP P. Saviankou (IKP-3)

Dr. H. Schaal (IKP-1)

PD Dr. S. Schadmand (IKP-1)

E. Schlauch (IKP-3) (until 14 January, 2007)

Dr. R. Schleichert (IKP-2)

DI M. Schmitt (IKP-4) (since 1 May, 2007)

DI H. Schneider (IKP-4) (until 30 September 2007)

DI G. Schug (IKP-4)

Dr. Th. Sefzick (IKP-TA)

DI E. Senicheva (IKP-4)

Dr. Y. Senichev (IKP-4)

DI M. Simon (IKP-4)

Dr. A. Sokolov (IKP-1)

Dr. R. Stassen (IKP-4)

Dr. H. Stockhorst (IKP-4)

Dr. T. Stockmanns (IKP-1)

DP Th. Strauch (IKP-2)

Prof. Dr. H. Ströher (IKP-2)

T. Tolba (IKP-1)

Dr. R. Tölle (IKP-4)

DI T. Vashegyi (IKP-4)

Dr. N. Vasiukhin (IKP-4)

DP P. Vlasov (IKP-1)

Chr. Weidemann (IKP-2)

DP D. Welsch (IKP-4)

M. P. Westig (IKP-2) (since 15 June 2007)

Dr. P. Wintz (IKP-1)

PD Dr. A. Wirzba (IKP-3)

DI J.-D. Witt (IKP-4)

Dr. M. Wolke (IKP-2)

Dr. E. Zaplatin (IKP-4)

F. Zarife (IKP-4) (since 15 March 2007)

DP D. Z. Zhang (IKP-1)

J.2 Technical and Administrative Staff

J. Ahlschläger (IKP-4) (since 1 March, 2007)

C. Berchem (IKP-TA)

P. Birx (IKP-4)

M. Böhnke (IKP-4)

H. Bongen (IKP-1)

J. Borsch (IKP-TA)

P. Brittner (IKP-4)

J. But (IKP-TA)

M. Comuth-Werner (IKP-TA)

B. Dahmen (IKP-4)

C. Deliege (IKP-4)

W. Derissen (IKP-TA)

N. Dolfus (IKP-TA)

G. D'Orsaneo (IKP-2)

R. Dosdall (IKP-1)

R. Enge (IKP-4)

B. Erkes (IKP-4)

W. Ernst (IKP-TA)

K. Esser (IKP-TA)

H.-P. Faber (IKP-4)

G. Fiori (IKP-TA)

H.-W. Firmenich (IKP-TA)

J. Göbbels (IKP-TA)

H. Hadamek (IKP-TA)

R. Hecker (IKP-4)

E. Heßler (IKP-TA)

M. Holona (IKP-TA)

H.-M. Jäger (IKP-1)

H. J. Jansen (IKP-TA)

M. Karnadi (IKP-2)

A. Kieven (IKP-4)

Ch. Krahe (IKP-TA)

M. Kremer (IKP-TA)

Th. Krings (IKP-TA)

G. Krol (IKP-4)

M. Küven (IKP-TA)

K.-G. Langenberg (IKP-4)

H. Metz-Nellen (IKP-TA)

S. Müller (IKP-TA)

R. Nellen (IKP-TA)

St. Nießen (IKP-TA)

H. Pütz (IKP-4)

G. Roes (IKP-TA)

N. Rotert (IKP-4)

D. Ruhrig (IKP-4)

T. Sagefka (IKP-4)

F. Scheiba (IKP-4)

H. Schiffer (IKP-TA)

J. Schmitz (IKP-4)

F. Schultheiß (IKP-TA)

H. Singer (IKP-4)

D. Spölgen (IKP-2)

G. Sterzenbach (IKP-1)

J. Strehl (IKP-TA)

J. Uehlemann (IKP-1)

P. Wieder (IKP-2)

J. Wimmer (IKP-1)

H. Zens (IKP-4)

IKP-1 = Experimental Hadron Structure
IKP-2 = Experimental Hadron Dynamics
IKP-3 = Theoretical Nuclear Physics
IKP-4 = Large-Scale Nuclear Physics Equipment
IKP-TA = Technical Services and Administration

K Contents of the Attached CD

1. This report as pdf file

2. Detailed reports for the Annual Report 2007